INFRARED SPECTROSCOPY OF HYDROCARBON RADICALS WITHIN SUPERFLUID HELIUM NANODROPLETS: EXPERIMENTAL AND THEORETICAL RESULTS WITH APPLICATIONS TO UNDERGRADUATE EDUCATION

by

ALAINA RACHEL BROWN

(Under the Direction of Gary E. Douberly)

ABSTRACT

Helium nanodroplet isolation is used to trap hydrocarbon radicals produced by the pyrolysis of appropriate precursors. The infrared spectra, predominantly in the CH stretching region, of a variety of hydrocarbon radicals is discussed. High-level theoretical computations using the VPT2+K method are used to compare the spectra of each radical and make assignments when feasible. Cyclobutylmethyl nitrite is used as a pyrolytic precursor to the cyclobutyl radical, the spectrum of which is presented herein. Upon higher temperature pyrolysis, decomposition products of the cyclobutyl radical are observed, specifically, products that occur as a result of a ring-opening mechanism. These results are compared to the existing potential energy surface (PES) for C_4H_7 species. The infrared spectra of fulvenallene and the fulvenallenyl radical are also discussed. Spectra in the acetylenic CH stretching region for the fulvenallenyl radical provide valuable information about the extent of the unpaired electron's delocalization throughout the conjugated propargyl and cyclopentadienyl subunits. These results are

aided by spin density calculations based on Mulliken populations. Anharmonic theoretical computations are used to make spectral assignments and provide insight into the identity of other species formed during the initial pyrolysis process. Finally, a previously published physical chemistry experiment is transformed into an undergraduate SCALE-UP activity. As an extension of fundamental physical chemistry research, this activity serves as an example of how undergraduate curriculum can benefit from merging research with classroom content. Two versions of the activity will be presented along with an analysis of student definitions for entropy before and after completing the activity.

INDEX WORDS: HELIUM NANODROPLETS, INFRARED SPECTROSCOPY, HYDROCARBON RADICALS, VIBRATIONAL SPECTROSCOPY, SCALE-UP, UNDERGRADUATE PHYSICAL CHEMISTRY

INFRARED SPECTROSCOPY OF HYDROCARBON RADICALS WITHIN SUPERFLUID HELIUM NANODROPLETS: EXPERIMENTAL AND THEORETICAL RESULTS WITH APPLICATIONS TO UNDERGRADUATE EDUCATION

by

ALAINA RACHEL BROWN

B.S., Newberry College, 2014

A Dissertation Submitted to the Graduate Faculty of The University of Georgia in Partial Fulfillment of the Requirements for the Degree

DOCTOR OF PHILOSOPHY

ATHENS, GEORGIA

2019

INFRARED SPECTROSCOPY OF HYDROCARBON RADICALS WITHIN SUPERFLUID HELIUM NANODROPLETS: EXPERIMENTAL AND THEORETICAL RESULTS WITH APPLICATIONS TO UNDERGRADUATE EDUCATION

by

ALAINA RACHEL BROWN

Major Professor:	Gary E. Douberly
Committee:	Michael A. Duncan
	Geoffrey D. Smith

Electronic Version Approved:

Suzanne Barbour
Dean of the Graduate School
The University of Georgia
May 2019

DEDICATION

In memory of Granny. You will always be my sunshine.

ACKNOWLEDGEMENTS

This work would not have been possible without the help and support of countless individuals. First, I would like to thank my advisor, Gary Douberly. The past five years have been an amazing learning experience, and I'm grateful to have been a part of his group. His enthusiasm for science sparked my interest in joining the group and gave me the motivation to put in the long hours of data collection, analysis and writing. Through his mentorship, I was also given the opportunity to TA for his undergraduate physical chemistry course and to help develop new teaching materials. These experiences led me to pursue my teaching certificate here at UGA and to landing my dream job at a PUI. Second, I'd like to thank Professor Michael Duncan for his advice, guidance, and instruction during my time here. As a novice to all things education related, Professor Norbert Pienta and Dr. Colleen Kuusinen were invaluable resources as I planned and completed my teaching project for the teaching certificate program. Lastly, thanks goes to Professor Geoffrey Smith for agreeing to sit on my committee at the last minute when it came time to defend this dissertation.

I had the pleasure of having two great advisors during my undergraduate career at Newberry College: Drs. Sid Parrish and Christina McCartha. Without their direction and teaching, I would not have become interested in research or have even known that going to graduate school (and getting paid for it) was a possibility! Dr. Bruce Ault served as my research advisor during my undergraduate REU at the University of Cincinnati, which led

me to pursue experimental physical chemistry research during graduate school. His group not only made me feel at home in a new city for a summer but also showed me how exciting and rewarding physical chemistry research could be.

During my first year of graduate school, our postdoc Bernadette Broderick gave me the confidence I needed to work in an experimental physical chemistry lab and try new things. My colleagues, Joseph Brice and Peter Franke, were instrumental in helping with collecting spectra and performing theoretical calculations during my time at UGA. I owe Melissa Woodard my gratitude for keeping me sane and on track during graduate school. We did it! I'm also glad that I had the privilege of meeting some other amazing people while in graduate school and that we got to experience weekly trivia nights, game nights and many other events together. And to my fellow Douberly group members both past and present, thank you for paving the way and continuing to create a great work environment. I'm grateful to have had the chance to get to know you all and to do science with you all. Make helium great again!

Finally, my family and friends deserve my eternal gratefulness for many reasons. Thank you for listening to me vent about research and graduate school, for giving me pep talks when I needed the motivation to get through the rough patches, and for supporting me through it all. I love you all and can't thank you enough for all you have done for me especially over the past five years.

TABLE OF CONTENTS

Page

ACKNOWLEDGEMENTS v

LIST OF TABLES ix

LIST OF FIGURES x

CHAPTER

1 INTRODUCTION 1

1.1 History of Matrix Isolation and Helium Nanodroplet Isolation 1

1.2 Infrared Spectroscopy of Hydrocarbon Radicals 4

1.3 Applications to Undergraduate Education 7

References 8

2 EXPERIMENTAL METHODS 13

2.1 Formation of Helium Nanodroplets 13

2.2 Doping Process 17

2.3 Infrared Laser System and Action Spectroscopy 23

References 29

3 HELIUM NANODROPLET ISOLATION OF THE CYCLOBUTYL, 1-METHYLALLYL AND ALLYLCARBINYL RADICALS: INFRARED SPECTROSCOPY AND AB INITIO COMPUTATIONS ..31

3.1 Introduction 32

3.2 Experimental Section 34

3.3 Theoretical Methods 40

3.4 Results and Discussion 47

3.5 Conclusions.....73

References.....75

4 INFRARED SPECTRUM OF FULVENALLENE AND FULVENALLENYL IN HELIUM DROPLETS 81

4.1 Introduction.....82

4.2 Experimental Section.....84

4.3 Computational Details 86

4.4 Results and Discussion 92

4.5 Conclusions.....118

References.....120

5 A RESEARCH-BASED ACTIVITY FOR USE IN A SCALE-UP CLASSROOM ON STUDENTS' DEFINITIONS OF ENTROPY: CREATION IMPLEMENTATION AND RESULTS.....126

5.1 Introduction.....126

5.2 Project Methods 130

5.3 Results and Discussion 134

5.4 Conclusions.....136

References.....139

6 CONCLUSIONS AND OUTLOOK.....169

References.....174

LIST OF TABLES

Page

Table 3.1: Qualitative descriptions, symmetries, and harmonic frequencies of the cyclobutyl radical 55

Table 3.2: Comparison of experimental band centers for methylallyl 61

Table 4.1: Fulvenallene: comparison of experimental bands to VPT2+K predictions (cm^{-1}) 101

Table 4.2: Qualitative descriptions, symmetries and CCSD(T)/ANO1 harmonic frequencies and intensities of the normal modes of vibration of fulvenallene 102

Table 4.3: Experimental frequencies (cm^{-1}), intensities and assignments of the acetylenic CH stretch region measured with hot pyrolysis conditions 106

Table 4.4: Qualitative descriptions, symmetries, and ROHF-CCSD(T)/ANO1 harmonic frequencies and intensities of the normal modes of vibration of fulvenallenyl 107

Table 4.5: Symmetries, identities, and VPT2+K frequencies and intensities of vibrational transitions of 5-ethynylcyclopentadiene between 2800 and 3400 cm^{-1} 108

Table 4.6: Symmetries, identities, and VPT2+K frequencies and intensities of vibrational transitions of 1-ethynylcyclopentadiene between 2800 and 3400 cm^{-1} 109

Table 4.7: Symmetries, identities, and VPT2+K frequencies and intensities of vibrational transitions of 2-ethynylcyclopentadiene between 2800 and 3400 cm^{-1} 110

LIST OF FIGURES

Page

Figure 2.1: Schematic of the helium nanodroplet isolation (HENDI) instrument.....14

Figure 2.2: Log-normal distribution curves showing number of helium atoms per droplet at varying temperatures between 15 and 20 K.....15

Figure 2.3: Image of the quartz/tantalum pyrolysis source used in the experiments outlined in Chapter 3.....19

Figure 2.4: Circuit diagram for quartz/tantalum source (top) and silicon carbide source (bottom).....20

Figure 2.5: Depiction of the silicon carbide (SiC) source used in these experiments 21

Figure 2.6: Probability curves for droplets picking up *n* molecules under various pickup cell pressures based on Poisson statistics (Equation 2.1) 24

Figure 2.7: Evolution of the mass spectrum during the cyclobutyl radical experiment 27

Figure 3.1: The mass spectrum of the neat droplet beam is shown in trace (A).....38

Figure 3.2: Difference depletions mass spectra under various pyrolysis conditions and various frequencies 39

Figure 3.3: Computed structures for (A) C_s cyclobutyl, (B) C_{2v} cyclobutyl, (C) *trans*- and (D) *cis*-1-methylallyl, and (E) *gauche*- and (F) *cis*-allylcarbinyl 41

Figure 3.4: PES for the C_4H_7 species relevant to this study 48

Figure 3.5: IR survey spectra of the cyclobutyl radical (black) and its precursor, cyclobutylmethyl nitrite (blue) 50

Figure 3.6: Relaxed PES for the ring puckering of the cyclobutyl radical computed at the CCSD(T)/ANO1 level of theory 52
Figure 3.7: Experimental spectrum of the cyclobutyl radical (black) compared to the theoretical predictions for the C_{2v} structure (red) 54
Figure 3.8: IR survey spectrum of the 1-methylallyl radical (red) as compared to the spectrum of its precursor (2-methyl-3-buten-1-yl nitrite) in blue 57
Figure 3.9: Experimental spectrum for 1-methylallyl radical (black) compared to the theoretical predictions for the *trans* and *cis* structures (red) 58
Figure 3.10: Simulated spectra for the *trans* (blue) and *cis* (red) conformers of the 1-methylallyl radical as compared to the experimental spectrum 59
Figure 3.11: IR survey spectrum of the allylcarbinyl radical (red) as compared to the spectrum of its precursor, 4-penten-1-yl nitrite (blue) 63
Figure 3.12: Experimental spectrum of allylcarbinyl radical (black) compared to the theoretical predictions for the *gauche* and *cis* structures combined (red) 64
Figure 3.13: Experimental spectrum as compared to the theoretical simulated spectra for the *gauche* (blue) and *cis* (red) conformers of the allylcarbinyl radical 65
Figure 3.14: IR survey spectrum of allylcarbinyl radical (red) and 1-methylallyl radical (blue) as compared to the spectrum of cyclobutyl radical (black) 67
Figure 3.15: Laser-induced depletion spectrum of 1,3-butadiene in the CH stretching region, measured on mass channel m/z = 27 u 69
Figure 3.16: Pyrolysis of cyclobutyl methyl nitrite at 33 A 71
Figure 4.1: Structures and orbitals of theoretically investigated molecules and bonding nomenclature 87

Figure 4.2: Plot of the CCSD(T)/ANO1 potential energy (primary Y-axis) using UHF (red) and ROHF (blue) reference wavefunctions.....89

Figure 4.3: Schematic C_7H_6 potential energy surface (kcal/mol).....93

Figure 4.4: (A) Electron ionization mass spectrum of the neat droplet beam, showing peaks every 4 u (He_n^+ ions) and residual water at 18 u.....96

Figure 4.5: Difference depletion mass spectra measured with the laser frequency fixed to 3089.9 cm^{-1}.....97

Figure 4.6: Mass channel 63 u comparison for cold pyro (black) and hot pyro (red).....99

Figure 4.7: Infrared spectrum of fulvenallene in the CH stretching region, measured on mass channel 89 u.....100

Figure 4.8: Comparison of 89 u depletion spectra between 3000 and 3140 cm^{-1} with cold (A) and hot (B) pyrolysis source conditions.....103

Figure 4.9: VPT2+K spectra of (bottom to top) fulvenallene, fulvenallenyl, 5-ethynylcyclopentadiene, 1-ethynylcyclopentadiene, and 2-ethynylcyclopentadiene.....105

Figure 4.10: Acetylenic CH stretching region measured on mass channels 89 and 63 u.....112

Figure 4.11: (A) Experimental acetylenic CH stretch spectral region (channel 63 u) compared to VPT2+K simulations for fulvenallenyl radical (B), and three C_7H_6 isomers: (C) 5-ethynylcyclopentadiene, (D) 1-ethynylcyclopentadiene, and (E) 2-ethynylcyclopentadiene.....113

Figure 4.12: ROHF-CCSD(T)/ANO1 spin density plot for fulvenallenyl radical (ρ=0.01 ea_0^{-3}).....117

Figure 5.1: Simple schematic of a SCALE-UP classroom in the Science Learning Center at UGA 143
Figure 5.2: Student consent form used in Fall 2016 CHEM 3110 course 144
Figure 5.3: Preliminary activity used in fall 2016 class for CHEM 3110 145
Figure 5.4: Relevant survey questions and results from the 2016 survey given after the initial project 153
Figure 5.5: Modified activity used in CHEM 3110 fall 2017 semester 156
Figure 5.6: Student consent form used during the fall 2017 course 160
Figure 5.7: Student pre-test questionnaire given to students in the fall 2017 course 161
Figure 5.8: Post-test questionnaire and accompanying survey questions given to students in the fall 2017 course 164
Figure 5.9: Bar graphs indicating student responses for question 3 of the pre-test (top) and post-test (bottom) 168

CHAPTER 1

INTRODUCTION

1.1 History of Matrix Isolation and Helium Nanodroplet Isolation

In the mid-1950's, the term matrix isolation was coined by George Pimentel to describe experiments where an unreactive host gas is mixed and condensed with a target molecule onto a cold surface.[1] The target molecule is therefore *isolated* from other co-deposited molecules in a *matrix* of the host gas. During this time, pioneering experiments were performed by Pimentel[2, 3] and George Porter[4] in a variety of matrix materials such as CO_2, CCl_4, Xe, ether, and isopentane held at or slightly below liquid nitrogen temperatures. Lowering operating temperatures to ~ 20 K, the infrared spectra of methylene deposited into both Ar and N_2 matrices were collected upon pyrolysis of diazomethane.[5, 6] These experiments are the first examples of modern-day matrix isolation experiments. Since this time, a variety of radicals and transient species have been trapped by an assortment of host gasses and probed by various spectroscopic techniques.[1, 7-13] The most common matrix materials are noble gasses because they do not typically interact with the target molecules trapped inside.[10] However, there is generally a frequency shift associated with spectra collected under these conditions as opposed to gas-phase spectra.[7, 8] Warming of the matrix as well as secondary photolysis via a UV

laser can provide additional information about secondary reactions or decomposition mechanisms that can occur within the matrix environment.[14-16]

Solid para-hydrogen (p-H_2) is often used as an alternative matrix material to noble gas matrices. At room temperature, H_2 exists in a 3:1 ratio of ortho to para states; the ortho state (paired nuclear spin of I=1 and odd rotational quantum numbers, J) is converted to the para form (I=0 with even J quantum numbers) at low temperatures with the aid of a catalyst.[17, 18] Upon formation of the matrix, impurities of only 100 ppm ortho can be achieved depending upon the temperature of the gas during conversion.[17] Similar to rare gas matrices, spectra collected in p-H_2 matrices experience red-shifting of frequencies when compared to gas-phase values but tend to be on the order of 5-15 cm^{-1} and give sharper spectral lines.[18, 19] An early experiment from Oka and coworkers discovered the narrow 180 MHz linewidth of the tetrahexacontapole-induced (64-pole) p-H_2 J=6 ← 0 transition.[20] This prompted others to begin trapping molecules inside of p-H_2 matrices to study them spectroscopically. One of the first examples of this was performed by Momose and Shida; methane was trapped in a matrix held at 5 K and the vibrational spectrum was recorded.[21] Rotational fine structure was also observed, but because of matrix crystal-field effects, the transitions were split.

Halogen containing species can be used as precursors for radical formation when a beam of 266 nm light from a Nd:YAG is used for photodissociation once molecules are doped into the p-H_2 matrix.[22] Homolytic bond dissociation of the precursor forms a halogen radical which moves through the matrix and away from the newly formed hydrocarbon radical due to the matrix's softness and high thermal conductivity.[23] Similar experiments have been performed by depositing O_2 and CH_2I_2 simultaneously before

irradiating with UV light to form the peroxy species ICH_2OO.[24] In a p-H_2 matrix, the p-H_2 molecules are delocalized within the matrix and have a large zero-point motion; thus, it is considered a "quantum solid". Reactions of the host matrix with the radical dopant as well as quantum phenomena such as ortho-H_2 quantum diffusion and nuclear spin conversion have also been studied.[23, 25]

Many of the problems encountered when working with rare-gas or p-H_2 matrices can be overcome by using the helium nanodroplet isolation (HENDI) technique. Early work by Stephens and King studied the properties of helium nanodroplets by electron impact ionization.[26] In the early 1990's, this technique was used during a cross-beam experiment to trap Ne atoms in droplets; this was the first time that a dopant was solvated within the droplet environment.[27] The first instance where a molecule was picked up by a droplet beam and studied spectroscopically was in 1992 when Scoles and coworkers formed droplets of a few thousand He atoms to pick up SF_6 molecules. Using a line-tunable CO_2 laser overlapped with the droplet beam, they found two IR absorptions near 946 cm^{-1}.[28] At that time, it was thought the molecules resided on the surface of the droplet and were not solvated; a follow-up experiment found that it was more likely that molecules were located inside of the He clusters.[29] This latter experiment found two additional bands around 933 and 955 cm^{-1} which were attributed to the SF_6 dimer. Rotationally resolved spectra came a few years later; these results showed that molecules within droplets have a significantly reduced rotational constant when compared with gas-phase values and that the SF_6 embedded within the droplet had a rotational temperature of 0.37 ± 0.05 K.[30, 31] These results showed that HENDI is able to effectively and efficiently cool the degrees of freedom of the dopant like other matrix isolation techniques.

Another interesting property of helium nanodroplets are their superfluid character. This was first discovered by Toennies, Vilesov and coworkers when they doped glycoxyl ($C_2H_2O_2$) into droplets containing approximately 5500 He atoms to study the $S_1 \leftarrow S_0$ electronic transition.[32] OCS was doped into helium droplets containing about 10^4 atoms of ^{3}He, ^{4}He, or a mixture of both in a "microscopic Andronikashivili experiment".[33] Spectra collected in pure ^{3}He droplets did not show rotational resolution while spectra collected in pure ^{4}He droplets had narrow rotational lines. This was evidence that free rotations are a consequence of a superfluid environment. When adding ^{4}He atoms to a ^{3}He droplet, the ^{4}He atoms would cluster around the OCS dopants. Approximately 60 ^{4}He atoms were needed to give a rotationally resolved spectrum providing evidence that this is the number of ^{4}He atoms required to achieve superfluidity.

1.2 Infrared Spectroscopy of Hydrocarbon Radicals

As highlighted in the previous section, it is often easy to dope closed shell molecules into droplets and study them spectroscopically. However, radicals and other transient species are not as easy to study experimentally. In general, radical spectra are often more complex than closed-shell systems because the unpaired electron(s) undergoes a variety of interactions including orbital and spin angular momentum coupling with itself and other unpaired electrons if present.[34] High-resolution spectra of various radicals have been recorded by Nesbitt and co-workers with rotational temperatures of < 25 K.[35-43] Although this temperature is relatively cold, the spectra are still quite

complicated because of the many rotational states that are occupied. Similar results were found by Curl and coworkers during their many experiments probing radicals with their high-resolution infrared spectroscopy technique.[44-48] The complexity found in spectra like these not only provides a challenge for spectroscopists to make assignments but for computational chemists as well; current methods are not always able to reproduce a radical's spectrum.

With the use of HENDI, molecules are doped and subsequently cooled to their ground electronic and vibrational states and are in low rotational quantum states that are dependent upon the rotational constant of the molecule and the droplet temperature.[49] This greatly simplifies complicated spectra when compared to other matrix techniques and can be illustrated by comparing the spectra of the allyl radical trapped in a neon matrix held at 10 K[50] vs. a helium droplet at ~0.4 K[51]. In particular, the ν_1 fundamental shows a large band with a small shoulder in the neon matrix, but this band is resolved into 1 large band with a shoulder and 1 smaller band, all with varying degrees of rotational resolution, in the helium droplet spectrum.

With any gas-phase technique, the density of the molecule of interest is vital for achieving significant signal to noise ratios. This is one advantage of matrix techniques when compared to traditional gas-phase or HENDI. When carrying out a matrix isolation experiment, the deposition period can be extended until a sufficient concentration of dopant is achieved. This is not possible with the HENDI technique as molecular dopants are housed in a "pick-up chamber" and are picked up by droplets as the beam enters this region of the instrument. Densities of radicals are even lower when using a pyrolysis method as the probability for each droplet picking up one radical of interest is reduced by

the presence of other pyrolytic products.[52] Pressures must be carefully monitored in the pick-up chamber to avoid doping more than one molecule into the same droplet, as this would cause unwanted dimer/complex peaks or evidence of radical recombination within a particular spectrum.

Infrared spectroscopy of these radicals has implications in many areas, but in particular, the chemistry of these radicals in combustion environments is interesting and an area for further exploration.[53] There are hundreds of fuel-type molecules with thousands of possible reactions in a combustion environment; this does not include trying to characterize a radical's secondary reaction with other radicals or molecular oxygen. Because of their short lifetimes, high reactivity, and instability, direct observation by traditional methods are difficult.[10] This is why techniques such as HENDI are employed to record a radical's infrared spectrum to be used for future identification and analysis. Chapters 3 and 4 of this dissertation focus on initial identification and band assignments of a handful of hydrocarbon radicals via infrared spectroscopy and HENDI. The hope is that this data is used as a benchmark for future studies involving hydrocarbon radicals produced in similar manner and/or once reacted with molecular oxygen to form peroxy radicals. These experiments also provide computational chemists benchmarks for calibrating and developing new methods.

1.3 Applications to Undergraduate Education

The remainder of this dissertation focuses on applying experimental physical chemistry data to undergraduate education. Specifically, the model dipeptide N-acetylglycine methylamide (NAGMA)[54] was used to teach students in the CHEM 3110 course at the University of Georgia about thermodynamic concepts in a SCALE-UP setting. Based on the research article, an activity was created so that students were exposed to current physical chemistry research, which related to topics they were learning in class. Through this activity, students in the course gained an appreciation for real-world applications to the concepts they were learning in class while also expanding their previous definitions of entropy, an extremely abstract physical chemistry concept. Details of this project are given in Chapter 5.

References

(1) Bally, T. Matrix Isolation. In *Reactive Intermediate Chemistry*, Platz, M. S.; Moss, R. A.; Jones, M. J., Eds. John Wiley & Sons, Inc.: Hoboken, New Jersey, 2005.

(2) Whittle, E.; Dows, D. A.; Pimentel, G. C. Matrix Isolation Method for the Experimental Study of Unstable Species. *J. Chem. Phys.* **1954**, *22*, 1943.

(3) Becker, E. D.; Pimentel, G. C. Spectroscopic Studies of Reactive Molecules by the Matrix Isolation Method. *J. Chem. Phys.* **1956**, *25*, 224-228.

(4) Norman, I.; Porter, G. Trapped Atoms and Radicals in a Glass 'Cage'. *Nature.* **1954**, *174*, 508-509.

(5) DeMore, W. B.; Pritchard, H. O.; Davidson, N. Photochemical Experiments in Rigid Media at Low Temperatures. II. The Reactions of Methylene, Cyclopentadienylene and Diphenylmethylene. *J. Am. Chem. Soc.* **1959**, *81*, 5874-5879.

(6) Milligan, D. E.; Pimentel, G. C. Matrix Isolation Studies: Possible Infrared Spectra of Isomeric Forms of Diazomethane and of Methylene, CH_2. *J. Chem. Phys.* **1958**, *29*, 1405-1412.

(7) Dunkin, I. R. The Matrix Isolation Technique and its Application to Organic Chemistry. *Chem. Soc. Rev.* **1980**, *9*, 1-23.

(8) Bondybey, V. E.; Smith, A. M.; Agreiter, J. New Developments in Matrix Isolation Spectroscopy. *Chem. Rev.* **1996**, *96*, 2113-2134.

(9) Sander, W.; Bucher, G.; Wierlacher, S. Carbenes in Matrixes: Spectroscopy, Structure, and Reactivity. *Chem. Rev.* **1993**, *93*, 1583-1621.

(10) Andrews, L. Infrared Spectra of Free Radicals and Chemical Intermediates in Inert Matrices. *Annu. Rev. Phys. Chem.* **1971**, *22*, 109-132.

(11) Andrews, L. Spectroscopy of Molecular Ions in Noble Gas Matrices. *Annu. Rev. Phys. Chem.* **1979**, *30*, 79-101.

(12) Frei, H.; Pimentel, G. C. Infrared Induced Photochemical Processes in Matrices. *Annu. Rev. Phys. Chem.* **1985**, *36*, 491-524.

(13) Nagarajan, R.; Maier, J. P. Electronic Spectra of Carbon Chains and Derivatives. *Int. Rev. Phys. Chem.* **2010**, *29*, 521-554.

(14) Amicangelo, J. C.; Lee, Y. P. Infrared Spectra of the 1-Chloromethyl-1-Methylallyl and 1-Chloromethyl-2-Methylallyl Radicals Isolated in Solid Para-Hydrogen. *J. Phys. Chem. A.* **2017**, *121*, 8771-8784.

(15) Pinelo, L. F.; Klotz, E. R.; Wonderly, W. R.; Paulson, L. O.; Kettwich, S. C.; Kubelka, J.; Anderson, D. T. Solid Parahydrogen Infrared Matrix Isolation and Computational Studies of Li_n–$(C_2H_4)_m$ Complexes. *J. Phys. Chem. A.* **2018**, *122*, 985-991.

(16) Lee, Y. P.; Wu, Y. J.; Lees, R. M.; Xu, L. H.; Hougen, J. T. Internal Rotation and Spin Conversion of CH_3OH in Solid Para-Hydrogen. *Science.* **2006**, *311*, 365-368.

(17) Silvera, I. F. The Solid Molecular Hydrogens in the Condensed Phase: Fundamentals and Static Properties. *Rev. Mod. Phys.* **1980**, *52*, 393-452.

(18) Fajardo, M. E. Matrix Isolation Spectroscopy in Solid Parahydrogen: A Primer. In *Physics and Chemistry at Low Temperatures*, Khriachtchev, L., Ed. Pan Stanford Publishing: Singapore, 2011.

(19) Oka, T. High-Resolution Spectroscopy of Solid Hydrogen. *Annu. Rev. Phys. Chem.* **1993**, *44*, 299-333.

(20) Okumura, M.; Chan, M.-C.; Oka, T. High-Resolution Infrared Spectroscopy of Solid Hydrogen: The Tetrahexacontapole-Induced $\Delta J=6$ Transitions. *Phys. Rev. Lett.* **1989**, *62*, 32-35.

(21) Takamasa, M.; Tadamasa, S. Matrix-Isolation Spectroscopy Using Solid Parahydrogen as the Matrix: Application to High-Resolution Spectroscopy, Photochemistry, and Cryochemistry. *Bull. Chem. Soc. Jpn.* **1998**, *71*, 1-15.

(22) Sato, H. Photodissociation of Simple Molecules in the Gas Phase. *Chem. Rev.* **2001**, *101*, 2687-2726.

(23) Fushitani, M.; Shida, T.; Momose, T.; Räsänen, M. UV-Photolysis of $HI\cdots CO_2$ Complexes in Solid Parahydrogen: Formation of CO and H_2O. *J. Phys. Chem. A.* **2000**, *104*, 3635-3641.

(24) Lee, Y. F.; Lee, Y. P. Infrared Absorption of Iodomethylperoxy (Syn-ICH_2OO) Radical Generated Upon Photolysis of CH_2I_2 and O_2 in Solid Para-H_2. *Mol. Phys.* **2015**, *113*, 2148-2158.

(25) Yoshioka, K.; Raston, P. L.; Anderson, D. T. Infrared Spectroscopy of Chemically Doped Solid Parahydrogen. *Int. Rev. Phys. Chem.* **2006**, *25*, 469-496.

(26) Stephens, P. W.; King, J. G. Experimental Investigation of Small Helium Clusters: Magic Numbers and the Onset of Condensation. *Phys. Rev. Lett.* **1983**, *51*, 1538-1541.

(27) Scheidemann, A.; Toennies, J. P.; Northby, J. A. Capture of Neon Atoms by ^{4}He Clusters. *Phys. Rev. Lett.* **1990**, *64*, 1899-1902.

(28) Goyal, S.; Schutt, D. L.; Scoles, G. Vibrational Spectroscopy of Sulfur Hexafluoride Attached to Helium Clusters. *Phys. Rev. Lett.* **1992**, *69*, 933-936.

(29) Goyal, S.; Schutt, D. L.; Scoles, G. Infrared Spectroscopy in Highly Quantum Matrixes: Vibrational Spectrum of Sulfur Hexafluoride ($(SF_6)n=1,2$) Attached to Helium Clusters. *J. Phys. Chem.* **1993**, *97*, 2236-2245.

(30) Fröchtenicht, R.; Toennies, J. P.; Vilesov, A. High-Resolution Infrared Spectroscopy of SF_6 Embedded in He Clusters. *Chem. Phys. Lett.* **1994**, *229*, 1-7.

(31) Hartmann, M.; Miller, R. E.; Toennies, J. P.; Vilesov, A. Rotationally Resolved Spectroscopy of SF_6 in Liquid Helium Clusters: A Molecular Probe of Cluster Temperature. *Phys. Rev. Lett.* **1995**, *75*, 1566-1569.

(32) Hartmann, M.; Mielke, F.; Toennies, J. P.; Vilesov, A. F.; Benedek, G. Direct Spectroscopic Observation of Elementary Excitations in Superfluid He Droplets. *Phys. Rev. Lett.* **1996**, *76*, 4560-4563.

(33) Grebenev, S.; Toennies, J. P.; Vilesov, A. F. Superfluidity Within a Small Helium-4 Cluster: The Microscopic Andronikashvili Experiment. *Science.* **1998**, *279*, 2083-2086.

(34) Herzberg, G. *Molecular Spectra and Molecular Structure*, 2nd ed.; Van Nostrand: New York, 1950.

(35) Anderson, D. T.; Davis, S.; Zwier, T. S.; Nesbitt, D. J. An Intense Slit Discharge Source of Jet-Cooled Molecular Ions and Radicals (T_{rot} < 30 K). *Chem. Phys. Lett.* **1996**, *258*, 207-212.

(36) Schiffman, A.; Nelson, D. D.; Robinson, M. S.; Nesbitt, D. J. High-Resolution Infrared Flash Kinetic Spectroscopy of Hydroxyl Radicals. *J. Phys. Chem.* **1991**, *95*, 2629-2636.

(37) Dong, F.; Roberts, M.; Nesbitt, D. J. High-Resolution Infrared Spectroscopy of Jet-Cooled Vinyl Radical: Symmetric CH_2 Stretch Excitation and Tunneling Dynamics. *J. Chem. Phys.* **2008**, *128*, 044305.

(38) Sharp, E. N.; Roberts, M. A.; Nesbitt, D. J. Rotationally Resolved Infrared Spectroscopy of a Jet-Cooled Phenyl Radical in the Gas Phase. *Phys. Chem. Chem. Phys.* **2008**, *10*, 6592-6596.

(39) Dong, F.; Davis, S.; Nesbitt, D. J. Slit Discharge IR Spectroscopy of a Jet-Cooled Cyclopropyl Radical: Structure and Intramolecular Tunneling Dynamics. *J. Phys. Chem. A.* **2006**, *110*, 3059-3070.

(40) Häber, T.; Blair, A. C.; Nesbitt, D. J.; Schuder, M. D. CH Stretch/Internal Rotor Dynamics in Ethyl Radical: High-Resolution Spectroscopy in the CH_3-Stretch Manifold. *J. Chem. Phys.* **2006**, *124*, 054316.

(41) Davis, S.; Uy, D.; Nesbitt, D. J. Laser Spectroscopy of Jet-Cooled Ethyl Radical: Infrared Studies in the CH_2 Stretch Manifold. *J. Chem. Phys.* **2000**, *112*, 1823-1834.

(42) Uy, D.; Davis, S.; Nesbitt, D. J. High-Resolution Infrared Spectroscopy of Jet-Cooled Allyl Radical (CH_2–CH–CH_2): In-Phase (ν_1) and Out-of-Phase (ν_{13}) Antisymmetric CH_2 Stretching Vibrations. *J. Chem. Phys.* **1998**, *109*, 7793-7802.

(43) Davis, S.; Anderson, D. T.; Duxbury, G.; Nesbitt, D. J. Jet-Cooled Molecular Radicals in Slit Supersonic Discharges: Sub-Doppler Infrared Studies of Methyl Radical. *J. Chem. Phys.* **1997**, *107*, 5661-5675.

(44) Unfried, K. G.; Glass, G. P.; Curl, R. F. Infrared Flash Kinetic Spectroscopy of the Ketenyl Radical. *Chem. Phys. Lett.* **1991**, *177*, 33-38.

(45) Morter, C. L.; Domingo, C.; Farhat, S. K.; Cartwright, E.; Glass, G. P.; Curl, R. F. Rotationally Resolved Spectrum of the ν_1 CH Stretch of the Propargyl Radical (H_2CCCH). *Chem. Phys. Lett.* **1992**, *195*, 316-321.

(46) Han, J. X.; Utkin, Y. G.; Chen, H. B.; Burns, L. A.; Curl, R. F. High-Resolution Infrared Spectra of the C-H Asymmetric Stretch Vibration of Jet-Cooled Methoxy Radical (CH_3O). *J. Chem. Phys.* **2002**, *117*, 6538-6545.

(47) DeSain, J. D.; Thompson, R. I.; Sharma, S. D.; Curl, R. F. The Rotationally Resolved Infrared Spectrum of the ν_1 Stretch of the Allyl Radical. *J. Chem. Phys.* **1998**, *109*, 7803-7809.

(48) Utkin, Y. G.; Han, J. X.; Sun, F.; Chen, H. B.; Scott, G.; Curl, R. F. High-Resolution Jet-Cooled and Room Temperature Infrared Spectra of the ν_3 CH Stretch of Vinoxy Radical. *J. Chem. Phys.* **2003**, *118*, 10470-10476.

(49) Choi, M. Y.; Douberly, G. E.; Falconer, T. M.; Lewis, W. K.; Lindsay, C. M.; Merritt, J. M.; Stiles, P. L.; Miller, R. E. Infrared Spectroscopy of Helium Nanodroplets: Novel Methods for Physics and Chemistry. *Int. Rev. Phys. Chem.* **2006**, *25*, 15-75.

(50) Nandi, S.; Arnold, P. A.; Carpenter, B. K.; Nimlos, M. R.; Dayton, D. C.; Ellison, G. B. Polarized Infrared Absorption Spectra of Matrix-Isolated Allyl Radicals. *J. Phys. Chem. A.* **2001**, *105*, 7514-7524.

(51) Leavitt, C. M.; Moradi, C. P.; Acrey, B. W.; Douberly, G. E. Infrared Laser Spectroscopy of the Helium-Solvated Allyl and Allyl Peroxy Radicals. *J. Chem. Phys.* **2013**, *139*, 234301.

(52) Lewerenz, M.; Schilling, B.; Toennies, J. P. Successive Capture and Coagulation of Atoms and Molecules to Small Clusters in Large Liquid Helium Clusters. *J. Chem. Phys.* **1995**, *102*, 8191-8207.

(53) McIlroy, A.; McRae, G. *Report of the Basic Energy Sciences Workshop on Clean and Efficient Combustion of 21st Century Transportation Fuels*; Combustion Research Facility, Sandia National Laboratories: Livermore, CA, 2007.

(54) Leavitt, C. M.; Moore, K. B.; Raston, P. L.; Agarwal, J.; Moody, G. H.; Shirley, C. C.; Schaefer, H. F.; Douberly, G. E. Liquid Hot NAGMA Cooled to 0.4 K: Benchmark Thermochemistry of a Gas-Phase Peptide. *J. Phys. Chem. A.* **2014**, *118*, 9692-9700.

CHAPTER 2

EXPERIMENTAL METHODS

2.1 Formation of Helium Nanodroplets

Figure 2.1 shows a schematic of the helium nanodroplet isolation (HENDI) instrument used for the work presented herein. Droplets are formed in the "Source Chamber" by an expansion of ultrapure (99.9995% or 99.9999%) ^{4}He gas through a cryogenically cooled nozzle with a 5 μm aperture. With a nozzle temperature of 17 K and a backing pressure of 35 bar, each helium droplet contains approximately 4200 atoms, on average, based on scaling laws.[1, 2] Under these conditions, droplets are formed via condensation of the gaseous expansion and undergo rapid evaporative cooling to reach an equilibrium temperature of 0.4 K.[3]

Adjustments to the nozzle temperature or backing pressure changes the average size of the droplets; this can be useful for optimizing the doping of various precursors or radicals.[4] A plot highlighting the log-normal size distribution of helium droplets at various nozzle temperatures is shown in Figure 2.2. The mean number of droplets, $P_N(N)$, can be determined from the number of helium atoms per droplet (N), as well as the mean and standard deviation (μ and σ) of the distribution. These expressions are shown as Equations 2.1-2.3, respectively.

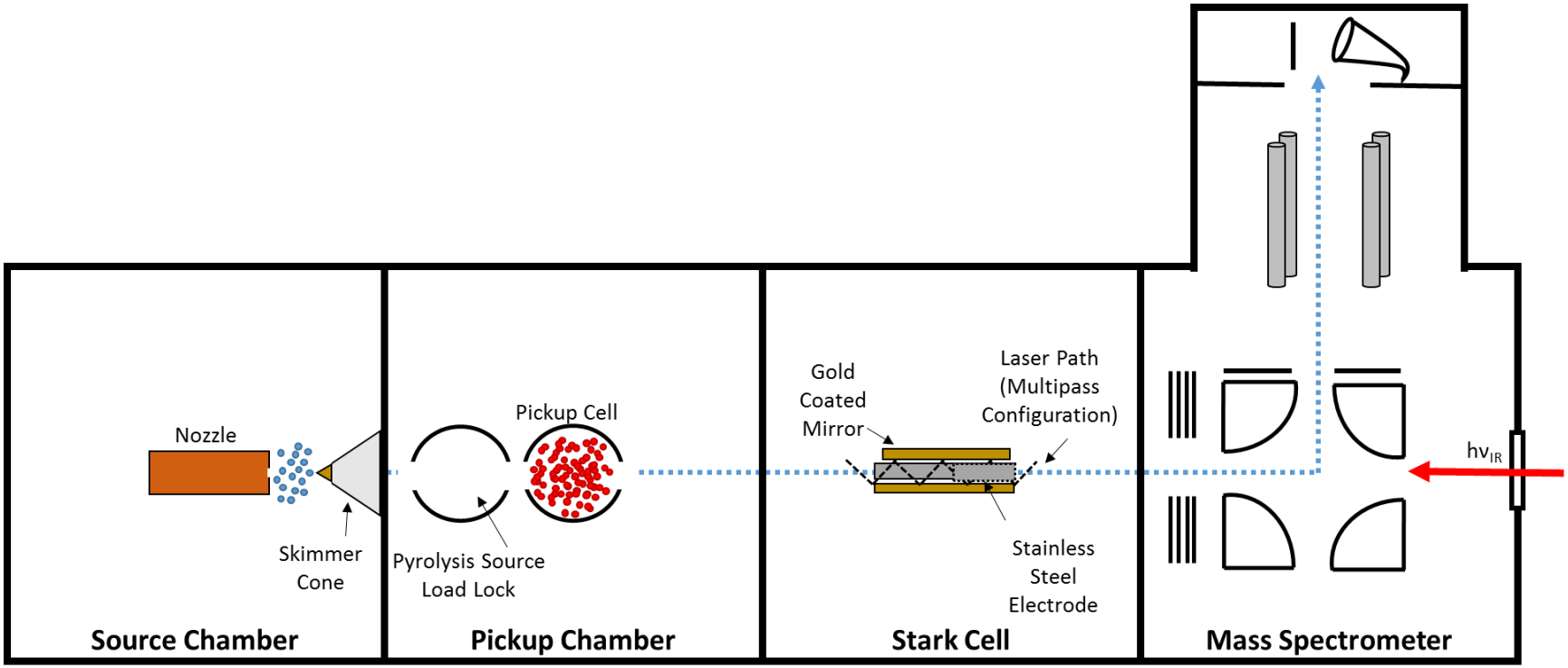

Figure 2.1: Schematic of the helium nanodroplet isolation (HENDI) instrument. Droplets are formed from a continuous expansion of helium gas through a cryogenically cooled nozzle with a 5 μm aperture. Newly formed droplets are skimmed into a beam and enter the pickup chamber where precursor or radical molecules are doped into the droplets. The Stark cell is used to find experimental dipole moments but is not used for the experiments described here. Finally, droplets and dopants are detected via the quadrupole mass spectrometer. Infrared light enters the instrument in a counterpropagating arrangement in relation to the droplet beam.

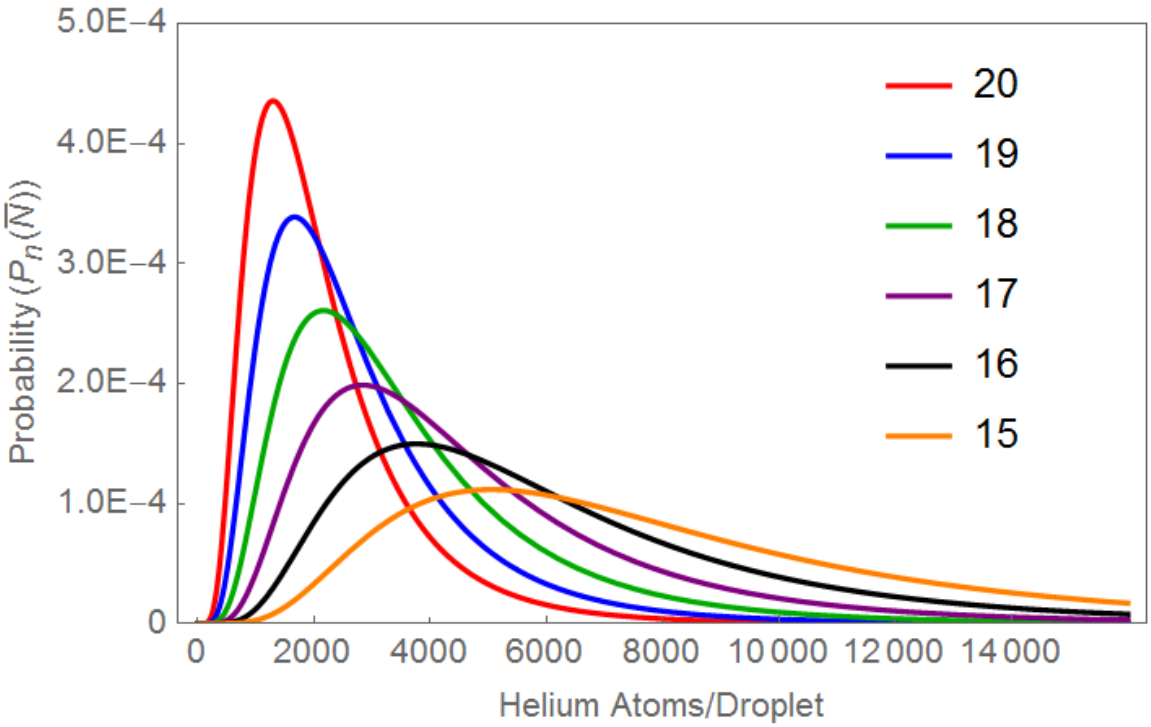

Figure 2.2: Log-normal distribution curves showing number of helium atoms per droplet at varying temperatures between 15 and 20 K. The scaling parameter, Γ, was calculated based on a nozzle diameter of 5 μm, and a backing pressure of 35 bar along with the corresponding temperature of each curve.

$$P_N(N) = \left(N\sigma\sqrt{2\pi}\right)^{-1} \exp\left[-\frac{(\ln N-\mu)^2}{2\sigma^2}\right] \quad \textbf{(Eq. 2.1)}$$

$$\mu = \ln(\bar{N}) - \frac{1}{2}\ln\left[\left(\frac{S}{\bar{N}}\right)^2 + 1\right] \quad \textbf{(Eq. 2.2)}$$

$$\sigma = \ln\left[\left(\frac{S}{\bar{N}}\right)^2 + 1\right]^{\frac{1}{2}} \quad \textbf{(Eq. 2.3)}$$

The variable S is the standard deviation of the size distribution. For the distribution curves shown in Figure 2.2, S was set to 0.65 $\bar{N}$. The average droplet size can be determined from the scaling law

$$\ln(\bar{N}) = 2.44 + 2.55\ln(\Gamma) \quad \textbf{(Eq. 2.4)}$$

where Γ is a dimensionless scaling parameter that relies on the nozzle diameter, temperature and pressure.[1] For Figure 2.2, the nozzle diameter was fixed to 5 μm, the temperature was varied between 15 and 20 K, and the backing pressure was held constant at 35 bar.

Droplets can also be formed by the expansion of liquid helium jets from a cooled nozzle usually held between 5 and 10 K.[5-7] This method produces droplets containing an average of 10^6 helium atoms per droplet but is extremely sensitive to the nozzle aperture diameter.[6] The liquid expansion fragments after exiting the nozzle to produce droplets which also undergo the evaporative cooling process mentioned above. Larger droplets (on the order of 1-3 μm in diameter) containing between 10^{10} and 10^{12} atoms are also formed from an expansion of pressurized helium when the nozzle temperature is below 4.2 K.[8] The liquid jet stays intact for longer periods of time after exiting the nozzle before breaking up into large, mostly uniform droplets.[9]

^{4}He nanodroplets are considered "superfluid" at temperatures below 2.2 K. Despite the ultra-cold environment, molecules that are doped inside of the droplet rotate freely and consequently give rotationally resolved spectra in many cases.[3, 4, 10] Although expansion of ^{3}He results in an overall colder droplet environment (0.15 K), the onset of superfluidity does not occur until T = 3 x 10^{-3} K.[3] Spectra of molecules within ^{3}He droplets can still be recorded but will not possess sharp rotational or rovibrational lines, which is a hallmark of the superfluid environment of ^{4}He droplets. Even within ^{4}He droplets, the doped molecules still experience slight coupling to the helium bath which contributes to the molecule's effective moment of inertia and results in a decrease of the B rotational constant as compared with gas phase values.[4] Based on an Andronikashvili-like experiment by Grebenev, Toennies, and Vilesov, a droplet must contain at least 60 ^{4}He atoms to have the characteristics of superfluidity.[10] Interestingly, if a droplet contains a mixture of both ^{3}He and ^{4}He atoms, the ^{4}He atoms form a superfluid core which is surrounded by the ^{3}He atoms.[3, 10, 11]

2.2 Doping Process

Once droplets are formed in the "Source Chamber", they are skimmed into a beam and enter the "Pickup Chamber". From here, molecules of interest are doped into the droplet by one of two ways: from the "pickup cell" or directly from an effusive pyrolysis source (*vide infra*). The pickup cell consists of a differentially pumped stainless steel tube that contains the molecule of interest at pressures around 10^{-6} torr. The droplet beam enters and exits the cell through two holes drilled on either side of the tube.

If a pyrolysis source is used, the density of the dopants is approximately an order of magnitude lower than when the pickup cell is employed. Two types of pyrolysis sources are primarily used: a quartz/tantalum source and a silicon carbide (SiC) source. An example of a quartz/tantalum pyrolysis source is shown in Figure 2.3 and the electrical circuit diagram is shown as the top image in Figure 2.4. Water cooled copper electrodes are used to transfer current to the tantalum wire wrapped around the quartz tube. A 0-130 V metered variable output AC converter (variac) is used to supply the voltage for the pyrolysis source. A step-down transformer is connected to the source in series and is used to decrease the initial voltage by a factor of 10 which corresponds to an increase in the initial current by a factor of 10; a power meter reads the initial, non-transformed current during experiments. Gas phase precursor molecules enter the source from a sample vial metered by a needle valve and travel through 1/8" Teflon tubing which is inserted into the end of a 6" section of quartz tube. Molecules thermally decompose after coming into contact with the hot walls of the quartz tube producing radicals and other small molecules as by-products. A variety of molecules can be made in this manner. For example, the cyclobutyl radical is formed from the pyrolysis of cyclobutylmethyl nitrite through this source (Chapter 3). With an operating voltage of approximately 1.5 V and final currents between 20 and 30 A, this corresponds to powers ranging from 30-45 W. The resistance of the tantalum under operating conditions is negligible.

The second pyrolysis source involves using a resistively heated SiC tube coupled to a quartz tube which extends the length of the source (Figure 2.5). The circuit diagram for this source is shown as the bottom image of Figure 2.4. This design is far more robust

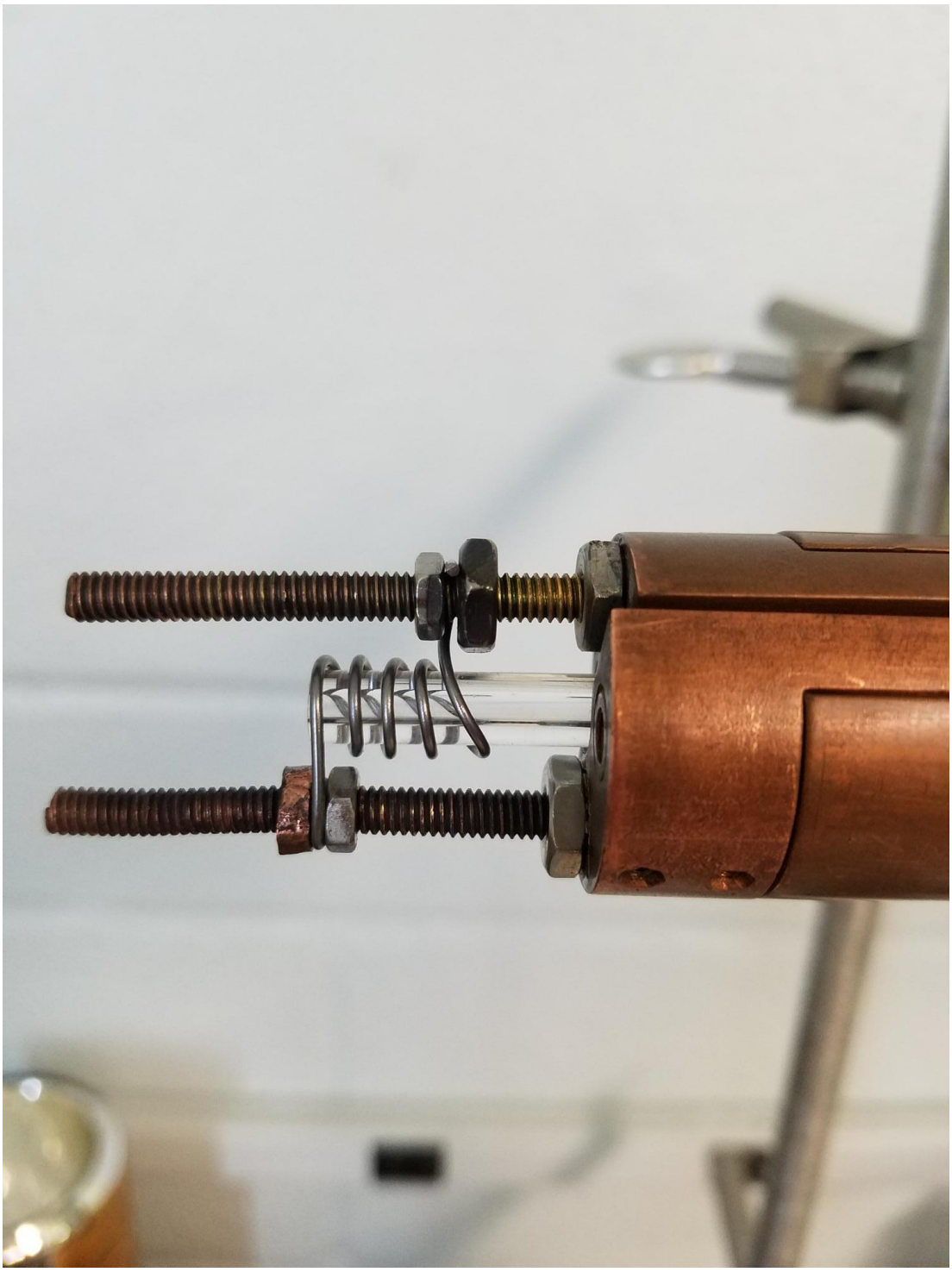

Figure 2.3: Image of the quartz/tantalum pyrolysis source used in the experiments outlined in Chapter 3. The droplet beam passes between the two copper posts as close to the end of the quartz tube as possible and perpendicular to the image.

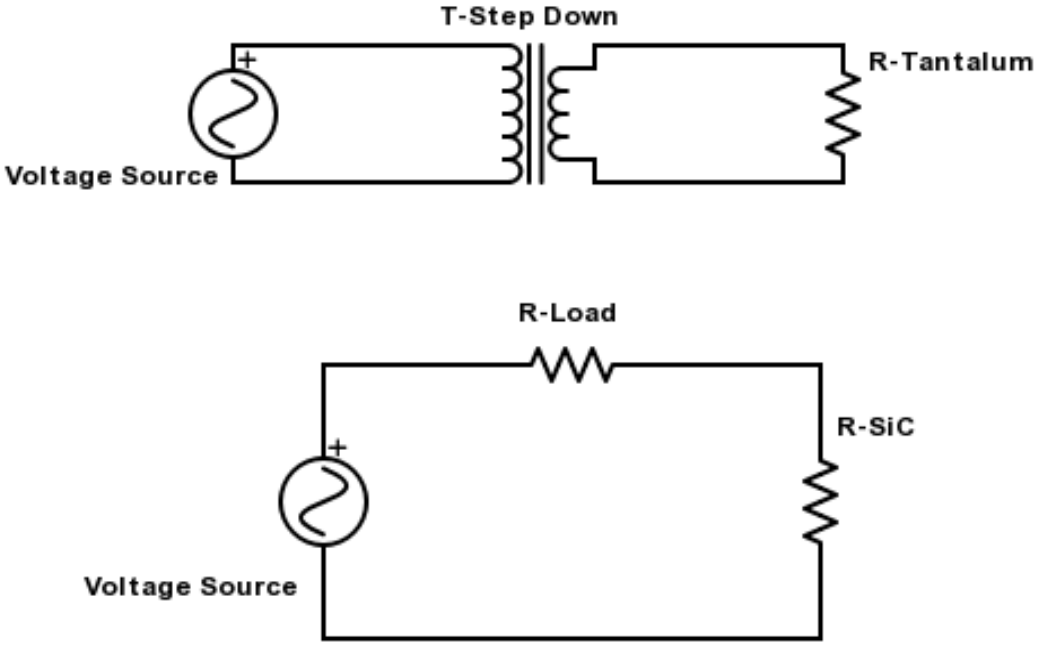

Figure 2.4: Circuit diagram for quartz/tantalum source (top) and silicon carbide source (bottom).

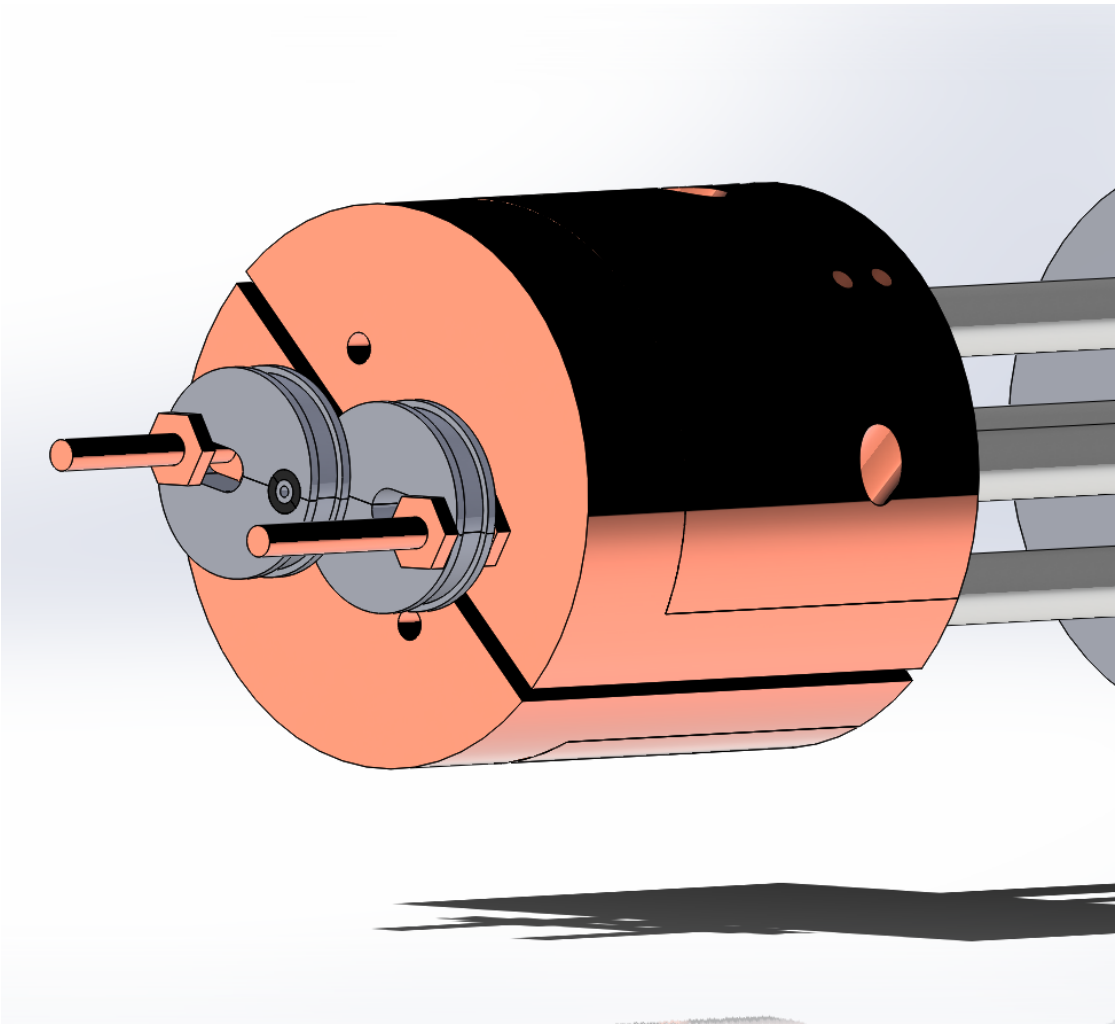

Figure 2.5: Depiction of the silicon carbide (SiC) source used in these experiments. A SiC tube (light grey) is coupled to a quartz tube and resistively heated by graphite electrodes (dark grey). The droplet beam passes perpendicular to the end of the SiC tube between the two copper posts to pick up radicals being studied.

and can reach temperatures exceeding 1500 K making it ideal for decomposition of more stable molecules. Chlorine atoms were formed utilizing this source with Cl_2 as the precursor.[12, 13] Similar to the quartz tantalum source, water cooled copper electrodes and additional graphite electrodes provide current to a 1 mm inner diameter SiC tube coupled to the quartz tube. Voltage is provided to the source by a 0-140 V variac. A current limiting resistor (R-Load = 5.5 Ω) is connected in series with the variac; the resistance of the SiC tube is small in comparison with the load resistor which allows the source to operate at a nearly constant current. Molecules in the sample vial are introduced into the source through a needle valve; those that come into contact with the walls of the heated SiC tube are broken apart to form radicals and other small molecules. The SiC source was used for the production of fulvenallenyl radical from the fulvenallene molecule as outlined in Chapter 4. During this particular experiment, a voltage of approximately 30 V was supplied by the variac to achieve the required current of 4.5 A to form fulvenallenyl from fulvenallene. Under these conditions, the source was operating with a total power of approximately 140 W.

Regardless of which method is employed, the pickup process obeys Poisson statistics (defined in Equation 2.5) since the doping of one molecule into the droplet does not affect the doping of subsequent molecules.[1, 3, 14]

$$P(n) = \frac{(\alpha L)^n e^{-\alpha L}}{n!} \qquad \textbf{(Eq. 2.5)}$$

The path length of the pickup cell (L) and α, given as the product of the number density of the gas within the chamber (ρ) and the geometric cross section of the droplet (σ), determine the probability (P) of picking up *n* molecules. The probability of each droplet

picking up one or more molecules as it passes through the pickup chamber is shown in Figure 2.6 as a function of pressure.

2.3 Infrared Laser System and Action Spectroscopy

Infrared light is produced by a continuous-wave optical parametric oscillator (cw-OPO) system (Lockheed-Martin Aculight ARGOS 2400-SF-15). A continuous-wave Yb-doped fiber laser (Koheras AdjustiK) is used to pump the OPO with 15 mW of 1064 nm light. This laser is both temperature and piezo tunable for up to a combined total of approximately 6 cm^{-1}. The light is then amplified to a maximum of 15 W by a fiber amplifier (IPG Photonics). This light then enters the bow-tie cavity of the OPO cavity and subsequently through a magnesium oxide doped periodicially poled lithium niobate (MgO:PPLN) crystal, which converts pump photons to signal and idler photons through optical parametric generation. The crystal is configured with a "fan out" design, which allows it to be translated within the cavity to give course 1 cm^{-1} tuning. Since the cavity is resonant with the signal frequency, changing the pump frequency consequently tunes the idler frequency. In the experiments described here, both the "B" and "C" modules are used which gives a tuning range of 2600-4000 cm^{-1} for the idler beams. Although it is not used in the current set-up, module "A" can extend this range up to 4300 cm^{-1}. The signal and pump beams are dumped and only the idler is used to collect the infrared spectra.

Portions of the idler beam are used for diagnostic purposes and enter a Bristol 621 wavemeter, a Fabry-Perot scanning etalon, and a power meter. Approximately 10-20 mW of the original beam enter each diagnostic after being reflected off CaF_2 windows. During

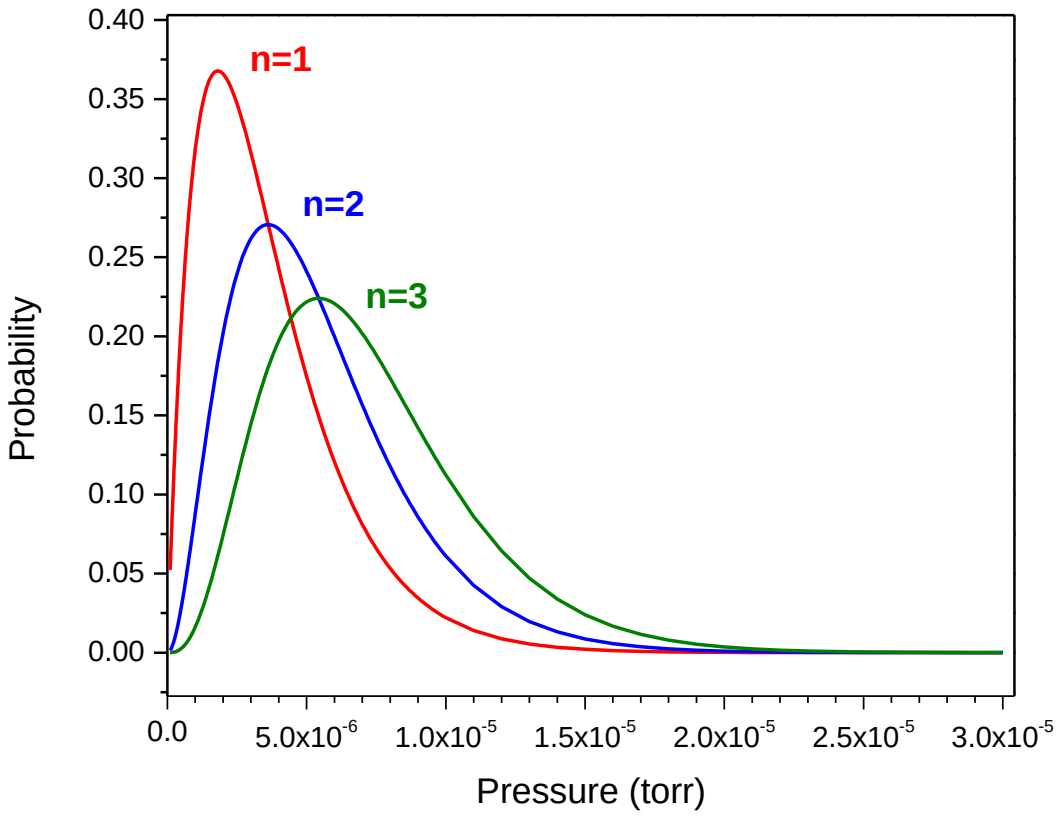

Figure 2.6: Probability curves for droplets picking up *n* molecules under various pickup cell pressures based on Poisson statistics (Equation 2.1). In the simulations, the droplets have a mean diameter of 7.05 nm and travel a path length of approximately 40 mm in the pickup region.

an experiment, the frequency and power are monitored and recorded by a custom LabVIEW program. The etalon is coupled to an oscilloscope to ensure that the etalon cavity only has one mode above the oscillation threshold at a time. From this point, the beam is chopped at 80 Hz before a small portion of the beam enters the power meter. The remaining portion of the beam enters the instrument either collinearly or through the Stark cell in a multipass arrangement. In the collinear arrangement, the counterpropagating infrared light is directed at the droplet beam to interact with the molecules solvated within the droplets. This arrangement was used to collect the infrared spectra shown in Chapters 3 and 4.

Although the Stark cell is not utilized for the experiments described in Chapters 3 and 4, a short description will be given here. The Stark cell consists of two parallel stainless steel electrodes, which are situated above and below the droplet beam and separated by approximately 3 mm, and two parallel gold coated mirrors arranged on either side of the droplet beam. Several kV of high voltage are applied to one electrode while the other is held at ground resulting in DC fields of up to 50 kV/cm. The two parallel gold mirrors are used to reflect the light such that the droplet beam interacts with the laser beam between 20 and 30 times while in this arrangement. A Fresnel rhomb is used to either align or misalign the laser polarization with the Stark field in a parallel or perpendicular manner. This causes shifts and splittings in the infrared spectrum which allows the vibrationally averaged permanent electric dipole of molecules within helium droplets to be determined.

Unlike typical infrared spectroscopy, the HENDI technique relies on an indirect method to record the spectrum of the molecule of interest. This is accomplished by an

"action" spectroscopy method, which uses an Extrel quadrupole mass spectrometer (QMS) for detection. Droplets undergo electron impact ionization and form He^+ ions, or He_n^+ clusters, separated by 4 u. Ionization of the droplet creates an electron "hole" which travels throughout the bath until either the droplet blows apart to form $(He)_n^+$ ions or it interacts with a molecular dopant. Since the ionization potential of He is 2-3 times higher than most dopants, this latter interaction will result in an ionized dopant and neutral He atoms. An example of a typical mass spectrum showing this phenomenon is shown in Figure 2.7. Typically, precursor dopants and radical dopants will become ionized and fragment into different mass channels making it easy to separate and identify them within a particular experiment. In Figure 2.7, an increase in mass channel 55 m/z is noticed when the precursor is doped into the droplets while mass channel 39 m/z increases as a result of pyrolysis of the precursor and formation of the new radical species, cyclobutyl radical. By setting the mass spectrometer to a narrow mass range, the QMS can be used as a mass filter and only allow certain species to be detected. This helps discriminate against precursor contributions when measuring the spectrum of a particular radical as long as the mass fragments are sufficiently different. When the mass spectrum of the precursor and radical have similar fragments, and therefore similar mass channels for collecting the infrared spectrum, differentiation can become more difficult but not impossible. This was the case for measuring the infrared spectrum of fulvenallene and fulvenallenyl, which is described in Chapter 4.

Detection of the droplets and dopants is based on the change in size of the droplets from initial production through ionization in the mass spectrometer. If a droplet is not doped with a molecule, it will stay approximately the same size as it travels

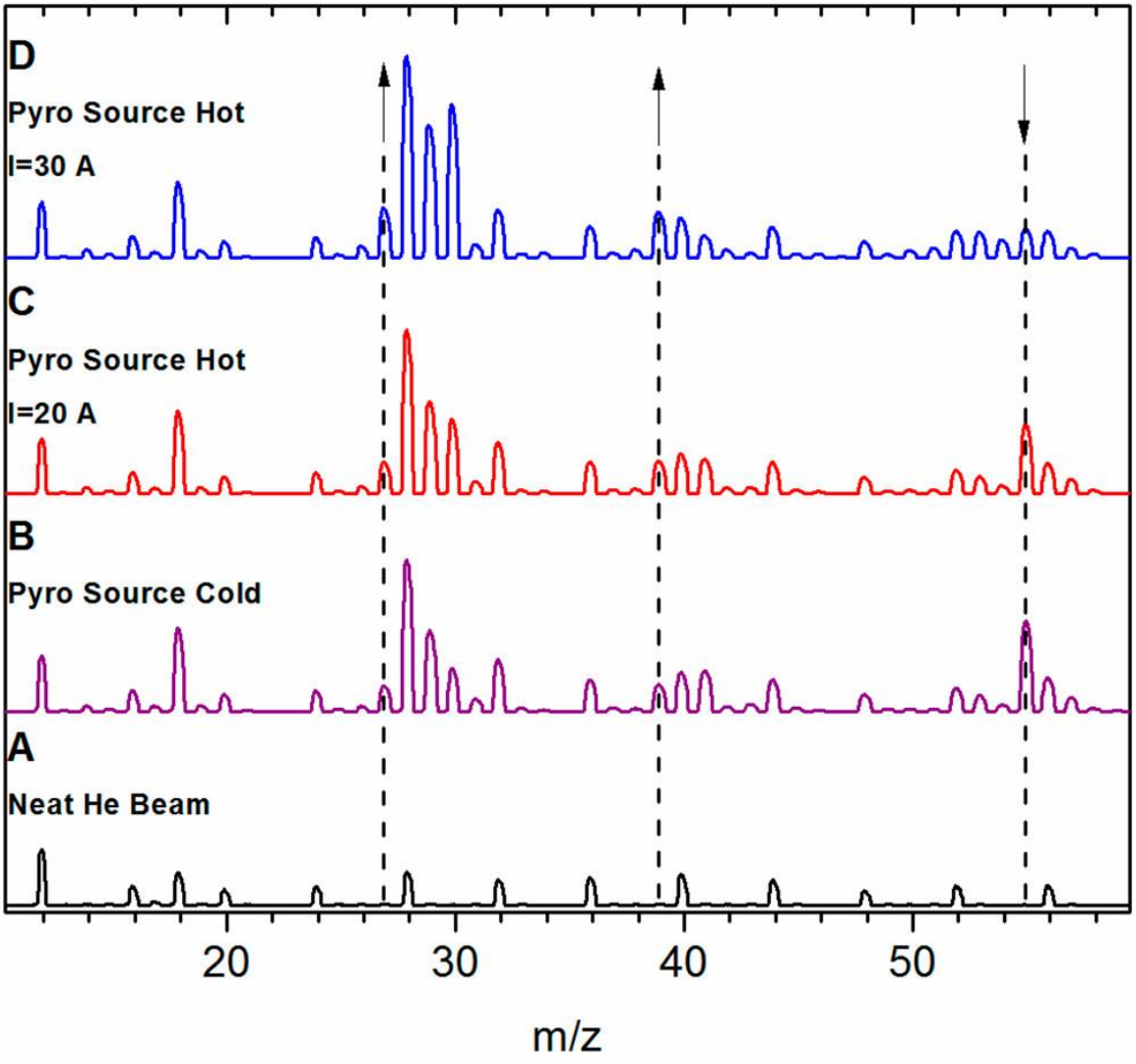

Figure 2.7: Evolution of the mass spectrum during the cyclobutyl radical experiment. The neat droplet beam is shown in trace (A). Traces (B)-(D) are mass spectra of the droplet beam with the precursor, cyclobutylmethyl nitrite, under various pyrolysis conditions. The increase of mass 55 u indicates that the droplets have been doped with the precursor molecule, cyclobutylmethyl nitrite. Upon pyrolysis, cyclobutyl radical is formed as indicated by the increase in m/z = 39 u and decrease of m/z = 55 u. At higher pyrolysis temperatures, an increase in mass channel 27 u is observed. See Chapter 3 for a more thorough discussion of the experiment.

through the instrument and into the mass spectrometer region. However, if a droplet is doped, excess energy from the dopant will be transferred the helium bath which will cause He atoms to evaporate from the surface of the droplet. In addition to this, if the dopant is rovibrationally excited by the infrared light from the OPO, more He atoms are evaporated from the droplet as the energy is quenched. Each He atom that is evaporated corresponds to a loss of ~5 cm^{-1} of energy.[15] The average geometric cross section of the doped droplets following vibrational excitation is approximately 10-20% smaller; this corresponds to a decrease in the QMS ionization signal as compared with unexcited droplets because smaller droplets cannot be ionized as efficiently. This is known as a laser-induced depletion and is what is used as the spectroscopy signal during an experiment. Each spectrum is a difference spectrum of the ion signal when the laser is "on" vs. "off" (blocked or unblocked by the 80 Hz chopper) as a function of laser frequency. The QMS current is converted into a voltage through a Stanford Research SR570 current preamplifier which is then processed by a lock-in amplifier and recorded with a custom LabVIEW program.

References

(1) Lewerenz, M.; Schilling, B.; Toennies, J. P. A New Scattering Deflection Method For Determining and Selecting the Sizes of Large Liquid Clusters of He-4. *Chem. Phys. Lett.* **1993**, *206*, 381-387.

(2) Knuth, E.; Schilling, B.; Toennies, J. P. Proceedings of the 19th International Symposium on Rarefield Gas Dynamics, 1995.

(3) Toennies, J. P.; Vilesov, A. F. Superfluid Helium Droplets: A Uniquely Cold Nanomatrix for Molecules and Molecular Complexes. *Angew. Chem.-Int. Edit.* **2004**, *43*, 2622-2648.

(4) Choi, M. Y.; Douberly, G. E.; Falconer, T. M.; Lewis, W. K.; Lindsay, C. M.; Merritt, J. M.; Stiles, P. L.; Miller, R. E. Infrared Spectroscopy of Helium Nanodroplets: Novel Methods for Physics and Chemistry. *Int. Rev. Phys. Chem.* **2006**, *25*, 15-75.

(5) Buchenau, H.; Knuth, E. L.; Northby, J.; Toennies, J. P.; Winkler, C. Mass Spectra and Time-of-Flight Distributions of Helium Cluster Beams. *J. Chem. Phys.* **1990**, *92*, 6875-6889.

(6) Knuth, E. L.; Henne, U. Average Size and Size Distribution of Large Droplets Produced in a Free-Jet Expansion of a Liquid. *J. Chem. Phys.* **1999**, *110*, 2664-2668.

(7) Jiang, T.; Northby, J. A. Fragmentation Clusters Formed in Supercritical Expansions of ^{4}He. *Phys. Rev. Lett.* **1992**, *68*, 2620-2623.

(8) Grisenti, R. E.; Toennies, J. P. Cryogenic Microjet Source for Orthotropic Beams of Ultralarge Superfluid Helium Droplets. *Phys. Rev. Lett.* **2003**, *90*, 234501.

(9) Toennies, J. P. Helium Clusters and Droplets: Microscopic Superfluidity and Other Quantum Effects. *Mol. Phys.* **2013**, *111*, 1879-1891.

(10) Grebenev, S.; Toennies, J. P.; Vilesov, A. F. Superfluidity Within a Small Helium-4 Cluster: The Microscopic Andronikashvili Experiment. *Science.* **1998**, *279*, 2083-2086.

(11) Dalfovo, F. Atomic and Molecular Impurities in ^{4}He Clusters. *Z. Phys. D.* **1994**, *29*, 61-66.

(12) Kohn, D. W.; Clauberg, H.; Chen, P. Flash Pyrolysis Nozzle for Generation of Radicals in a Supersonic Jet Expansion. *Rev. Sci. Instrum.* **1992**, *63*, 4003-4005.

(13) Moradi, C. P.; Douberly, G. E. Infrared Laser Spectroscopy of the L-Shaped Cl–HCl Complex Formed in Superfluid ^{4}He Nanodroplets. *J. Phys. Chem. A.* **2015**, *119*, 12028-12035.

(14) Toennies, J. P.; Vilesov, A. F. Spectroscopy of Atoms and Molecules in Liquid Helium. *Annu. Rev. Phys. Chem.* **1998**, *49*, 1-41.

(15) Brink, D. M.; Stringari, S. Density of States and Evaporation Rate of Helium Clusters. *Z. Phys. D: At., Mol. Clusters.* **1990**, *15*, 257-263.

CHAPTER 3

HELIUM NANODROPLET ISOLATION OF THE CYCLOBUTYL, 1-METHYLALLYL AND ALLYLCARBINYL RADICALS: INFRARED SPECTROSCOPY AND AB INITIO COMPUTATIONS

Gas phase cyclobutyl radical ($\cdot C_4H_7$) is produced *via* pyrolysis of cyclobutylmethyl nitrite ($C_4H_7(CH_2)ONO$). Other $\cdot C_4H_7$ radicals, such as 1-methylallyl and allylcarbinyl, are similarly produced from nitrite precursors. Nascent radicals are promptly solvated in liquid He droplets, allowing for the acquisition of infrared spectra in the CH stretching region. For the cyclobutyl and 1-methylallyl radicals, anharmonic frequencies are predicted by VPT2+K simulations based upon a hybrid CCSD(T) force field with quadratic (cubic and quartic) force constants computed using the ANO1 (ANO0) basis set. A density functional theoretical method is used to compute the force field for the allylcarbinyl radical. For all $\cdot C_4H_7$ radicals, resonance polyads in the 2800-3000 cm^{-1} region appear as a result of anharmonic coupling between the CH stretching fundamentals and CH_2 bend overtones and combinations. Upon pyrolysis of the cyclobutylmethyl nitrite precursor to produce the cyclobutyl radical, an approximately two-fold increase in the source temperature leads to the appearance of spectral signatures that can be assigned to 1-methylallyl and 1,3-butadiene. On the basis of a previously reported $\cdot C_4H_7$ potential energy surface, this result is interpreted as evidence for the unimolecular decomposition of the cyclobutyl radical *via* ring opening,

prior to it being captured by helium droplets. On the $\cdot C_4H_7$ potential surface, 1,3-butadiene is formed from cyclobutyl ring opening and H atom loss, and the 1-methylallyl radical is the most energetically stable intermediate along the decomposition pathway. The allylcarbinyl radical is a higher energy $\cdot C_4H_7$ intermediate along the ring opening path, and the spectral signatures of this radical are not observed under the same conditions that produce 1-methylallyl and 1,3-butadiene from the unimolecular decomposition of cyclobutyl.

3.1 Introduction

Hydrocarbon radicals are prevalent in combustion environments, namely those that originate from organic flames[1, 2] or pyrolysis of organic solvents.[3, 4] The reaction between CH and propene (C_3H_6) occurs in Titan's atmosphere and other methane containing gas clouds, in which CH is produced from methane photolysis.[5] The CH + C_3H_6 reaction produces 1,3-butadiene, which is a precursor to the formation of benzene and polycyclic aromatic hydrocarbons. Branching to other products has also been predicted *ab initio*, including pathways to 1,2-butadiene + H, ethylene + vinyl, and allene + methyl. All of these pathways involve C_4H_7 radical intermediates.[5] The spectroscopy of these C_4H_7 radicals is almost entirely missing. In this report, cyclobutyl, 1-methylallyl, and allylcarbinyl radicals are captured by helium droplets and probed with infrared (IR) laser spectroscopy.[6, 7]

The cyclobutyl radical and cation have been studied both experimentally,[8-15] and theoretically,[5, 16-18] although the IR spectra of these species have never been recorded.

The dissociation dynamics of cyclobutyl bromide were recently studied *via* velocity map imaging.[13] Liu et al. found that cyclobutyl radicals, formed from the 234 nm photodissociation of cyclobutyl bromide, are produced with 10 to 35 kcal/mol of internal energy. However, the radicals do not undergo isomerization; rather, the internal energy is largely funneled into rotational motion.

Allylcarbinyl radical, also known as 3-buten-1-yl, has also been studied experimentally[8, 18-23] and theoretically,[5, 24, 25] mostly relating to its rearrangement from the cyclopropylmethylcarbinyl radical. An IR spectrum for this radical has not been measured. However, Bahou et al.[24] computed harmonic and anharmonic frequencies at the B3PW91/6-311++g(2d,2p) level of theory for both the *trans* and *cis* conformers. At this level of theory, the *trans* conformer is lower in energy than *cis* by about 0.5 kcal/mol.[24]

The 1-methylallyl radical, hereafter shortened to methylallyl, has also been studied experimentally[8, 15, 18, 24, 26-32] and theoretically.[5, 16, 24, 25, 27, 33] Most notably, its IR spectrum was recorded following its isolation in a solid *para*-H_2 matrix. The radical was produced following UV irradiation of a co-deposited mixture of Cl_2 and 1,3-butadiene.[24] This experiment confirmed theoretical predictions that H atoms react with 1,3-butadiene to produce 1-methylallyl.[25] Harmonic and anharmonic frequencies of this radical were also computed for both the *trans* and *cis* conformers, where *trans* was found to be about 0.8 kcal/mol lower in energy than *cis*. These authors used the computed frequencies to assign the solid *para*-H_2 spectrum to the *trans* conformer.

We report here the IR spectra of several C_4H_7 radicals, including the cyclobutyl, 1-methylallyl, and allylcarbinyl radicals, all of which have been trapped and cooled to

less than 0.5 K using helium nanodroplets. These radicals are all produced *via* the pyrolytic decomposition of their respective nitrite precursors. We use the spectroscopy of these radical species, along with the spectrum of 1,3-butadiene (also reported here), to rationalize the observation of new features that grow into the cyclobutyl spectrum under high-temperature pyrolysis source conditions, which apparently promote the unimolecular decomposition of the gas-phase cyclobutyl radical.

3.2 Experimental Section

3.2.1 Droplet Production and Radical Doping

Ultrapure (99.9995%) helium is continuously expanded through a 5 μm pinhole nozzle to form He nanodroplets. The nozzle is held at ~17 K with a backing pressure of 35 bar. Under these conditions, the nanodroplets are estimated to contain 4000-6000 He atoms on average.[34] Newly formed droplets are skimmed into a beam and passed into a second vacuum chamber where they pick up nascent cyclobutyl radicals, formed from the pyrolysis of cyclobutylmethyl nitrite.[8] The methylallyl and allylcarbinyl radicals are similarly produced from nitrite precursors. Following solvation, the radicals are rapidly cooled to ~0.4 K.[6, 7] The pyrolysis source consists of a quartz tube (0.6 cm outer diameter), the end of which is wrapped in tantalum wire. This region of the source is positioned perpendicular and adjacent to the droplet beam. A relatively low source temperature (500-700˚C) is sufficient to cleave the precursor molecule to form the C_4H_7 radical.[8] Other by-products from this pyrolytic decomposition include formaldehyde

(CH_2O) and nitric oxide (NO). Dopant pressures are optimized such that less than one molecule is doped into a droplet on average. Conditions are optimized to render the sequential capture of two pyrolysate molecules improbable. Specifically, conditions are optimized such that less than a few percent of the interrogated droplets pick up two C_4H_7 radicals, or one C_4H_7 radical and either NO or CH_2O. Under these source conditions, we have also found repeatedly in past studies that the number density of radicals in the quartz tube is sufficiently low to suppress bimolecular reactions that lead to larger species.[35-38] The spectra reported here are therefore assumed to be free of spectral features associated with complexes or reaction products formed either in the pyrolysis source or within the droplets. This assumption is based on both the well-known Poisson capture statistics associated with droplet doping and our many previous studies of helium-solvated hydrocarbon radicals formed *via* an identical pyrolysis approach.[35-38]

3.2.2 Laser Spectroscopy

The doped droplet beam interacts with the counterpropagating mid-IR beam of an optical parametric oscillator (OPO), which vibrationally excites molecules within the droplet. The tuning and calibration of the laser system is given elsewhere.[39] Upon resonant excitation, the vibrational energy of the molecule is quenched by the evaporation of He atoms. For every ~5 cm^{-1} of vibrational energy, one He atom is lost; therefore, for a 3000 atom droplet, excitation of a dopant at 3000 cm^{-1} leads to an approximately 14% geometric cross section reduction. This size reduction is accompanied by a cross section reduction for electron impact ionization, which is

detected with a quadrupole mass spectrometer. The IR beam is chopped at 80 Hz, and the ion current measured in a specific mass channel is processed with a lock-in amplifier. The resulting IR spectrum is a difference spectrum of the ion signal with and without the laser present, normalized to the power of the laser beam.

3.2.3 Mass Spectrometry and Species-selective Spectroscopy

The mechanism by which doped helium droplets are ionized by electron bombardment has been discussed in detail elsewhere.[7, 40] Electron impact ionization of pure droplets leads to a distribution of helium cluster ions *via* the mechanism shown in equation (3.1).

$$(He)_n + e^- \rightarrow He^+(He)_{n-1} + 2e^- \rightarrow (He)_2^+(He)_{n-2} + 2e^- \rightarrow (He)_m^+ + (n-m)(He) + 2e^- \quad \textbf{(Eq. 3.1)}$$

Dopants are ionized *via* charge-transfer from He^+, because the IP difference between He and the molecular dopant is typically 10 to 15 eV.

$$(M)(He)_m + e^- \rightarrow (M)He^+(He)_{m-1} + 2e^- \rightarrow (M)^{+*} + m(He) + 2e^- \quad \textbf{(Eq. 3.2)}$$

Despite the presence of the helium bath, this large IP mismatch leads to the fragmentation of the ionized dopant, $(M)^{+*}$ and its ejection into the gas phase, where it is detected with quadrupole mass spectrometry. The observed fragmentation pathways are typically

analogous to those observed in gas-phase electron impact ionization, when comparisons are available.

Figures 3.1A, 3.1B, 3.1C and 3.1D show the mass spectra of the neat He beam (A) and the precursor and radical doped droplet beams (B-D). In trace A, peaks appearing every 4 u correspond to ionized $(He)_n^+$ clusters. Introduction of the precursor, cyclobutylmethyl nitrite, gives rise to an intense peak at 55 u, as well as peaks at 28, 29 and 30 u, indicative of a nitrite molecule (B).[35-38] Once the pyrolysis temperature is raised to a level that is sufficient to crack nitrite precursors,[8, 35-38] a reduction of 55 u is observed along with an increase in 39 u (C). Although the peak at 39 u is also present in the precursor mass spectrum, this increase only occurs at temperatures consistent with the decomposition of cyclobutylmethyl nitrite precursor. We therefore begin our search for the spectrum of the cyclobutyl radical by recording ion depletion in channel 39 u as the IR laser is tuned from 2800 to 3100 cm^{-1}. Indeed, as discussed extensively below, the IR spectrum of cyclobutyl appears cleanly in this mass channel.

The mass spectra of *either* cyclobutylmethyl nitrite doped helium droplets *or* cyclobutyl doped droplets can be obtained *via* a *difference depletion mass spectrometry* technique, the results from which are shown in Figures 3.2A, 3.2B, 3.2C, 3.2D and 3.2E. With the pyrolysis source at room temperature, the IR laser is tuned to 2990.0 cm^{-1}, *i.e.* a resonant frequency for cyclobutylmethyl nitrite, *vide infra*. The laser frequency is fixed and amplitude modulated at 80 Hz while the quadrupole mass spectrometer is slowly scanned across all mass channels. When processed with a lock-in amplifier, the resulting *difference* mass spectrum corresponds to the electron-impact ionization mass spectrum of *only* the subset of droplets that contain resonantly excited molecules. In Figure 3.2A,

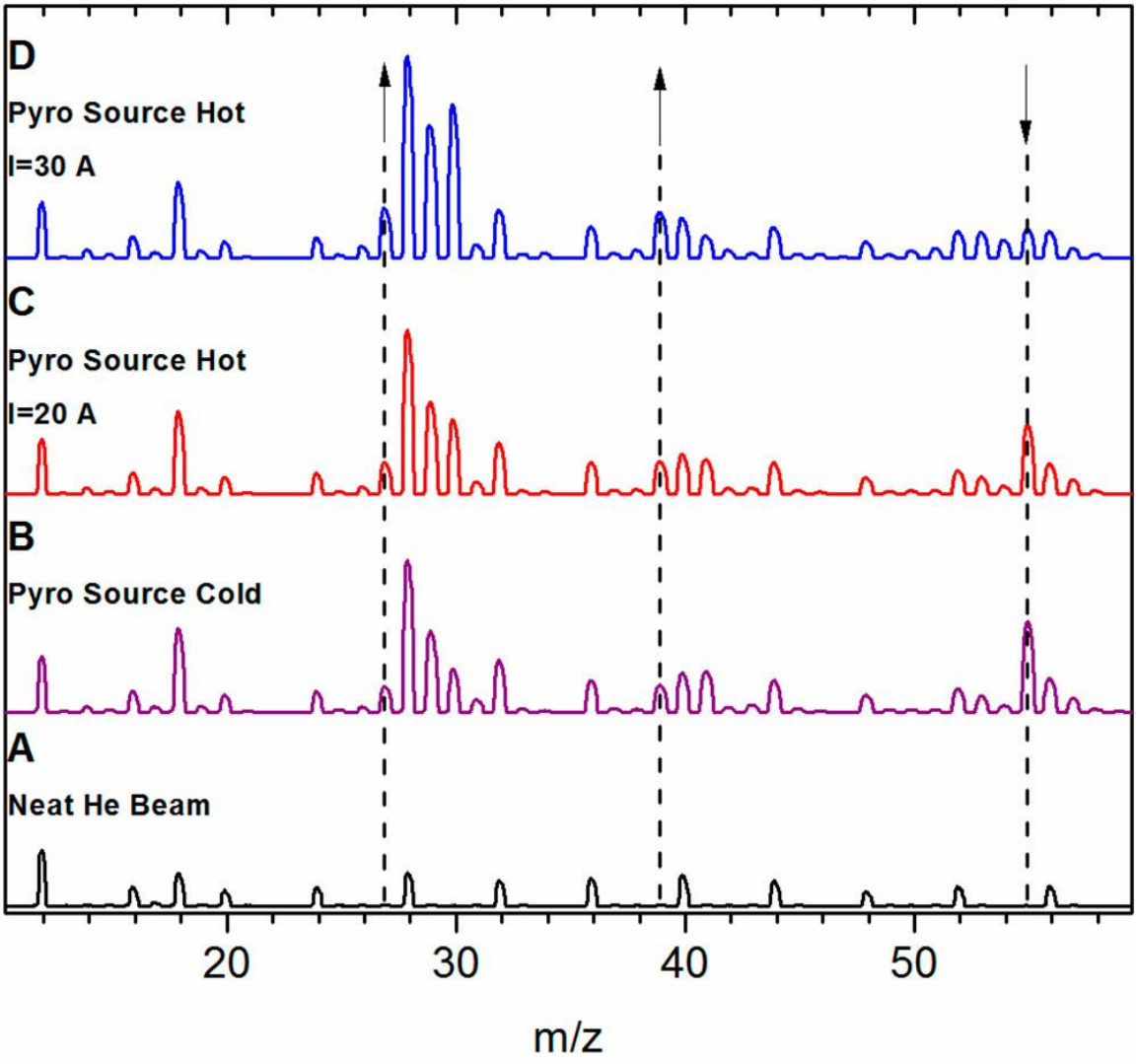

Figure 3.1: The mass spectrum of the neat droplet beam is shown in trace (A). Traces (B)-(D) are mass spectra of the droplet beam with the precursor, cyclobutylmethyl nitrite, under various pyrolysis conditions. The increase of mass 55 u indicates that the droplets have been doped with the precursor molecule, cyclobutylmethyl nitrite. Upon pyrolysis, cyclobutyl radical is formed as indicated by the increase in m/z = 39 u and decrease of m/z = 55 u. At higher pyrolysis temperatures, an increase in mass channel 27 u is observed.

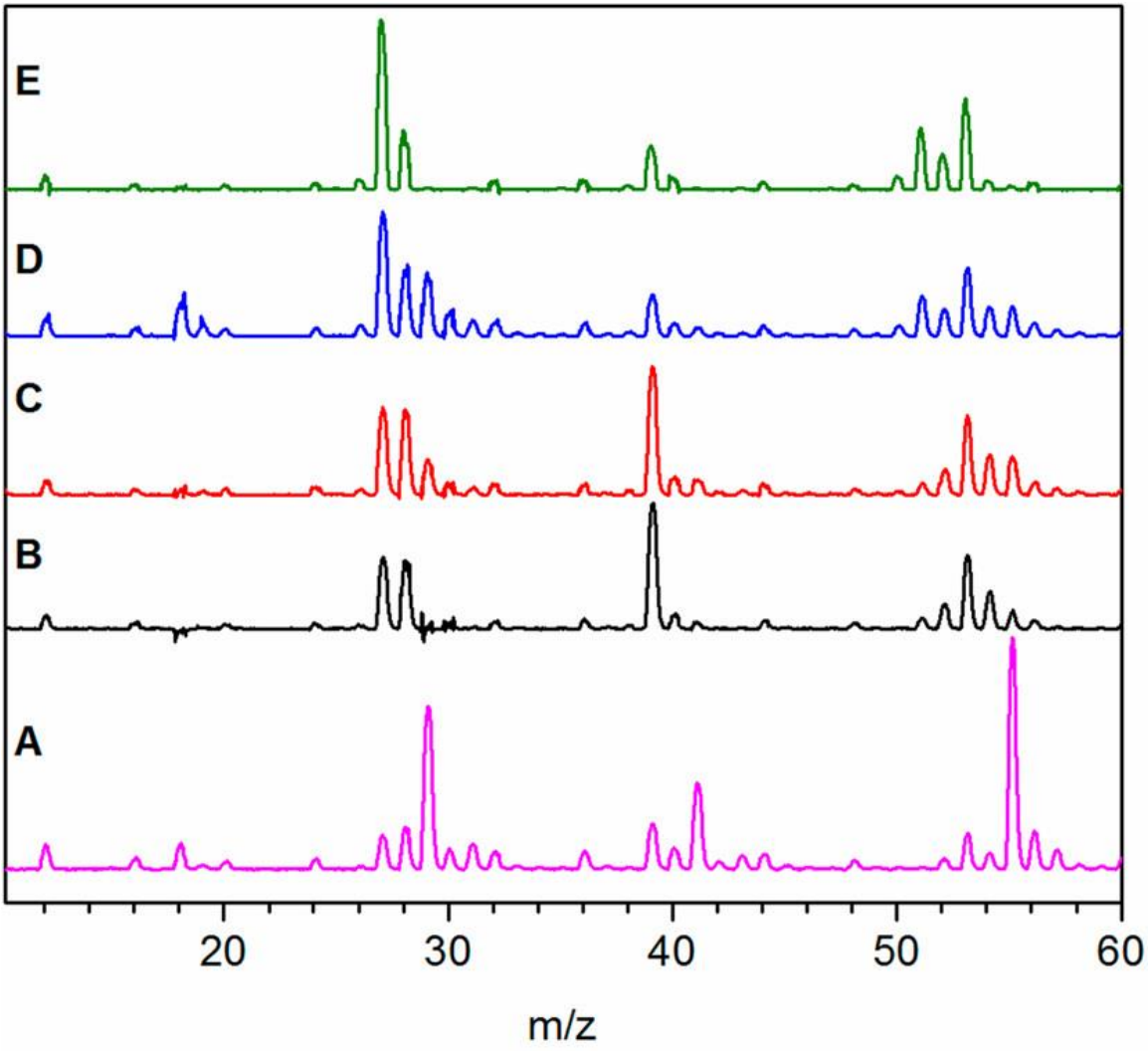

Figure 3.2: Difference depletions mass spectra under various pyrolysis conditions and various frequencies: (A) 0 A (2990.0 cm^{-1}) cyclobutylmethyl nitrite only; (B, C) 20 A (3069.7 and 2819.4 cm^{-1}, respectively) formation of cyclobutyl radical; (D) 30 A (3101.9 cm^{-1}) formation of 1,3-butadiene from cyclobutyl unimolecular decompositions; (E) 0 A (3101.9 cm^{-1}) neat 1,3-butadiene. (See section 3.4.2.4 for an explanation of traces D and E.)

mass channels 29 and 55 u are the most intense, indicating that these channels carry the largest laser-induced ion depletion signal at 2990 cm^{-1} when the pyrolysis source is kept at room temperature, *i.e.* indicating that these are the largest mass channels associated with cyclobutylmethyl nitrite doped helium droplets. With the pyrolysis source temperature raised to optimize for cyclobutyl production, difference mass spectra were measured with the laser fixed to either 3069.7 cm^{-1} (Figure 3.2B) or 2819.5 cm^{-1} (Figure 3.2C), *i.e.* the two sharpest transitions observed in the IR spectrum of the cyclobutyl radical, *vide infra*. Here we note the drastic signal reduction in channels 29 and 55 u, along with the enhanced signal in 39 u. Indeed, this confirms that the ionization of cyclobutyl doped helium droplets leads to the production of $C_3H_3^+$ ions. By recording the IR spectrum as a depletion in channel 39 u, we discriminate against residual precursor features and features due to other species populated in the droplet ensemble. This species-selective mass spectrometry was used throughout and provides a two-dimensional approach for assigning bands in the IR spectra described here.

3.3 Theoretical Methods

3.3.1 Cyclobutyl Radical

Two stationary points were characterized: a C_s electronic minimum and a C_{2v} first-order saddle point (Figures 3.3A and 3.3B). Geometries were optimized using the CCSD(T)[41-46] method combined with the ANO0 and ANO1 basis sets,[47] as implemented in CFOUR.[48] All computations utilized UHF reference wavefunctions. The frozen-core

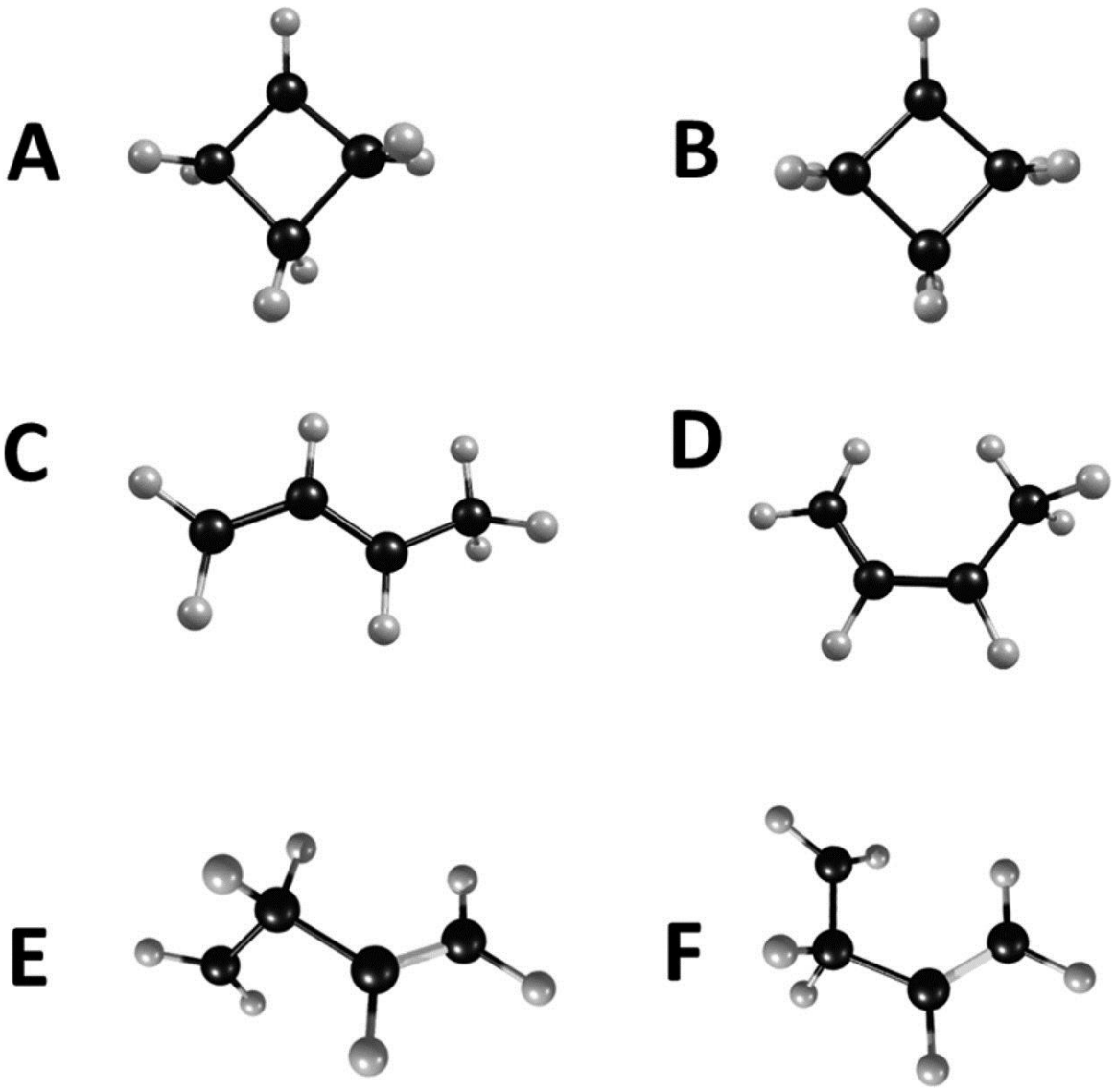

Figure 3.3: Computed structures for (A) C_s cyclobutyl, (B) C_{2v} cyclobutyl, (C) *trans*- and (D) *cis*-1-methylallyl, and (E) *gauche*- and (F) *cis*-allylcarbinyl. Structures A, C, and E are the lower-energy structures.

approximation was made, *i.e*. the carbon 1s electrons were not included in the post-HF treatment. Vibrational spectra were predicted using the VPT2+K method.[49-52] Quadratic force constants and first derivatives of the dipole moment were computed at CCSD(T)/ANO1 by numerical differentiation of analytic gradients. Cubic and semi-diagonal quartic force constants were computed by numerical differentiation of CCSD(T)/ANO0 analytic second derivatives.[53] To compute the anharmonicity constants, these cubic and semi-diagonal quartic force constants were combined into a "hybrid" force field[54] with which the standard VPT2 procedure was carried out using scripts written in Mathematica 10.[55] An effective Hamiltonian was then constructed, containing all but the highest frequency CH stretching fundamental (6 states) and all two-quanta HCH scissor overtones/combinations (6 states). The interactions between these two groups of states were anticipated to be the most important for modeling the CH stretching region.[38] The Martin diagnostic[56] was also computed to identify other strongly interacting states; no additional resonances were found that were relevant to this spectral region.

The diagonal elements of the effective Hamiltonian were the VPT2 frequencies of each state, deperturbed for interactions with all other states within the effective Hamiltonian. Off- diagonal elements are well-known harmonic oscillator matrix elements involving cubic force constants, which account for Fermi coupling, and Darling-Dennison resonance constants, which account for some small, higher-order couplings.[51, 52] Diagonalization of the effective Hamiltonian yields the anharmonic transition frequencies. Anharmonic intensities were determined from the CCSD(T)/ANO1 harmonic intensities under the electrical harmonicity approximation.

The intensity of each anharmonic transition is proportional to the amount of each zeroth-order CH stretching fundamental that it contains. To compare VPT2+K frequencies evaluated at the C_s and C_{2v} geometries, the ring-puckering normal coordinate that approximately carries one into the other, and for which the C_{2v} structure has an imaginary harmonic frequency, was simply ignored. Excitation or force constants involving this ring-puckering mode were not considered in the VPT2 procedure.

3.3.2 1-Methylallyl Radical

The electronic minima of both rotamers of methylallyl (*trans* and *cis*; Figures 3.3C and 3.3D) were characterized. VPT2+K simulations were performed for these systems, similar to the aforementioned cyclobutyl simulations. In deciding upon which vibrational states to include in the effective Hamiltonian, the 2-quanta combinations/overtones generated from the HCH scissoring normal modes (localized on the methylene carbons) were a relatively straightforward choice for cyclobutyl radical. However, more varied kinds of coupling could conceivably be important in lower-symmetry hydrocarbons, such as the methylallyl radical.

The states for these effective Hamiltonians were chosen in a systematic way. For *cis*- and *trans*-methylallyl, all CH stretching fundamentals were included except for the highest frequency mode. Then, all 2-quanta vibrational states (combinations and overtones) that could be built from a small pool of normal modes were included. The pool was constructed by first starting with the non-CH stretching normal coordinate having the largest harmonic frequency. A VPT2+K simulation was performed; the

normal coordinate with the next largest harmonic frequency was added to the pool, and the spectrum was re-simulated with the new, larger Hamiltonian matrix. This was continued until the frequencies and intensities were observed to be relatively converged. The desire for convergence was balanced with our desire to limit the simulations to the smallest and most economical effective Hamiltonians possible. While the most important interactions between vibrational states were included, expanding the effective Hamiltonian to include weak interactions is not expected to improve the simulation.[51] The normal coordinates comprising the methylallyl effective Hamiltonians can be approximately described as three CH_3 scissors, one CH_2 scissor, one CH in-plane bend, and one asymmetric skeletal stretch (6 total).

Each conformer presents one additional theoretical challenge. In *trans*-methylallyl, the asymmetric skeletal stretching and the CH_2 scissoring fundamentals are found to be in strong Fermi resonance with a handful of 2-quanta states characterized by out-of-plane wagging/twisting of the allyl group. The presence of these "connected" resonances complicates the resonance polyads and requires some additional treatment.[54] A simplified form of this kind of problem can be dealt with *via* the Hamiltonian matrix:

$$\begin{pmatrix} v_a^* & \frac{\phi_{abc}}{2\sqrt{2}} & 0 \\ \frac{\phi_{abc}}{2\sqrt{2}} & (v_b + v_c)^* & \frac{\phi_{cdf}}{2\sqrt{2}} \\ 0 & \frac{\phi_{cdf}}{2\sqrt{2}} & (v_b + v_d + v_f)^* \end{pmatrix}$$

where the off-diagonal elements contain cubic force constants, and the diagonal elements are the deperturbed VPT2 frequencies of an arbitrary 1-quantum state, a 2-quanta state in resonance with it, and a 3-quanta state in resonance with the 2-quanta state. The 3-quanta state is a contrivance to correct the 2-quanta state for the resonance, $\omega_c \approx \omega_d + \omega_f$, which in-turn affects the fundamental. A total of 18 three-quanta states were added to correct for all connected resonances. Their inclusion gives rise to many additional low intensity transitions. Although an identical treatment could not be applied to *cis*-methylallyl, as the normal modes of *cis* do not always have clear *trans* analogs, every attempt was made to make their simulations comparable.

Specifically in *cis*-methylallyl, there is a low methyl torsional frequency (44 cm^{-1}), and very strong coupling was predicted between that mode and the methyl CH stretches. Attempts to treat this coupling in the effective Hamiltonian were not successful, so this mode was thrown out. The methyl torsional coordinate was also thrown out of the *trans*-methylallyl simulations to be fair.

3.3.3 Allylcarbinyl Radical.

The electronic minima of both rotamers of allylcarbinyl (*gauche* and *cis*; Figures 3.3E and 3.3F) were characterized. Strange behavior precluded the application of the same CCSD(T) electronic structure methods used for the cyclobutyl and methylallyl radicals. For both conformers of allylcarbinyl, we noted small but pervasive numerical inconsistencies in the cubic force constants and unreasonably large (-700 cm^{-1}) anharmonic corrections to the C=C stretching fundamentals. We found that this is not

simply indicative of an untreated Fermi resonance. The numerical errors also manifest in the force constants that involve the C=C stretch. For diagnostic purposes, we computed harmonic frequencies using ROHF-CCSD(T)/ANO0 and observed that the C=C stretch harmonic frequency for *cis*-allylcarbinyl was 1689 cm^{-1}, whereas in comparison, the frequency shifts to 1794 cm^{-1} with UHF-CCSD(T)/ANO0. Similarly, the C=C stretch harmonic frequencies for *gauche*-allylcarbinyl are predicted to be 1689 cm^{-1} and 1802 cm^{-1} using ROHF and UHF references, respectively. In addition to the strong dependence on the choice of reference wave function in these highly-correlated calculations, each of these systems is of doublet multiplicity and possesses a multiple-bond. This combination has previously been identified as a warning-sign for unreliable force constant calculations.[57, 58] We suspect that near-instabilities in the reference wave function(s) are degrading the quality of the computed CCSD(T) frequencies.[57, 58]

Because of these challenges associated with the CCSD(T) computations, we chose instead to compute quadratic (cubic and quartic) force constants at the B2PLYP/aug-cc-pVTZ (B3LYP/aug-cc-pVTZ) level of theory.[59-61] These were all obtained with analytic second derivative techniques in Gaussian 09.[62] Inspection of the DFT force fields does not reveal anything out of the ordinary. There is some evidence to suggest that DFT force constants are less susceptible to the influence of orbital near-instabilities.[63, 64]

For *cis*- and *gauche*-allylcarbinyl, the symmetric and antisymmetric CH stretch fundamentals localized on the radical site were not included in the effective Hamiltonians. This is analogous to the structurally similar *n*-propyl radical, where these

states are not involved in strong anharmonic coupling.[38] Indeed, the Martin diagnostic fails to find any strong couplings between them and any of the 2-quanta bends. Their predicted frequencies are simply the full VPT2 values. Otherwise, the process used to construct the effective Hamiltonians was the same as with methylallyl. The allylcarbinyl simulations considered combinations and overtones of three CH_2 scissors, one in-plane CH bend, and the C=C stretch coordinate. The stretch-torsion couplings were not a cause for concern, and there were no strong connected resonances in these systems.

3.4 Results and Discussion

3.4.1 C_4H_7 Potential Energy Surface

The potential energy surface (PES) shown in Figure 3.4 was adapted from the work of Ribeiro and Mebel[5] and simplified for the purpose of this discussion. All values are in kcal/mol and are relative to the *trans*-methylallyl structure. Upon unimolecular decomposition of the cyclobutyl radical *via* ring-opening (barrier at 50.3 kcal/mol), both the *trans*- and *cis*-methylallyl radicals and 1,3-butadiene are energetically accessible. Both of these pathways pass through the allylcarbinyl radical intermediate. The allylcarbinyl radical can also rearrange over barriers below the cyclobutyl ring-opening barrier to form either the 1-buten-1yl or cyclopropylmethylcarbinyl radicals.

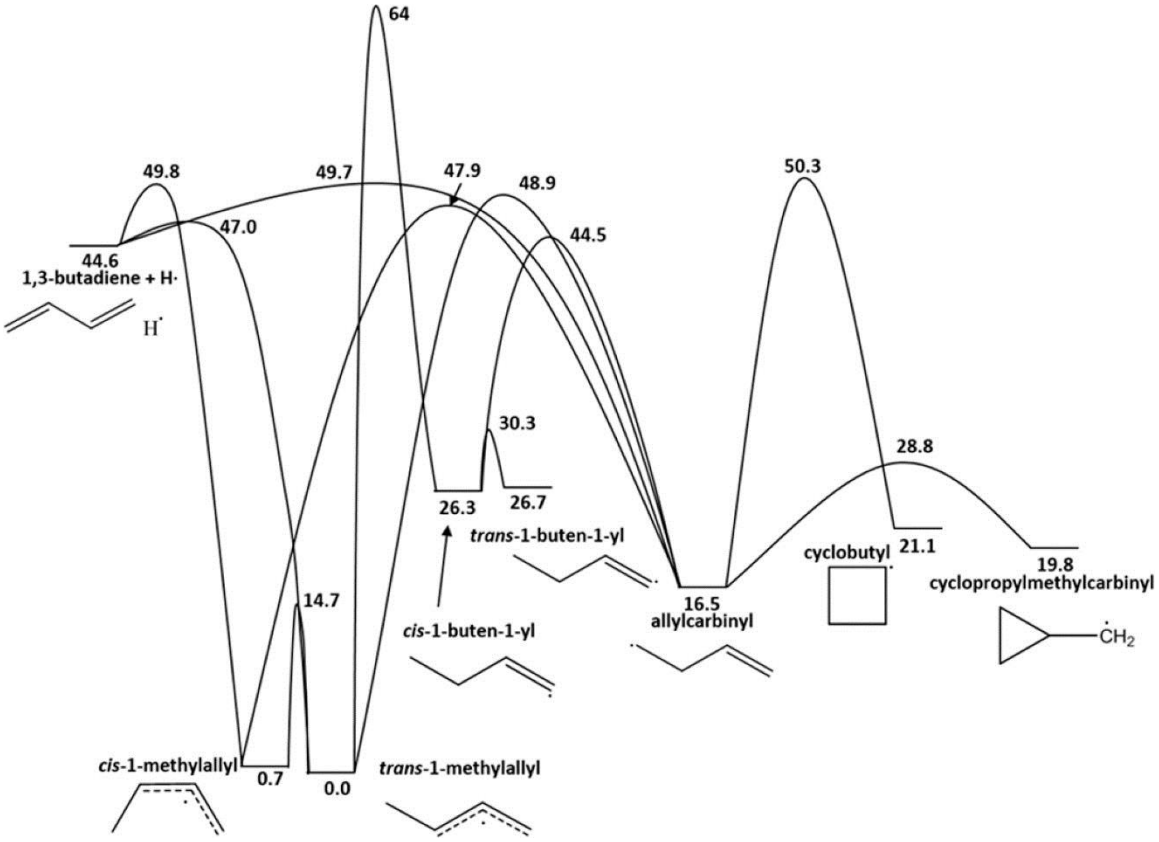

Figure 3.4: PES for the C_4H_7 species relevant to this study. Note the pathways that connect the cyclobutyl radical to the methylallyl radicals, through the formation of allylcarbinyl radical. Several pathways having barriers below the cyclobutyl ring-opening barrier lead toward 1,3-butadiene. Adapted from ref 5.

3.4.2 Infrared Spectroscopy

3.4.2.1 Cyclobutyl Radical

The laser induced depletion IR spectrum of the cyclobutyl radical and its precursor are shown in Figure 3.5. The precursor spectrum (blue) was acquired on mass channel 55 u with a pyrolysis current of 0 A, while the radical spectrum (black) was obtained on mass channel 39 u with a pyrolysis current of 20 A. Two distinctly new bands, located at 2819.5 and 3069.6 cm^{-1}, are only present in the radical spectrum. Although not necessarily obvious by eye, the collection of features in the radical spectrum between 2850 and 3000 cm^{-1} are different from those observed in the precursor spectrum. The collection of spectral features observed in the cyclobutyl spectrum can be mostly assigned *via* a comparison to the VPT2+K anharmonic frequency computation.

To investigate the question of what geometry provides the most physically meaningful description of cyclobutyl, a fully-relaxed CCSD(T)/ANO1 one-dimensional PES was computed for the ring-puckering coordinate. Two dihedral angles were simultaneously scanned, while the system was constrained to C_s symmetry (C_{2v} at the saddle point). The scan coordinates are the angle between the plane made by the right, bottom, and top (radical) carbon atoms and the C_s symmetry plane (see Figure 3.3A), which was scanned from 70 to 90 degrees in 0.5 degree steps, and the corresponding angle between the left, bottom, and top carbon plane and the symmetry plane, scanned from -70 to -90.

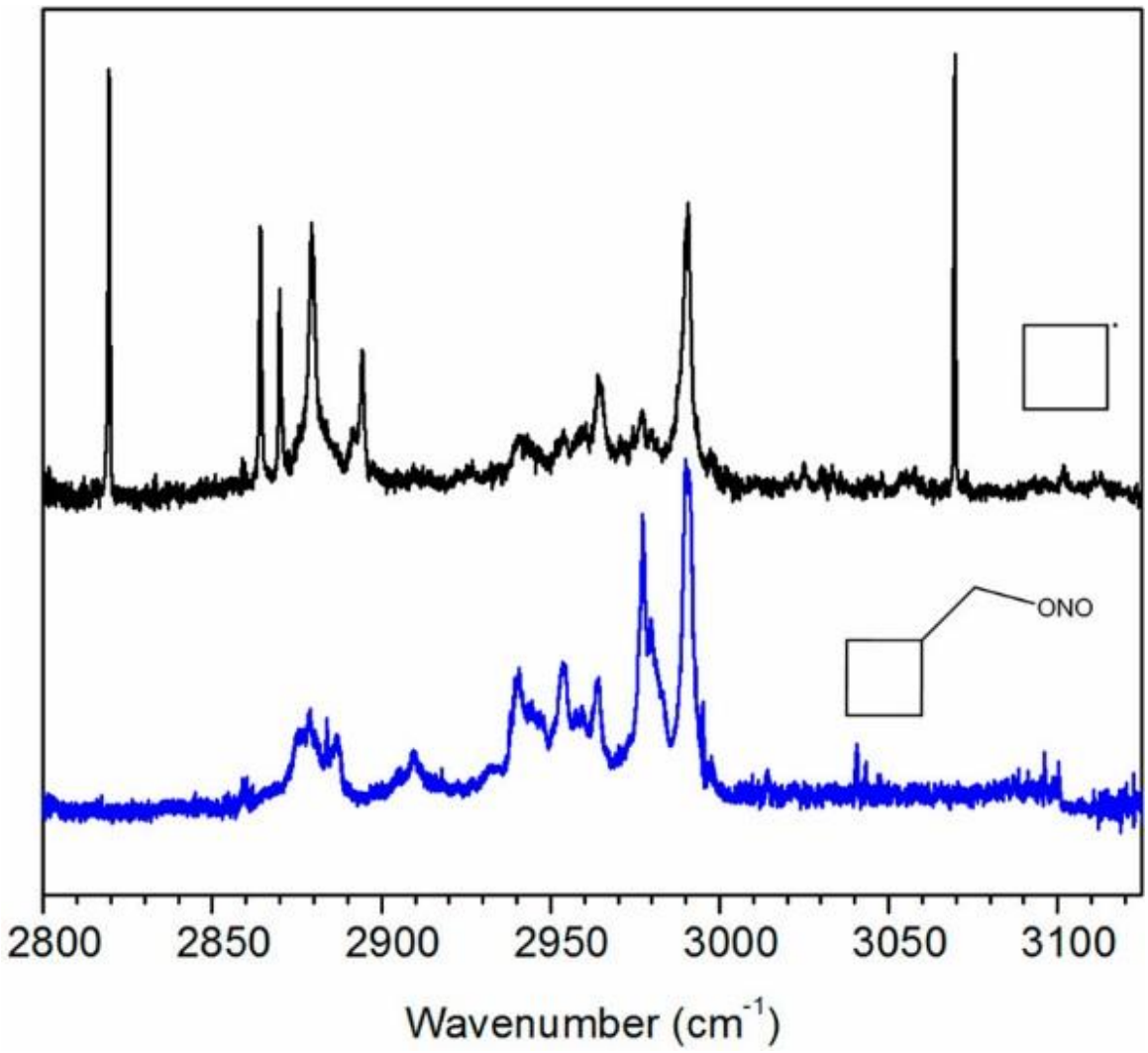

Figure 3.5: IR survey spectra of the cyclobutyl radical (black) and its precursor, cyclobutylmethyl nitrite (blue). The precursor spectrum was measured on mass channel 55 u, and the radical spectrum was measured on channel 39 u. Formation of the cyclobutyl radical is achieved at a pyrolysis current of 20 A (500-700 °C). Although some features appear to be present in both spectra, the bands in the 2950-3000 cm^{-1} region differ in frequency on the order of 0.5 cm^{-1}.

The geometries for the cyclobutyl radical and the relaxed ring-puckering potential energy surface are shown in Figures 3.3A, 3.3B and Figure 3.6, respectively. The one dimensional general internal motion Hamiltonian used is given in Equation 3.3.[65]

$$\hat{H}_{LAM}^{1D} = -\frac{\hbar^2}{2}\left[\begin{array}{c}\frac{\partial}{\partial\phi}\left(g_{4,4}(\phi)\right)\frac{\partial}{\partial\phi} - \frac{1}{4}\frac{\partial}{\partial\phi}\left(g_{4,4}(\phi)\right)\left(\frac{\partial \ln|G(\phi)|}{\partial\phi}\right) \\ + \frac{1}{16}\left(g_{4,4}(\phi)\right)\left(\frac{\partial \ln|G(\phi)|}{\partial\phi}\right)^2\end{array}\right] + \hat{V} \qquad \textbf{(Eq. 3.3)}$$

The ring-puckering coordinate is ϕ, $g_{4,4}(\phi)$ is the pure vibrational G-matrix element, and $|G(\phi)|$ is the G-matrix determinant. The 1D potential and reduced mass functions were fit to Fourier series and the wavefunctions were solved for variationally in a basis of sine and cosine functions.[66] A basis set of periodic functions is not an obvious choice, as this potential is not periodic; however, we note that this procedure succeeds at predicting eigenstates in the umbrella potential of ammonia, as shown by Rush and Wiberg,[67] where the fitting functions were even-order polynomials, and the solution was carried out with a Numerov algorithm. It is anticipated that the predominant source of error in our analysis is the failure to explicitly consider the α-CH wagging normal coordinate (b_1 symmetry with ω_e = 218 cm^{-1}) in a 2D treatment. Adiabatic separation may not be totally valid between this coordinate and the ring-puckering. The wavefunctions corresponding to the first four quantum states are overlaid on the potential. The calculated fundamental frequency of the ring-puckering motion is approximately 63 cm^{-1}. This motion connects the equivalent C_s electronic minima through a C_{2v} first-order saddle point. The ground state wave function lies above the barrier to interconversion, implying a vibrationally averaged C_{2v} structure; therefore, the C_{2v} stationary point was adopted for vibrational frequency calculations.

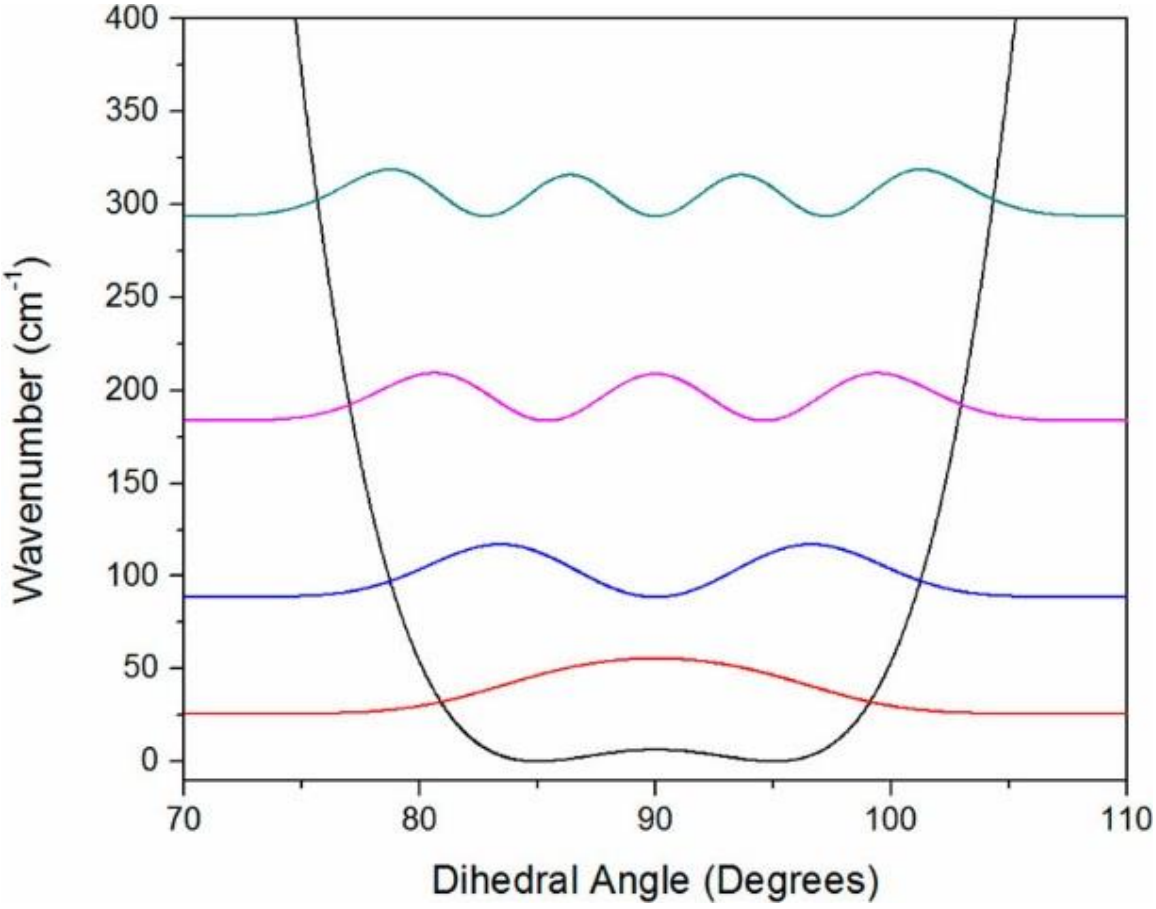

Figure 3.6: Relaxed PES for the ring puckering of the cyclobutyl radical computed at the CCSD(T)/ANO1 level of theory. The fundamental vibrational frequency of the ring-puckering motion is approximately 63 cm^{-1}. The electronic energy difference between the two stationary points is 6 cm^{-1}.

The anharmonic frequencies for the C_{2v} structure are shown as the red trace in Figure 3.7. The C_{2v} structure is most similar to the vibrationally averaged structure of the radical. A simulation performed with this geometry better captures the number and position of bands present in the experimental spectrum in comparison to simulations for the C_s structure. A table of the computed frequencies of both structures can be found in Table 3.1.

In the CH stretching region, cyclobutyl radical has 6 IR-active modes, one of which (β-CH_2 symmetric in phase) has ~0 intensity. Nevertheless, this mode was accounted for in the VPT2+K simulation, and was shown to not play a significant role. Three of the IR-active modes are not strongly coupled to other modes; these are the α-CH stretch, γ-CH_2 antisymmetric stretch, and β-CH_2 antisymmetric stretch. The remaining two IR-active modes, the β-CH_2 symmetric out-of-phase (b_2) and γ-CH_2 symmetric stretch (a_1), participate in anharmonic resonance polyads with various 2-quanta HCH bending states. This gives rise to the spectral complexity in the lower frequency region.

The highest frequency band, located around 3069 cm^{-1}, agrees well with the prediction for the α-CH stretch fundamental localized on the radical site (3078 cm^{-1}). The two bands located at 2990 and 2964 cm^{-1} closely match the theoretical predictions corresponding to the γ-CH_2 antisymmetric and symmetric stretches located at 2984 and 2963 cm^{-1} respectively. The lowest frequency band in this region (2819 cm^{-1}) agrees well with the predicted value of 2814 cm^{-1}, corresponding to the transition with about 40% β-CH_2 symmetric stretching character. Theory is unable to provide a quantitatively accurate picture for the cluster of peaks between 2850 and 2900 cm^{-1}. Similar deficiencies were seen when VPT2+K was applied to the *i*-propyl radical, which shares

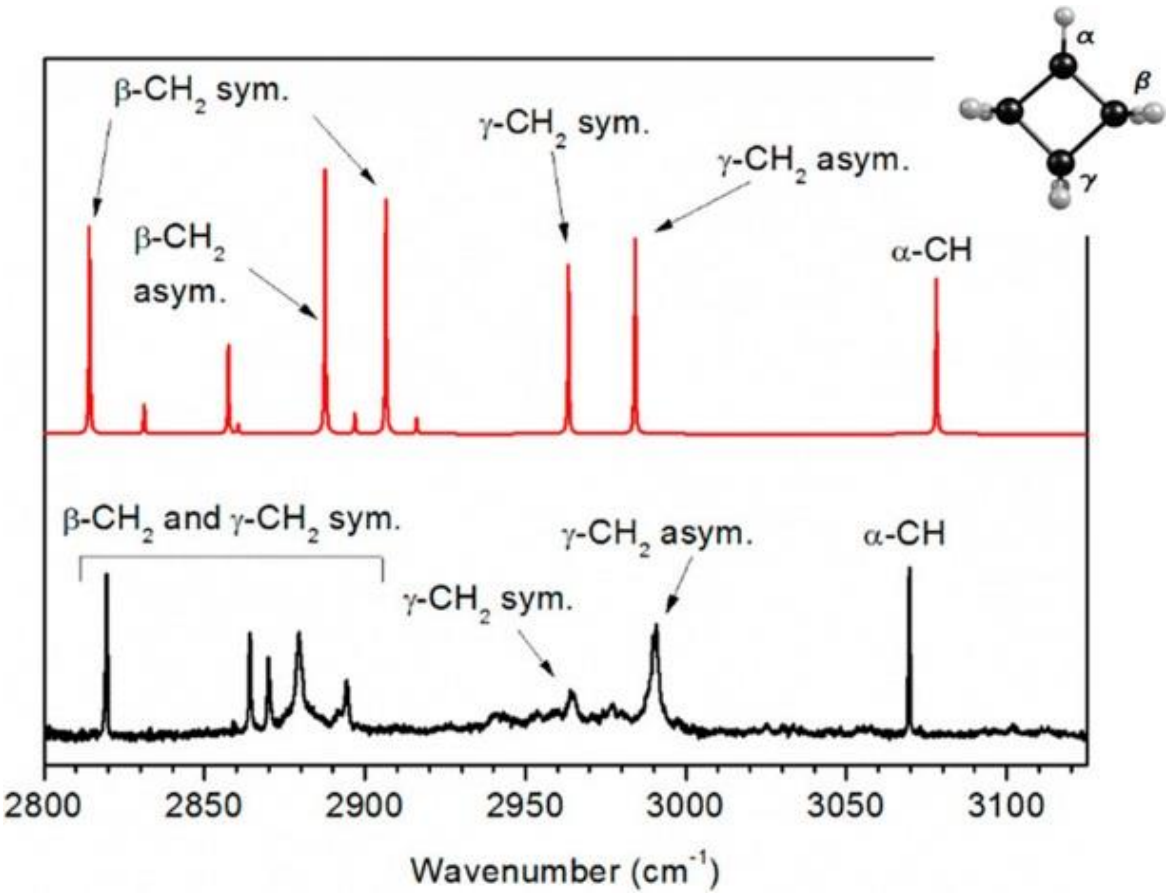

Figure 3.7: Experimental spectrum of the cyclobutyl radical (black) compared to the theoretical predictions for the C_{2v} structure (red).

Table 3.1: Qualitative descriptions, symmetries, and harmonic frequencies of the cyclobutyl radical.

Mode[a]	$\Gamma(C_{2v})^a$	$\Gamma(C_s)^b$	$\omega(C_{2v})^c$	$\omega(C_s)^c$	$\Delta\omega$	Description
1	a_1	a'	3210.00	3206.97	3.03	α-CH stretch
2	a_1	a'	3080.04	3079.75	0.30	γ-CH_2 symmetric stretch
3	a_1	a'	3015.37	3010.29	5.08	β-CH_2 symmetric stretch in-phase
4	a_1	a'	1497.75	1497.68	0.06	β,γ-CH_2 scissors in-phase
5	a_1	a'	1464.80	1466.18	-1.39	β,γ-CH_2 scissors out-of-phase
6	a_1	a'	1280.88	1280.37	0.52	β-CH_2 wag in-phase
7	a_1	a'	1037.72	1039.18	-1.46	ring-breathing
8	a_1	a'	905.78	904.08	1.69	ring-bending
9	a_1	a'	793.94	815.94	-22.00	ring-deformation
10	a_2	a''	3048.28	3056.13	-7.85	β-CH_2 antisymmetric stretch out-of-phase
11	a_2	a''	1221.91	1229.86	-7.95	β,γ-CH_2 twisting in-phase
12	a_2	a''	1003.36	1001.77	1.59	β,γ-CH_2 twisting out-of-phase
13	a_2	a''	742.27	742.89	-0.62	β-CH_2 rock out-of-phase
14	b_1	a'	3136.77	3136.60	0.18	γ-CH_2 antisymmetric stretch
15	b_1	a'	3045.22	3053.23	-8.01	β-CH_2 antisymmetric stretch in-phase
16	b_1	a'	1188.06	1191.91	-3.85	β,γ-CH_2 symmetric twisting
17	b_1	a'	1006.26	1015.72	-9.46	β-CH_2 rock in-phase
18	b_1	a'	733.69	716.35	17.34	β,γ-CH_2 symmetric rock
19	b_1	a'	218.31	269.58	-51.27	α-CH wag out-of-ring-plane
20	b_1	a'	56.91i	77.97	---	ring-puckering
21	b_2	a''	3012.76	3007.95	4.81	β-CH_2 symmetric stretch out-of-phase
22	b_2	a''	1460.23	1459.92	0.32	β-CH_2 antisymmetric scissors
23	b_2	a''	1315.67	1313.27	2.40	α-CH wag in-ring-plane
24	b_2	a''	1246.31	1246.10	0.21	β,γ-CH_2 wag in-phase
25	b_2	a''	1214.19	1203.71	10.48	β,γ-CH_2 wag out-of-phase
26	b_2	a''	972.44	968.43	4.01	c-axis antisymmetric ring stretch
27	b_2	a''	911.67	911.19	0.48	b-axis antisymmetric ring stretch

[a] The modes are ordered based on the symmetries at the average C_{2v} geometry.
[b] Symmetry labels were determined at the C_s electronic minimum.
[c] Harmonic frequencies were computed at the CCSD(T)/ANO1 level of theory.

some structural features with cyclobutyl.[38] One of the bands located here must be the (b_1) β-CH_2 antisymmetric stretching fundamental, and it should not be resonant, but because of the poor frequency agreement, no assignment is attempted.

3.4.2.2 1-Methylallyl Radical

The IR spectra of the 1-methylallyl and allylcarbinyl radicals were also recorded so as to rule out any contributions of these species to the previously recorded spectrum of the cyclobutyl radical. The methylallyl radical was formed from the pyrolysis of 2-methyl-3-buten-1-yl nitrite. Figure 3.8 shows the IR spectrum of this radical as compared to its precursor, recorded with pyrolysis currents of 29 A and 0 A, respectively. Band centers for radical peaks include 2970.8, 3025.0, 3057.6, 3110.9, and 3112.7 cm^{-1}.

Figure 3.9 shows the experimental spectrum of methylallyl compared to theoretical predictions for both conformers, shown as C and D in Figure 3.3. These predictions are shown and compared separately to the experimental spectrum in Figure 3.10. The *trans* conformer is lower in energy than the *cis* conformer by approximately 0.5 kcal/mol (CCSD(T)/ANO1). This electronic energy difference agrees with previous theoretical calculations.[5, 24] On the basis of that energy difference, it is conceivable that appreciable amounts of both conformers could result from pyrolysis of the nitrite precursor and that these would be cooled by the helium droplets into their respective potential wells. The simulation presented is simply the sum of the individual *cis* and *trans* simulations. The highest frequency band contains contributions from both conformers, and the ratio of each was adjusted to best reproduce the doublet feature. An equal ratio of

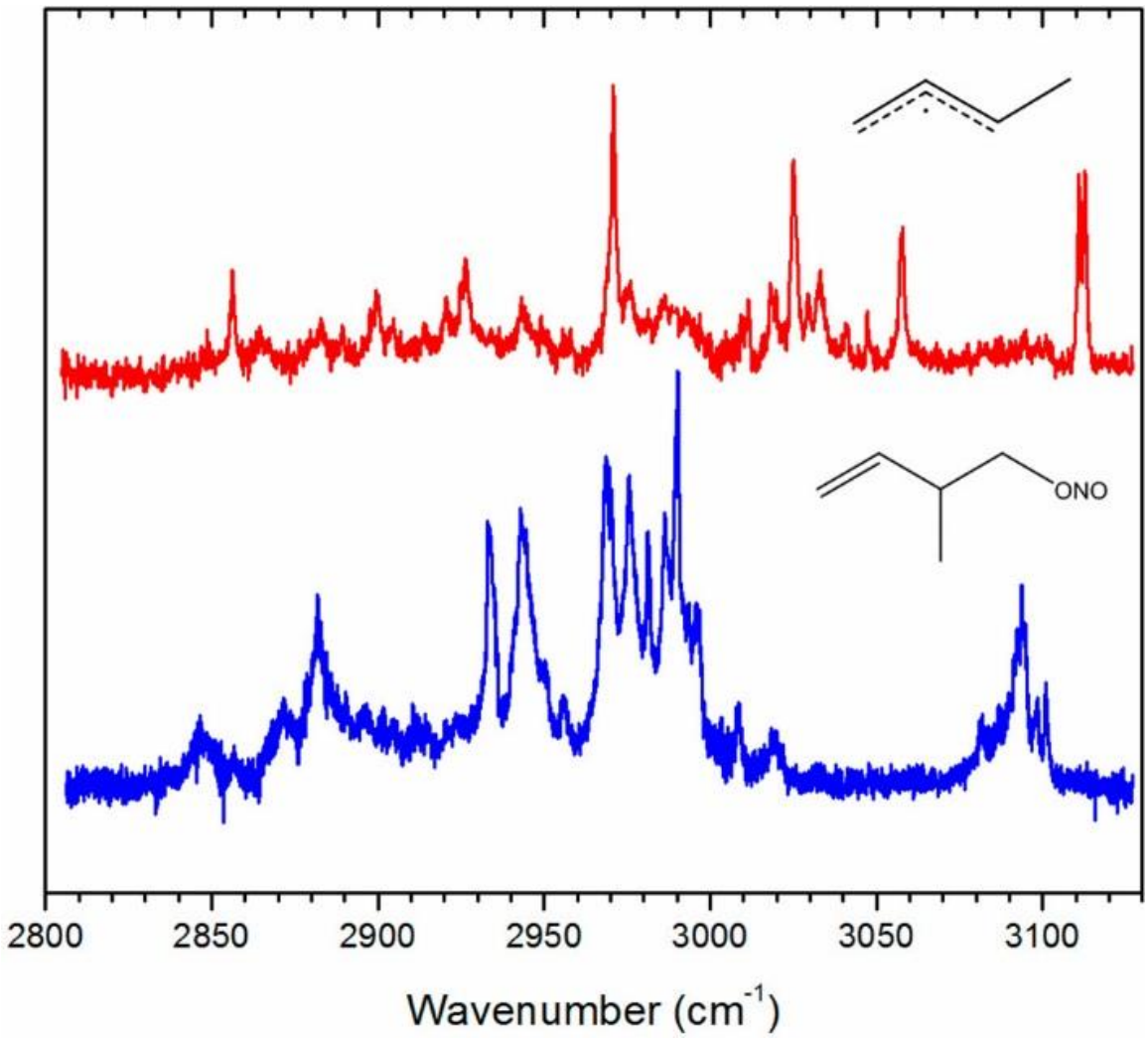

Figure 3.8: IR survey spectrum of the 1-methylallyl radical (red) as compared to the spectrum of its precursor (2-methyl-3-buten-1-yl nitrite) in blue. There is no evidence of precursor contamination in the radical spectrum.

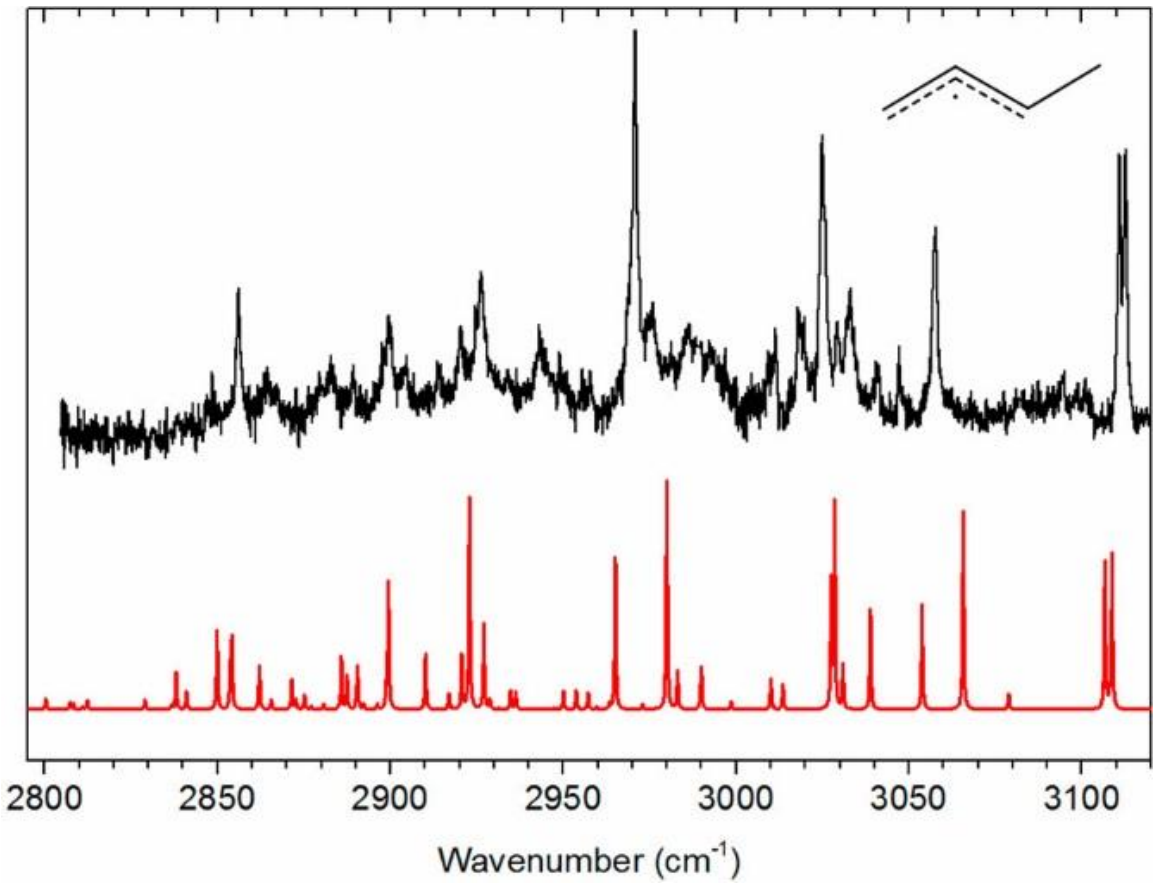

Figure 3.9: Experimental spectrum for 1-methylallyl radical (black) compared to the theoretical predictions for the *trans* and *cis* structures (red). Another figure having the *trans* and *cis* simulations shown separately is given in Figure 3.10.

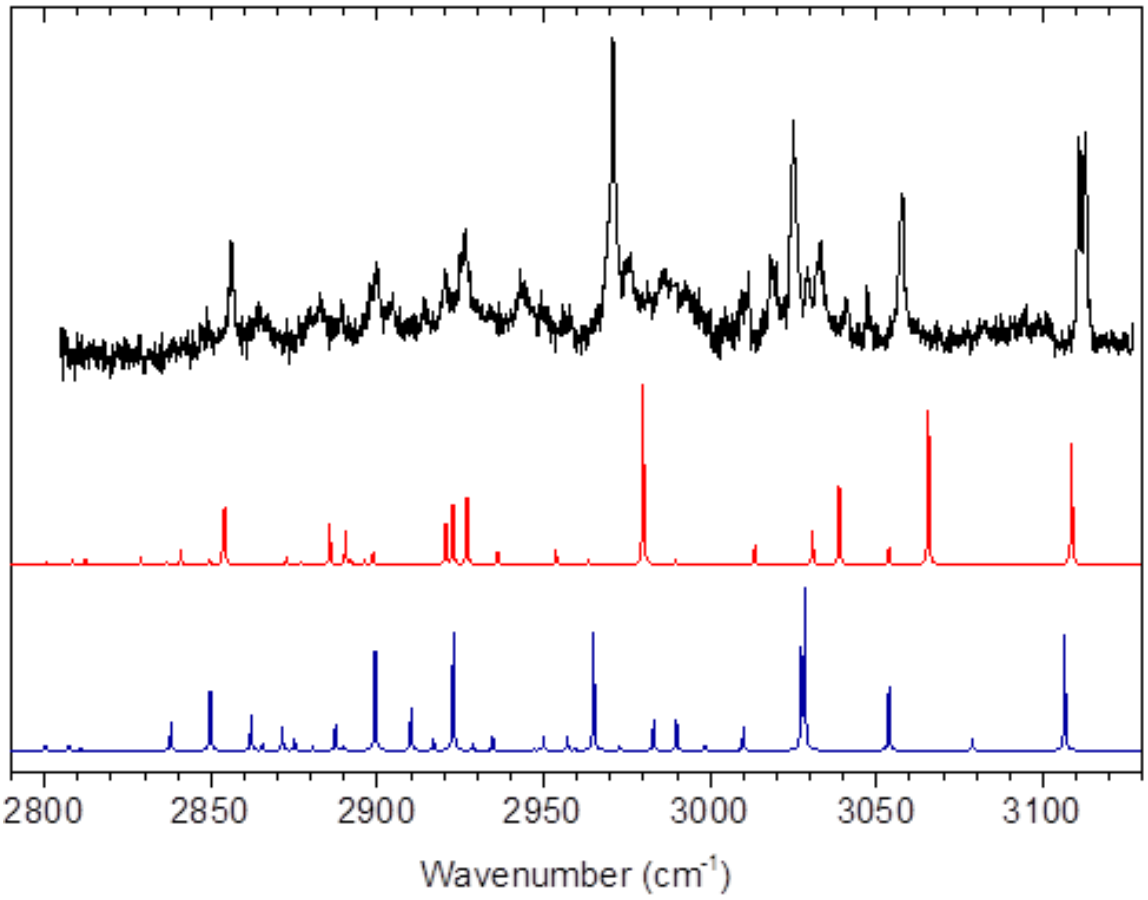

Figure 3.10: Simulated spectra for the *trans* (blue) and *cis* (red) conformers of the 1-methylallyl radical as compared to the experimental spectrum.

each was found to do a rather good job of explaining this feature. This doublet (3110.9 and 3112.7 cm^{-1}) is assigned to the antisymmetric CH_2 stretching fundamentals of both the *cis* and *trans* conformers, predicted at 3108.7 cm^{-1} and 3106.6 cm^{-1}, respectively. However, a confident conformer assignment is not within the accuracy of these calculations. This assignment is also in agreement with previous work by Bahou et al.[24] who assigned the highest frequency band in their spectrum to *trans*-1-methylallyl. However, their experiment did not resolve a doublet for the highest frequency band.

The band at 3057.6 cm^{-1} matches best with the lone CH stretch, nearest the methyl group, of *cis*-methylallyl. The 3025 cm^{-1} band is assigned to *trans*-methylallyl (predicted bands at 3027.4 and 3028.5 cm^{-1}). These overlapping transitions are characterized by symmetric stretching of the allyl unit; although, they cannot be assigned to any single normal mode. Bahou et al. also found a transition for the *trans* conformer in this region at 3023.5 cm^{-1}.[24] See Table 3.2 for a comprehensive comparison of methylallyl frequencies from this and the work of Bahou et al.

There is a strong transition at 2970.8 cm^{-1}. The most intense theoretical transitions in the vicinity, 2980.1 cm^{-1} from *trans* and 2965.3 cm^{-1} from *cis*, are both well-described as the *a′* components of the antisymmetric methyl stretch fundamentals. Theory is unambiguous regarding the character of this transition; however, it is not clear which conformer gives rise to it. The broad features located to the blue of this band are not predicted by theory. No assignments are attempted for the lower half of the spectrum. These transitions all possess some fraction of methyl stretching character: either the fully

Table 3.2: Comparison of experimental band centers for methylallyl.

Experiment (Helium Droplets)	**Experiment (p-H_2)[24]**
2856.2	2851.3
2899.8	
2926.4	2917.1/2922.2
2970.8	2968.8
3025.0	3023.5
3057.6[a]	
3110.9/3112.7[b]	3107.3

[a.] Bahou and et al. did not observe this feature. Our calculations suggest that this band is derived from the *cis* conformer.
[b.] Considering both the matrix shifts and the accuracy of the anharmonic frequencies, comparison to the spectrum of Bahou et al. cannot establish which conformer gives rise to each component of our doublet feature.

symmetric or the *a″* component of the antisymmetric stretch. Pure stretching fundamentals do not fall in this lower frequency region.

3.4.2.3 Allylcarbinyl Radical

Allylcarbinyl radical was produced from the pyrolysis of 4-penten-1-yl nitrite. Figure 3.11 shows the IR spectrum of allylcarbinyl as compared to its precursor. The radical spectrum was measured with a pyrolysis current of 25 A so as to minimize the formation of decomposition products of the radical. Among others, sharp bands found at 2900.0, 2932.1, 2952.7, 2955.7, 2976.1, 2992.8, 3030.2, 3079.6, 3093.2, 3117.2 cm^{-1} are signatures of the allylcarbinyl radical. As was the case with cyclobutyl radical, and methylallyl, a comparison of the radical and precursor spectra reveal a general sharpening and slight shifting of the vibrational bands in the 2900 to 3000 cm^{-1} region.

Figure 3.12 shows the experimental spectrum of allylcarbinyl as compared with the theoretical predictions for the two conformers combined. The radical has two rotamers, *gauche* (Figure 3E) and *cis* (Figure 3F), having an energy difference of approximately 0.5 kcal/mol (B2PLYP/aug-cc-pVTZ), the *gauche* conformer being lower in energy than *cis*. The predictions for these structures are shown separately and compared with the experimental spectrum in Figure 3.13. The computed structures are comparable to those computed by Bahou et al.[24] As with methylallyl, it is reasonable to expect that both conformers will make contributions to the measured vibrational spectrum. The simulation shown assumes a 1:1 conformer ratio, the same as used for methylallyl; although, in this case there were no obvious spectral features to which the ratio could be fit. Overall, the

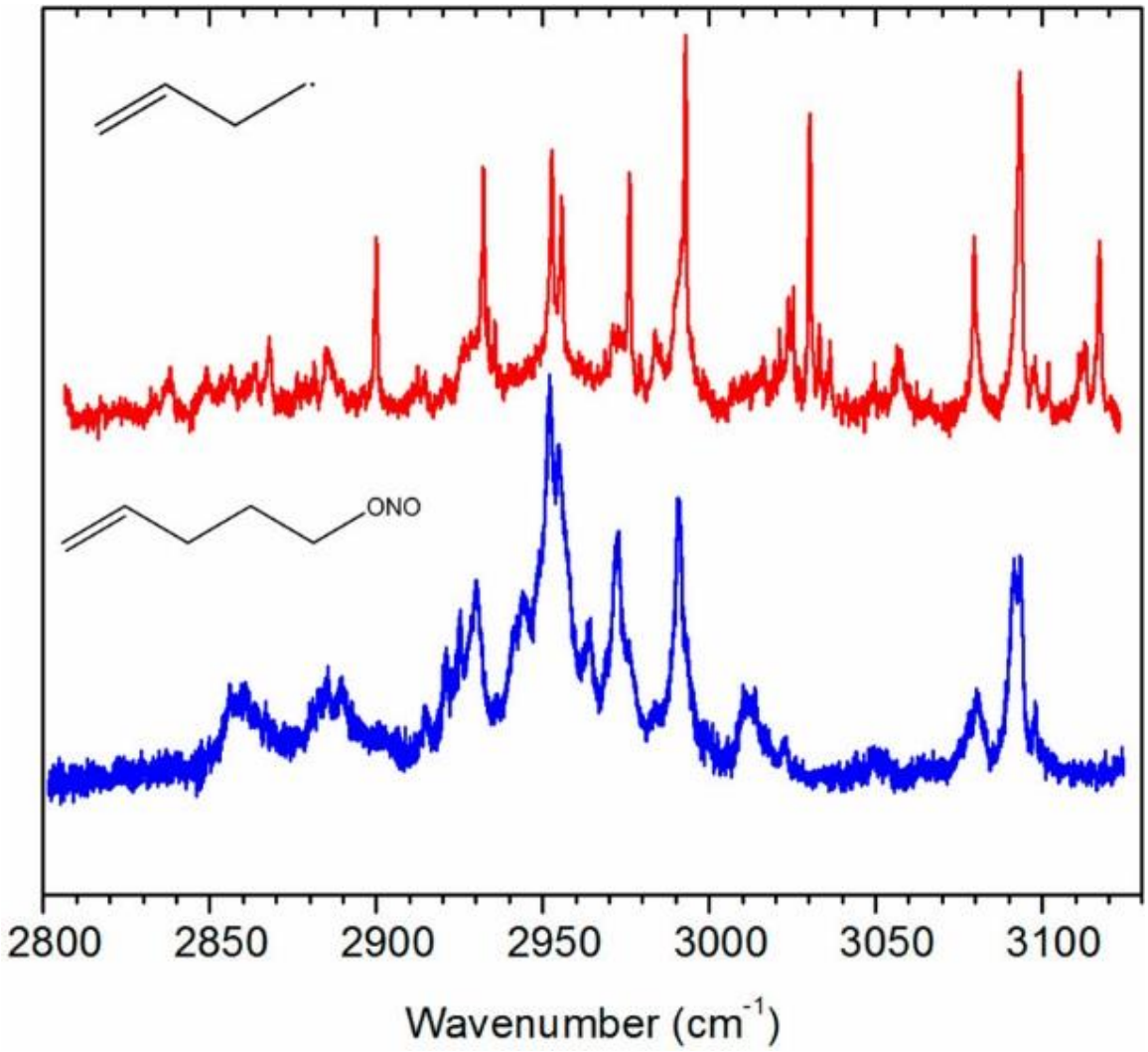

Figure 3.11: IR survey spectrum of the allylcarbinyl radical (red) as compared to the spectrum of its precursor, 4-penten-1-yl nitrite (blue). Although there is a resemblance of features in the 2900-3000 cm^{-1} region, contributions of the precursor are absent in the radical spectrum as all bands in this region are unique, differing from the precursor peaks by approximately 0.5 cm^{-1}.

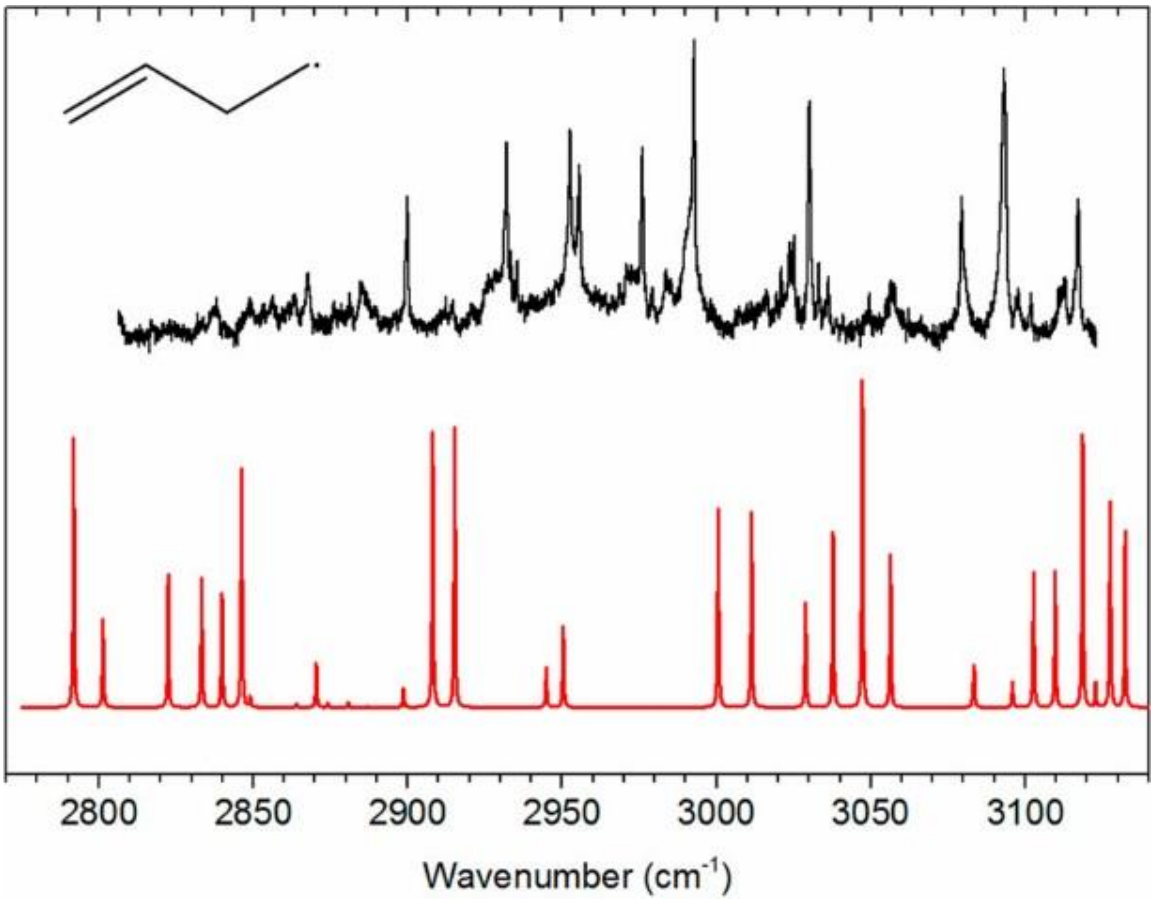

Figure 3.12: Experimental spectrum of allylcarbinyl radical (black) compared to the theoretical predictions for the *gauche* and *cis* structures combined (red). Separate theoretical spectra for the two different isomers are available in Figure 3.13.

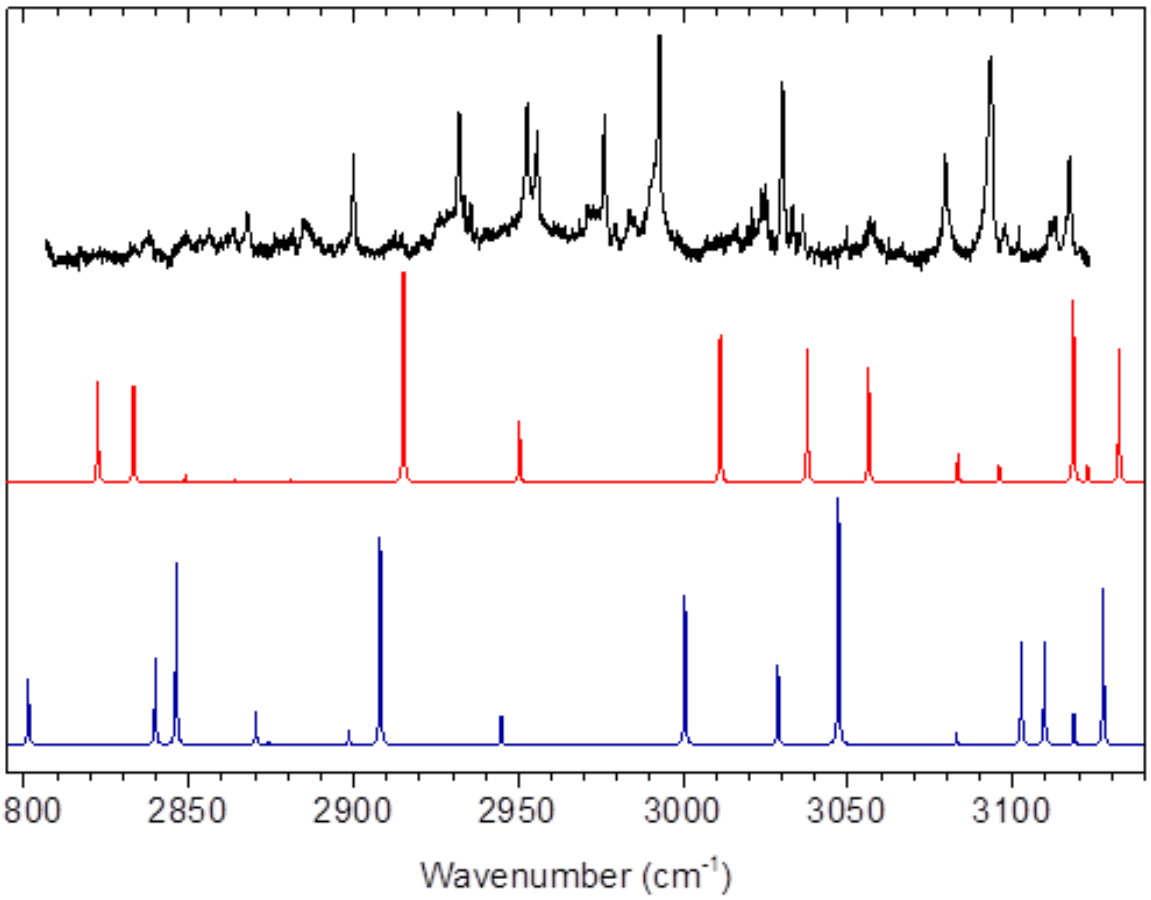

Figure 3.13: Experimental spectrum as compared to the theoretical simulated spectra for the *gauche* (blue) and *cis* (red) conformers of the allylcarbinyl radical.

agreement with theory is poor despite the history of good performance of B2PLYP and/or B3LYP for open shell systems.[60] There is some qualitative agreement with the features in the higher-frequency part of the spectrum, but the predictions for the highly-resonant, lower-frequency region are not satisfactory. Intense spectral features are present whereas theoretical intensity is absent, and the most intense theoretical features are found in regions where the experimental features are weak and sparse.

As discussed in the theoretical methods section, the problems here might be due to the influence of orbital near-instabilities, as suspected with UHF-CCSD(T). The B2PLYP and B3LYP functionals both incorporate fractions of UHF exchange, B2PLYP (53%) having somewhat more than B3LYP (20%).[59, 61] They may also inherit some of the problems that UHF has with allylcarbinyl. Due to the far greater importance of having accurate quadratic force constants (*vs*. cubic and quartic) in VPT2+K, the use of B2PLYP (which performs better for obtaining quadratic force constants generally),[60] may actually be counterproductive since it includes more Hartree-Fock exchange.

Allylcarbinyl differs structurally from *n*-propyl by having a terminal vinyl group rather than a methyl group. The radical CH_2 symmetric and antisymmetric stretch fundamentals of *n*-propyl were assigned to 3026.9 and 3110.1 cm^{-1}, respectively.[38] If the vinyl group does not have a great effect upon the frequencies of these transitions, then the features located at 3030.2 and 3117.2 cm^{-1} are good candidates for the analogous allylcarbinyl transitions. However, a conformer assignment cannot be made for these. Moreover, we attempt no further assignments for this spectrum.

For comparison purposes, Figure 3.14 shows the experimental spectra for cyclobutyl, allylcarbinyl and 1-methylallyl radicals. This is further evidence that the

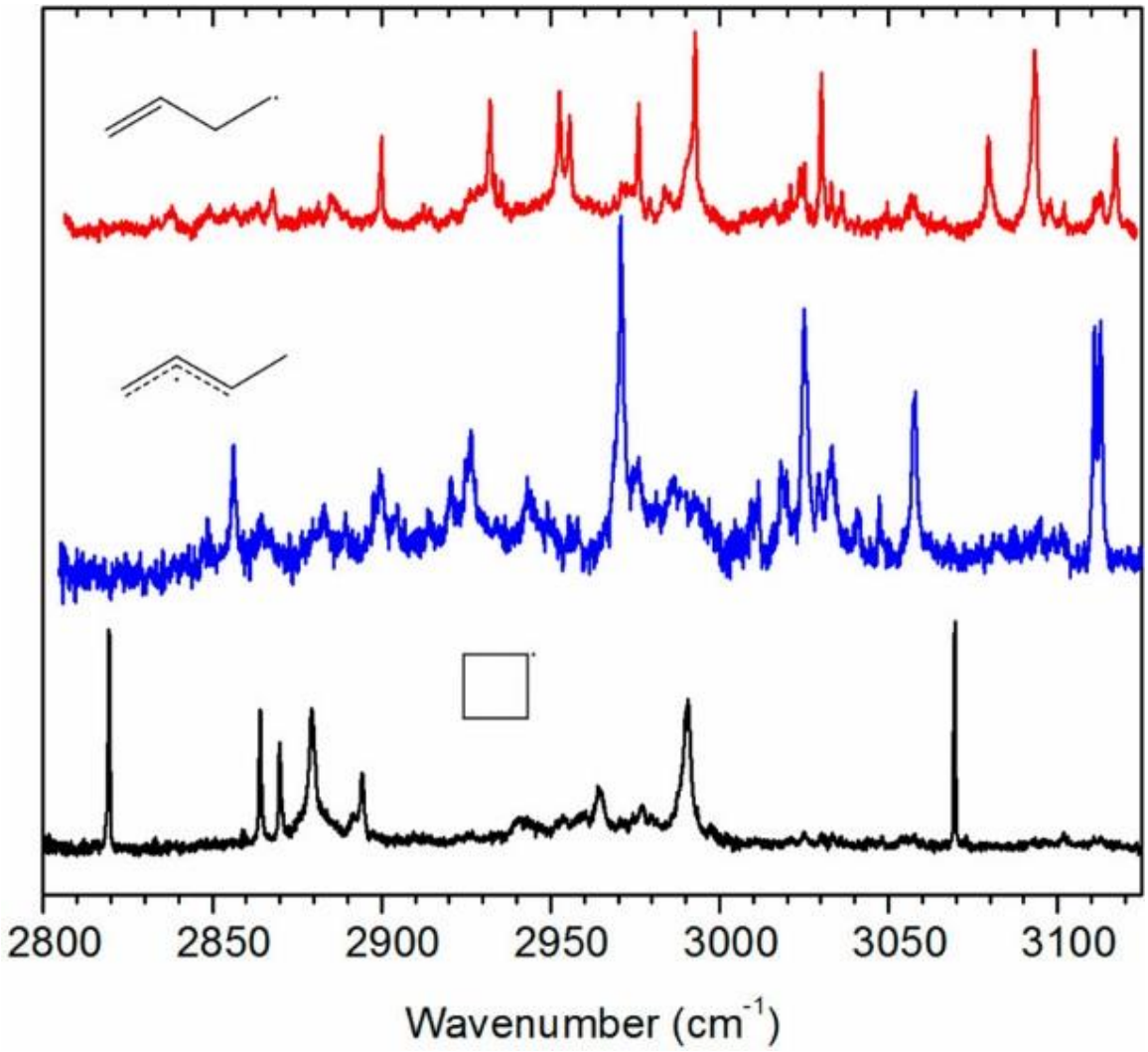

Figure 3.14: IR survey spectrum of allylcarbinyl radical (red) and 1-methylallyl radical (blue) as compared to the spectrum of cyclobutyl radical (black).

precursors selected to form these radicals are selective to which radical is produced and there are little to no common features in these spectra.

3.4.2.4 1,3-Butadiene

The IR spectrum of 1,3-butadiene (Sigma Aldrich, ≥99%) was also measured and is shown in Figure 3.15. This was motivated by the possibility of forming 1,3-butadiene upon cyclobutyl radical ring opening, given sufficient internal energy to overcome the barrier labeled 50.3 shown in Figure 3.2.[5, 8, 13, 27] A closer look at Figure 3.7 reveals that a small amount of 1,3-butadiene is being formed upon pyrolytic decomposition of cyclobutylmethyl nitrite (as evidenced by the small peak at 3101.9 cm^{-1}) when conditions are optimized for the production of cyclobutyl radical. Indeed, the 3101.9 cm^{-1} transition is the most intense peak in the CH stretching region of 1,3-butadiene spectrum. An explanation for this is that pyrolytic decomposition of the nitrite precursor can produce cyclobutyl radicals with sufficient internal energy (~30 kcal/mol) to overcome the ring-opening barrier, which is predicted to be above all but one barrier leading to the 1,3-butadiene + H atom product channel.

These results were further corroborated by recording a difference depletion mass spectrum at a laser frequency of 3101.9 cm^{-1} and a pyrolysis current of 30 A (pyrolysis of cyclobutylmethyl nitrite), shown in Figure 3.2D. Figure 3.2E shows the difference depletion mass spectrum for the *neat* 1,3-butadiene sample. These two traces have similar features, indicating that, at the 20 A pyrolysis source condition, a small amount of

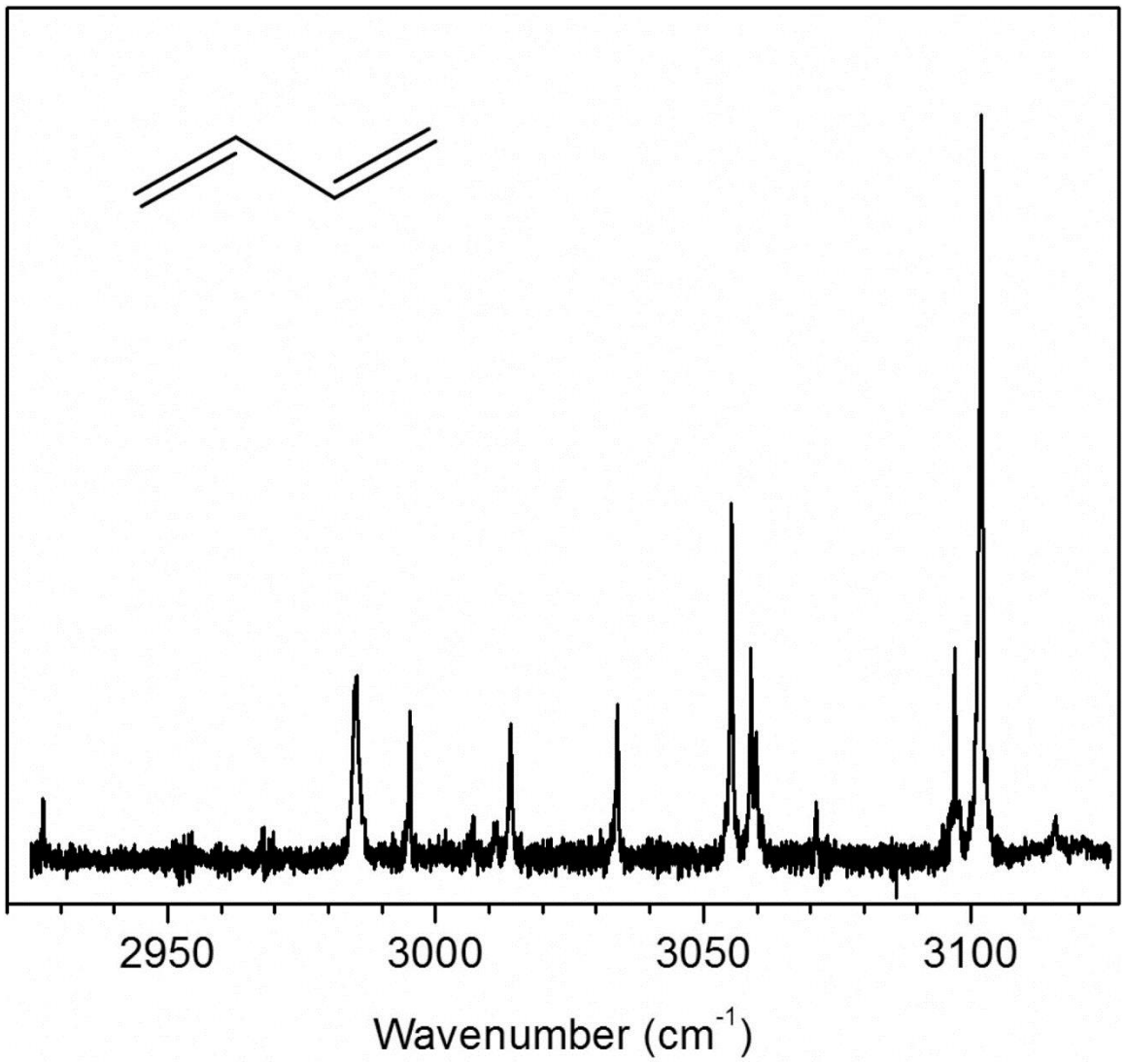

Figure 3.15: Laser-induced depletion spectrum of 1,3-butadiene in the CH stretching region, measured on mass channel m/z = 27 u.

1,3-butadiene is formed, most likely from the unimolecular ring-opening of the cyclobutyl radical prior to it being captured by a helium droplet. Most notably, upon increasing the current from 20 A (Figures 3.2B and 3.2C) to 30 A (Figure 3.2D), the largest depletion signal shifts to mass channel 27 u, which is indicative of the production of more 1,3-butadiene at the higher source temperature. These results are consistent with a mechanism, by which, through H atom loss, 1,3-butadiene is formed from the unimolecular ring-opening of the cyclobutyl radical. This mechanism is completely consistent with previous theoretical predictions of the C_4H_7 potential energy surface.[5, 8]

3.4.2.5 Higher Temperature Pyrolysis

Another IR survey scan (shown in Figure 3.16) was recorded at an even higher pyrolysis source temperature (33 A) to explore the decomposition products formed from cyclobutyl ring-opening. Features from both 1,3-butadiene and methylallyl are clearly present in the higher temperature scan (see caption for label descriptions), although there is no evidence for allylcarbinyl production. These results are consistent with the photoelectron spectroscopic work carried out by Beauchamp and co-workers,[8] as well as more recent sophisticated *ab initio* work carried out by Ribeiro and Mebel, where barriers out of the allylcarbinyl well are all below the barrier associated with cyclobutyl ring-opening.[5] In Figure 3.14, the peak at 3018.2 cm^{-1} is currently unassigned, as it cannot be attributed to either cyclobutyl, methylallyl, 1,3-butadiene, or allylcarbinyl. The cyclopropylmethylcarbinyl radical is another C_4H_7 isomer on the potential energy surface, but the pathway for formation involves a 12.3 kcal/mol barrier from the

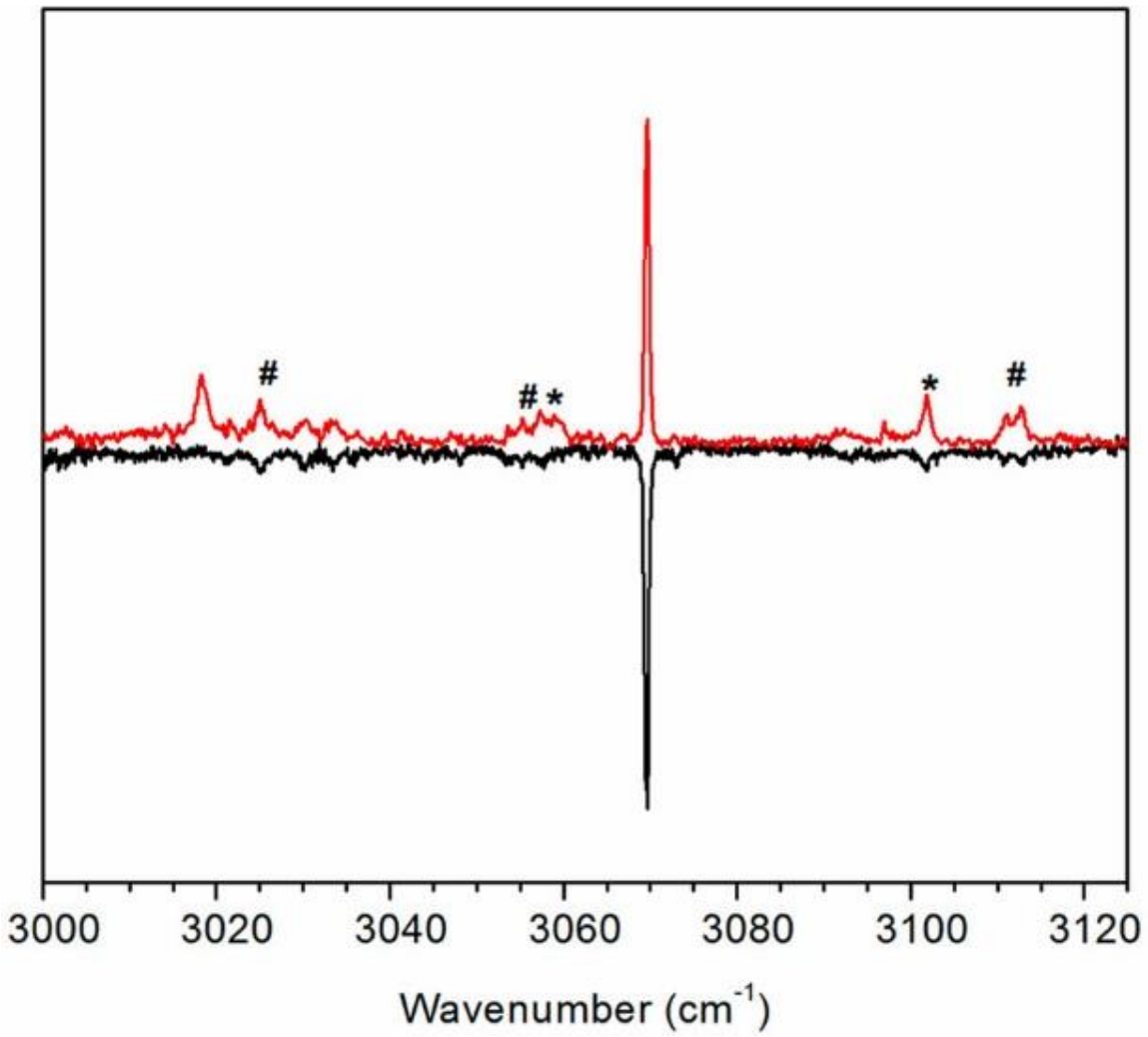

Figure 3.16: Pyrolysis of cyclobutyl methyl nitrite at 33 A. The IR scan (red) is compared to the original cyclobutyl radical scan taken at 20 A (black). Features that were present in small quantities in the lower trace become more pronounced in the upper trace, indicating that more cyclobutyl unimolecular decomposition products are being formed at the higher pyrolysis temperature. Evidence for both 1-methylallyl (#) and 1,3-butadiene (*) can be seen in the upper trace. There appears to be little to no contribution of the allylcarbinyl radicals. Another peak at 3018 cm^{-1} cannot be assigned and is not present in the spectra of 1-methylallyl, allylcarbinyl or 1,3-butadiene.

allylcarbinyl local minimum.[5] Given the excess internal energy available upon cyclobutyl ring-opening, it is perhaps unlikely that the cyclopropylmethylcarbinyl radical will be particularly abundant upon sample capture by the helium droplet beam. Moreover, there is currently no evidence for the allylcarbinyl radical in the spectrum obtained here. Nevertheless, this cyclopropylmethylcarbinyl radical should still be studied by IR spectroscopy to rule out its contribution to the spectrum. Also along the surface proposed by Ribeiro and Mebel, the 1-buten-1-yl radical, $CH_3CH_2CH{\cdot}CH$, is another intermediate species. This butenyl radical lies between allylcarbinyl radical and methylallyl, but it is unlikely that it will rearrange to methylallyl following the ring-opening of cyclobutyl, given the ~37 kcal/mol barrier.[5] Even though there is no evidence of allylcarbinyl formation, this 1-buten-1-yl radical cannot be ruled out as a possible source of this unassigned peak and should also be explored spectroscopically in future work. We note in closing that the above discussion assumes a sequential mechanism, by which the cyclobutylmethyl nitrite precursor first decomposes to cyclobutyl + CH_2O + NO; then the energized cyclobutyl radical rearranges unimolecularly *via* ring-opening, eventually decomposing by H atom loss to produce 1,3-butadiene. The experiment reported here cannot distinguish this mechanism from a concerted process involving only the nitrite species, in which it decomposes directly to 1,3-butadiene + H + CH_2O + NO. This pathway should be explored computationally in the future.

3.5 Conclusions

The IR spectra of cyclobutyl, 1-methylallyl, and allylcarbinyl radicals, as well as 1,3-butadiene were recorded in the CH stretching region. Rapid cooling of the radicals to ~0.4 K by helium nanodroplet isolation prevents these highly reactive species from interconverting to other species on the time scale of the spectroscopic measurement. Pyrolysis of the respective nitrite precursors cleanly produces these radicals with little evidence of precursor signatures in the IR spectra. However, higher temperature pyrolysis of cyclobutylmethyl nitrite produces the cyclobutyl radical with enough internal energy to overcome the ring-opening barrier leading to 1-methylallyl and 1,3-butadiene + H.

Anharmonic frequencies for the cyclobutyl radical match best with experiment when they are computed at the higher-symmetry C_{2v} structure. The theoretical predictions for methylallyl agree well with experiment and suggest that both conformers contribute to the measured spectrum. Multiple bands within the experimental spectrum are also in agreement with previous measurements by Bahou et al. using solid-pH_2 matrix isolation.[24] Predictions for allylcarbinyl (3-buten-1-yl) radical are overall poor and not very useful in assigning the spectrum. A dedicated theoretical study of allylcarbinyl should prove interesting and useful. The orbital near-instabilities in these systems would likely be alleviated with some form of orbital-optimized electronic structure method.[58] It does not appear that allylcarbinyl is captured by the He droplets following the unimolecular ring-opening of the cyclobutyl radical, despite the fact that allylcarbinyl lies between cyclobutyl and 1,3-butadiene on the potential surface. Apparently, allylcarbinyl rearranges to methylallyl or undergoes H atom loss to produce 1,3-butadiene on a

timescale that is fast in comparison to the ~10 μs transit time of the radicals through the hot pyrolysis source. An unidentified band at 3018 cm^{-1} is produced following cyclobutyl ring-opening, which cannot be attributed to either cyclobutyl, methylallyl, allylcarbinyl radicals or 1,3-butadiene. Additional studies of other C_4H_7 isomers along this interesting potential energy surface, such as cyclopropylmethylcarbinyl and 1-buten-1-yl radicals, should be explored.

References

(1) Lin, Z. K.; Wang, T. F.; Han, D. L.; Han, X.; Li, S. F.; Li, Y. Y.; Tian, Z. Y. Study of Combustion Intermediates in Fuel-Rich Methyl Methacrylate Flame with Tunable Synchrotron Vacuum Ultraviolet Photoionization Mass Spectrometry. *Rapid Commun. Mass Spectrom.* **2009**, *23*, 85-92.

(2) Yang, B.; Oßwald, P.; Li, Y.; Wang, J.; Wei, L.; Tian, Z.; Qi, F.; Kohse-Höinghaus, K. Identification of Combustion Intermediates in Isomeric Fuel-Rich Premixed Butanol–Oxygen Flames at Low Pressure. *Combust. Flame.* **2007**, *148*, 198-209.

(3) Zhang, T.; Wang, J.; Yuan, T.; Hong, X.; Zhang, L.; Qi, F. Pyrolysis of Methyl Tert-Butyl Ether (MTBE). 1. Experimental Study with Molecular-Beam Mass Spectrometry and Tunable Synchrotron VUV Photoionization. *J. Phys. Chem. A.* **2008**, *112*, 10487-10494.

(4) Davis, S. G.; Law, C. K.; Wang, H. Propyne Pyrolysis in a Flow Reactor: An Experimental, RRKM, and Detailed Kinetic Modeling Study. *J. Phys. Chem. A.* **1999**, *103*, 5889-5899.

(5) Ribeiro, J. M.; Mebel, A. M. Reaction Mechanism and Product Branching Ratios of the CH + C_3H_6 Reaction: A Theoretical Study. *J. Phys. Chem. A.* **2016**, *120*, 1800-1812.

(6) Toennies, J. P.; Vilesov, A. F. Superfluid Helium Droplets: A Uniquely Cold Nanomatrix for Molecules and Molecular Complexes. *Angew. Chem.-Int. Edit.* **2004**, *43*, 2622-2648.

(7) Choi, M. Y.; Douberly, G. E.; Falconer, T. M.; Lewis, W. K.; Lindsay, C. M.; Merritt, J. M.; Stiles, P. L.; Miller, R. E. Infrared Spectroscopy of Helium Nanodroplets: Novel Methods for Physics and Chemistry. *Int. Rev. Phys. Chem.* **2006**, *25*, 15-75.

(8) Schultz, J. C.; Houle, F. A.; Beauchamp, J. L. Photoelectron Spectroscopy of Isomeric C_4H_7 Radicals. Implications for the Thermochemistry and Structures of the Radicals and Their Corresponding Carbonium Ions. *J. Am. Chem. Soc.* **1984**, *106*, 7336-7347.

(9) Pottie, R. F.; Harrison, A. G.; Lossing, F. P. Free Radicals by Mass Spectrometry. XXIV. Ionization Potentials of Cycloalkyl Free Radicals and Cycloalkanes. *J. Am. Chem. Soc.* **1961**, *83*, 3204-3206.

(10) Bowen, R. D.; Williams, D. H.; Schwarz, H.; Wesdemiotis, C. Experimental Evidence for the Existence of Gaseous Cyclobutyl Cation. *J. Chem. Soc.-Chem. Commun.* **1979**, *1*, 261-262.

(11) Gordon, A. S.; Drew, C. M.; Smith, S. R. Photolysis of Mixtures of Cyclobutane and Acetone-d_6. Reactions of the Cyclobutyl Radical. *J. Chem. Phys.* **1962**, *36*, 824-829.

(12) Bischof, P.; Friedrich, G. Pyrolyses of Azoalkanes. Photoelectron Spectra of Some Hydrocarbon Radicals. *Tetrahedron Lett.* **1985**, *26*, 2427-2430.

(13) Liu, Y.; Lau, K. C.; Butler, L. J. Photodissociation of Cyclobutyl Bromide at 234 nm Studied Using Velocity Map Imaging. *J. Phys. Chem. A.* **2006**, *110*, 5379-5385.

(14) Cacace, F.; Speranza, M. Proof of Existence of Cyclic $C_4H_7^+$ Ions in the Dilute Gas Phase. *J. Am. Chem. Soc.* **1979**, *101*, 1587-1589.

(15) Lossing, F. P. Free Radicals by Mass Spectrometry. XLV. Ionization Potentials and Heats of Formation of C_3H_3, C_3H_5, and C_4H_7 Radicals and Ions. *Can. J. Chem.-Rev. Can. Chim.* **1972**, *50*, 3973-3981.

(16) Lau, K. C.; Zheng, W. X.; Wong, N. B. Theoretical Prediction of the Ionization Energies of the C_4H_7 Radicals: 1-Methylallyl, 2-Methylallyl, Cyclopropylmethyl, and Cyclobutyl Radicals. *J. Chem. Phys.* **2007**, *127*, 12.

(17) Zhidomirov, G. M.; Abronin, I. A.; Micheikin, I. D.; Chuvylkin, N. D. Calculation of Isotropic Hyperfine Coupling Constants in Cyclobutyl Radical. *J. Magn. Reson.* **1975**, *17*, 161-165.

(18) Lau, K. C.; Liu, Y.; Butler, L. J. Photodissociation of 1-Bromo-2-Butene, 4-Bromo-1-Butene, and Cyclopropylmethyl Bromide at 234 nm Studied Using Velocity Map Imaging. *J. Chem. Phys.* **2006**, *125*, 15.

(19) McEwen, C. N.; Rudat, M. A. Isomerization of Gas-Phase Hydrocarbon Ions. Radical Trapping. 3. *J. Am. Chem. Soc.* **1981**, *103*, 4355-4359.

(20) Effio, A.; Griller, D.; Ingold, K. U.; Beckwith, A. L. J.; Serelis, A. K. Allylcarbinyl-Cyclopropylcarbinyl Rearrangement. *J. Am. Chem. Soc.* **1980**, *102*, 1734-1736.

(21) Chen, K. S.; Edge, D. J.; Kochi, J. K. Conformations and Rotation Barriers in Allylcarbinyl Radicals by Electron-Spin Resonance. *J. Am. Chem. Soc.* **1973**, *95*, 7036-7043.

(22) Montgomery, L. K.; Matt, J. W. Rearrangement of Allylcarbinyl Radical. *J. Am. Chem. Soc.* **1967**, *89*, 3050-3051.

(23) Montgomery, L. K.; Matt, J. W. Homolytic Free-Radical Rearrangements. IV. Rearrangements of Allylcarbinyl Radical. *J. Am. Chem. Soc.* **1967**, *89*, 6556-6564.

(24) Bahou, M.; Wu, J. Y.; Tanaka, K.; Lee, Y. P. Infrared Absorption of Trans-1-Chloromethylallyl and Trans-1-Methylallyl Radicals Produced in Photochemical Reactions of Trans-1,3-Butadiene and Cl_2 in Solid Para-Hydrogen. *J. Chem. Phys.* **2012**, *137*, 084310.

(25) Miller, J. L. Theoretical Study of the Straight-Chain C_4H_7 Radical Isomers and Their Dissociation and Isomerization Transition States. *J. Phys. Chem. A.* **2004**, *108*, 2268-2277.

(26) Lang, M.; Holzmeier, F.; Hemberger, P.; Fischer, I. Threshold Photoelectron Spectra of Combustion Relevant C_4H_5 and C_4H_7 Isomers. *J. Phys. Chem. A.* **2015**, *119*, 3995-4000.

(27) Gasser, M.; Frey, J. A.; Hostettler, J. M.; Bach, A. Probing for Non-Statistical Effects in Dissociation of the 1-Methylallyl Radical. *Chem. Commun.* **2011**, *47*, 301-303.

(28) Knyazev, V. D.; Slagle, I. R. Thermochemistry and Kinetics of the Reaction of 1-Methylallyl Radicals with Molecular Oxygen. *J. Phys. Chem. A.* **1998**, *102*, 8932-8940.

(29) Tarrant, D. H.; Getty, J. D.; Liu, X.; Kelly, P. B. Resonance Raman Spectroscopy of the 1-Methylallyl Radical. *J. Phys. Chem.* **1996**, *100*, 7772-7777.

(30) Dibble, T. S.; Sha, Y.; Thornton, W. F.; Zhang, F. Cis–Trans Isomerization of Chemically Activated 1-Methylallyl Radical and Fate of the Resulting 2-Buten-1-Peroxy Radical. *J. Phys. Chem. A.* **2012**, *116*, 7603-7614.

(31) Gorton, P. J.; Walsh, R. The Kinetics of Cis-Trans-Isomerization of 1-Methylallyl Radical: New Technique for Study of Unimolecular Radical Reactions. *J. Chem. Soc.-Chem. Commun.* **1972**, *1*, 783-784.

(32) Driscoll, D. J.; Martir, W.; Lunsford, J. H. Formation of Gas-Phase Methylallyl Radicals During the Oxidations of 1-Butene and Isobutylene Over Bismuth Oxide. *J. Phys. Chem.* **1987**, *91*, 3585-3588.

(33) Ismail, H.; Goldsmith, C. F.; Abel, P. R.; Howe, P. T.; Fahr, A.; Halpern, J. B.; Jusinski, L. E.; Georgievskii, Y.; Taatjes, C. A.; Green, W. H. Pressure and Temperature Dependence of the Reaction of Vinyl Radical with Ethylene. *J. Phys. Chem. A.* **2007**, *111*, 6843-6851.

(34) Lewerenz, M.; Schilling, B.; Toennies, J. P. A New Scattering Deflection Method For Determining and Selecting the Sizes of Large Liquid Clusters of He-4. *Chem. Phys. Lett.* **1993**, *206*, 381-387.

(35) Leavitt, C. M.; Moradi, C. P.; Acrey, B. W.; Douberly, G. E. Infrared Laser Spectroscopy of the Helium-Solvated Allyl and Allyl Peroxy Radicals. *J. Chem. Phys.* **2013**, *139*, 234301.

(36) Moradi, C. P.; Morrison, A. M.; Klippenstein, S. J.; Goldsmith, C. F.; Douberly, G. E. Propargyl + O_2 Reaction in Helium Droplets: Entrance Channel Barrier or Not? *J. Phys. Chem. A.* **2013**, *117*, 13626-13635.

(37) Raston, P. L.; Agarwal, J.; Turney, J. M.; Schaefer, H. F.; Douberly, G. E. The Ethyl Radical in Superfluid Helium Nanodroplets: Rovibrational Spectroscopy and Ab Initio Computations. **2013**, *138*, 194303.

(38) Franke, P. R.; Tabor, D. P.; Moradi, C. P.; Douberly, G. E.; Agarwal, J.; Schaefer, H. F.; Sibert, E. L. Infrared Laser Spectroscopy of the n-Propyl and i-Propyl Radicals: Stretch-Bend Fermi Coupling in the Alkyl CH Stretch Region. *J. Chem. Phys.* **2016**, *145*, 224304.

(39) Morrison, A. M.; Liang, T.; Douberly, G. E. Automation of an "Aculight" Continuous-Wave Optical Parametric Oscillator. *Rev. Sci. Instrum.* **2013**, *84*, 013102.

(40) Hernandez, F. J.; Brice, J. T.; Leavitt, C. M.; Liang, T.; Raston, P. L.; Pino, G. A.; Douberly, G. E. Mid-Infrared Signatures of Hydroxyl Containing Water Clusters: Infrared Laser Stark Spectroscopy of OH–H_2O and OH(D_2O)n (n = 1-3). *J. Chem. Phys.* **2015**, *143*, 164304.

(41) Raghavachari, K.; Trucks, G. W.; Pople, J. A.; Head-Gordon, M. A Fifth-Order Perturbation Comparison of Electron Correlation Theories. *Chem. Phys. Lett.* **1989**, *157*, 479-483.

(42) Hampel, C.; Peterson, K. A.; Werner, H.-J. A Comparison of the Efficiency and Accuracy of the Quadratic Configuration Interaction (QCISD), Coupled Cluster (CCSD), and Brueckner Coupled Cluster (BCCD) Methods. *Chem. Phys. Lett.* **1992**, *190*, 1-12.

(43) Watts, J. D.; Gauss, J.; Bartlett, R. J. Open-Shell Analytical Energy Gradients for Triple Excitation Many-Body, Coupled-Cluster Methods: MBPT(4), CCSD+T(CCSD), CCSD(T),and QCISD(T). *Chem. Phys. Lett.* **1992**, *200*, 1-7.

(44) Watts, J. D.; Gauss, J.; Bartlett, R. J. Coupled-Cluster Methods with Noniterative Triple Excitations for Restricted Open-Shell Hartree–Fock and Other General Single Determinant Reference Functions: Energies and Analytical Gradients. *J. Chem. Phys.* **1993**, *98*, 8718-8733.

(45) Deegan, M. J. O.; Knowles, P. J. Perturbative Corrections to Account for Triple Excitations in Closed and Open Shell Coupled Cluster Theories. *Chem. Phys. Lett.* **1994**, *227*, 321-326.

(46) Stanton, J. F. Why CCSD(T) Works: A Different Perspective. *Chem. Phys. Lett.* **1997**, *281*, 130-134.

(47) Almlöf, J.; Taylor, P. R. General Contraction of Gaussian Basis Sets. I. Atomic Natural Orbitals for First- and Second-Row Atoms. *J. Chem. Phys.* **1987**, *86*, 4070-4077.

(48) CFOUR, A Quantum Chemical Program Package Written by, J. F. Stanton, J. Gauss, M. E. Harding, P. G. Szalay with Contributions from A. A. Auer, R. J. Bartlett, U. Benedikt, C. Berger, D. E. Bernholdt, Y. J. Bomble, et. al., and the Integral Packages Molecule (J. Almlöf and P. R. Taylor), Props (P. R. Taylor), Abacus (T. Helgaker, H. J. Aa. Jensen, P. Jørgensen, and J. Olsen), and ECP Routines by A. V. Mitin and C. Van Wüllen.

(49) Nielsen, H. H. The Vibration-Rotation Energies of Molecules. *Rev. Mod. Phys.* **1951**, *23*, 90-136.

(50) Clabo, D. A.; Allen, W. D.; Remington, R. B.; Yamaguchi, Y.; Schaefer, H. F. A Systematic Study of Molecular Vibrational Anharmonicity and Vibration—Rotation Interaction by Self-Consistent-Field Higher-Derivative Methods: Asymmetric Top Molecules. *J. Chem. Phys.* **1988**, *123*, 187-239.

(51) Matthews, D. A.; Vázquez, J.; Stanton, J. F. Calculated Stretching Overtone Levels and Darling–Dennison Resonances in Water: A Triumph of Simple Theoretical Approaches. *Mol. Phys.* **2007**, *105*, 2659-2666.

(52) Rosnik, A. M.; Polik, W. F. VPT2+K Spectroscopic Constants and Matrix Elements of the Transformed Vibrational Hamiltonian of a Polyatomic Molecule with Resonances Using Van Vleck Perturbation Theory. *Mol. Phys.* **2014**, *112*, 261-300.

(53) Gauss, J.; Stanton, J. F. Analytic CCSD(T) Second Derivatives. *Chem. Phys. Lett.* **1997**, *276*, 70-77.

(54) Schneider, H.; Vogelhuber, K. M.; Schinle, F.; Stanton, J. F.; Weber, J. M. Vibrational Spectroscopy of Nitroalkane Chains Using Electron Autodetachment and Ar Predissociation. *J. Phys. Chem. A.* **2008**, *112*, 7498-7506.

(55) Wolfram Research Inc., Mathematica, Version 10.0, Champaign, IL (2014).

(56) Martin, J. M. L.; Lee, T. J.; Taylor, P. R.; François, J. P. The Anharmonic Force Field of Ethylene, C_2H_4, by Means of Accurate Ab Initio Calculations. *J. Chem. Phys.* **1995**, *103*, 2589-2602.

(57) Crawford, T. D.; Stanton, J. F.; Allen, W. D.; Henry F. Schaefer, I. Hartree–Fock Orbital Instability Envelopes in Highly Correlated Single-Reference Wave Functions. *J. Chem. Phys.* **1997**, *107*, 10626-10632.

(58) Szalay, P. G.; Vázquez, J.; Simmons, C.; Stanton, J. F. Triplet Instability in Doublet Systems. *J. Chem. Phys.* **2004**, *121*, 7624-7631.

(59) Grimme, S. Semiempirical Hybrid Density Functional with Perturbative Second-Order Correlation. *J. Chem. Phys.* **2006**, *124*, 034108.

(60) Bloino, J.; Biczysko, M.; Barone, V. General Perturbative Approach for Spectroscopy, Thermodynamics, and Kinetics: Methodological Background and Benchmark Studies. *J. Chem. Theory Comput.* **2012**, *8*, 1015-1036.

(61) Becke, A. D. Density-Functional Thermochemistry. III. The Role of Exact Exchange. *J. Chem. Phys.* **1993**, *98*, 5648-5652.

(62) Frisch, J.; Trucks, G. W.; Schlegel, H. B.; Scuseria, G. E.; Robb, M. A.; Cheeseman, J. R.; Scalmani, G.; Barone, V.; Mennucci, B.; Petersson, G. A.; et. al., *Gaussian 09*, Revision E.01; Gaussian, Inc.: Wallingford, CT, USA, 2009.

(63) Ayala, P. Y.; Schlegel, H. B. A Nonorthogonal CI Treatment of Symmetry Breaking in Sigma Formyloxyl Radical. *J. Chem. Phys.* **1998**, *108*, 7560-7567.

(64) Hrušák, J.; Iwata, S. The Vibrational Spectrum of $H_2O_2^{+\cdot}$ Radical Cation: An Illustration of Symmetry Breaking. *J. Chem. Phys.* **1997**, *106*, 4877-4888.

(65) Meyer, R.; Günthard, H. H. General Internal Motion of Molecules, Classical and Quantum-Mechanical Hamiltonian. *J. Chem. Phys.* **1968**, *49*, 1510-1520.

(66) Lewis, J. D.; Malloy, T. B.; Chao, T. H.; Laane, J. Periodic Potential Functions for Pseudorotation and Internal Rotation. *J. Mol. Struct.* **1972**, *12*, 427-449.

(67) Rush, D. J.; Wiberg, K. B. Ab Initio CBS-QCI Calculations of the Inversion Mode of Ammonia. *J. Phys. Chem. A.* **1997**, *101*, 3143-3151.

CHAPTER 4

INFRARED SPECTRUM OF FULVENALLENE AND FULVENALLENYL IN HELIUM DROPLETS

Fulvenallene is the global minimum on the C_7H_6 potential energy surface. Rearrangement of fulvenallene to other C_7H_6 species and dissociation to produce fulvenallenyl radical (C_7H_5) is carried out in a continuous-wave SiC pyrolysis furnace at 1500 K. Prompt pick-up and solvation by helium droplets allows for the acquisition of vibrational spectra of these species in the CH stretching region. Anharmonic frequencies for fulvenallene, fulvenallenyl, and three isomers of ethynylcyclopentadiene are computed *ab initio*; VPT2+K spectral simulations are based on hybrid CCSD(T) force fields with quadratic (cubic and quartic) force constants computed using the ANO1 (ANO0) basis set. The acetylenic CH stretch of the fulvenallenyl radical is a sensitive marker of the extent by which the unpaired electron is delocalized throughout the conjugated propargyl and cyclopentadienyl subunits. The nature of this electron delocalization is explored with spin density calculations at the ROHF-CCSD(T)/ANO1 level of theory. Atomic partitioning of the spin density allows for a description of the fulvenallenyl radical in terms of two resonance structures: fulvenallenyl is approximately 24% allenic and 76% acetylenic.

4.1 Introduction

It is now accepted that fulvenallene is the most stable C_7H_6 isomer.[1-3] Experimental and theoretical studies have shown fulvenallene to be a major decomposition product of toluene[3-6] and benzyl radical.[7-11] In cyclopentene flames, photoionization mass spectrometry confirmed significant quantities of C_7H_6, and photoionization efficiencies were used to assign these species to fulvenallene and/or 1-ethynylcyclopentadiene.[4] Due to its high reactivity and abundance in flames, fulvenallene and its dissociation/isomerization products have been implicated as important intermediates in the formation and molecular weight growth chemistry of polycyclic aromatic hydrocarbons (PAHs).[12-14] In this report, we employ helium droplet isolation spectroscopy to show that pyrolysis of fulvenallene at 1500 K produces the fulvenallenyl radical as a dissociation product; moreover spectroscopic evidence for the production of multiple isomerization products is also observed.

Cavallotti and co-workers have reported a detailed analysis of the C_7H_6 potential energy surface; for fulvenallene, they computed energetics for its decomposition and its interconversion.[2, 3] Two separate fulvenallene decomposition pathways have been discussed: either loss of an allenic H-atom to form fulvenallenyl or formation of cyclopentadienylidene (C_5H_4) and acetylene.[3, 15] Barrierless homolytic bond rupture producing H + fulvenallenyl is the lowest energy channel, involving an 82.5 kcal/mol thermodynamic barrier from the fulvenallene minimum.[3, 13] The second pathway towards cyclopentadienylidene and acetylene requires an intersystem crossing from the singlet to triplet surface prior to its dissociation over an 96.0 kcal/mol exit barrier.[3] In experimental

248 and 193 nm photodissociation studies, Ramphal *et al*. found that fulvenallene dissociation produces fulvenallenyl exclusively, indicating a low probability for intersystem crossing.[16]

Fulvenallene has been probed with rotational spectroscopy[17] and gas-phase infrared (IR) spectroscopy.[18] The IR spectrum was obtained at room temperature with a grating based spectrometer having a few cm^{-1} resolution. Additionally, photoelectron spectroscopy revealed the ionization energy to be 8.22 eV (adiabatic)[19, 20] and 8.29 eV (vertical).[21]

Fulvenallenyl is the global minimum on the C_7H_5 potential energy surface.[12] As a resonantly stabilized system delocalized over allenic and acetylenic limiting structures (Figure 1), fulvenallenyl is believed to be relatively long lived within flame environments, which enhances the probability for self-reactions.[13] Computations predict that fulvenallenyl self-reactions can produce 2 and 3 ring PAH species directly.[13]

Many theoretical studies[2, 3, 9, 12-14, 22] have been carried out for the fulvenallenyl radical, but experimental studies are lacking.[16, 22-24] The electronic spectrum of fulvenallenyl in a neon matrix was recorded following mass selective deposition of its anion and UV irradiation.[24] The $1\ ^2B_1 \leftarrow X\ ^2B_1$ transition was observed at $\lambda = 401.3$ nm along with 3 vibrational bands at 365 (ν_{19}), 1984 (ν_4), and 3958 cm^{-1} ($2\nu_4$). Photoelectron spectroscopy of fulvenallenyl determined its adiabatic ionization energy to be 8.19 eV.[19] The photodissociation dynamics of fulvenallenyl were also studied at 248 and 193 nm.[16] Two dissociation channels were observed at both wavelengths: production of C_5H_3 radical and acetylene, and formation of diacetylene and propargyl radical.

We report here an IR spectroscopy study of fulvenallene and its decomposition and rearrangement products following its pyrolysis in a 1500 K SiC furnace. Helium droplets passing by the exit of the pyrolysis furnace capture the gas-phase molecules and rapidly quench their internal energy, producing an equilibrium molecular ensemble at 0.4 K. This allows for the acquisition of well-resolved vibrational spectra. Spectra are compared to high-level anharmonic frequency computations for fulvenallene, fulvenallenyl and three geometric isomers of ethynylcyclopentadiene (ECPD). The electronic structure of the fulvenallenyl radical is investigated with quantum chemistry, revealing the nature of the electron delocalization that leads to resonance stabilization.

4.2 Experimental Section

The helium nanodroplet apparatus has been described in detail elsewhere.[25] Helium nanodroplets are formed by the continuous expansion of chromatographic grade helium (99.9999%) through a 5 μm diameter nozzle. A backing pressure of 35 bar and a nozzle temperature of 17 K leads to the production of droplets having approximately 4000-6000 atoms.[26] The droplet expansion is skimmed into a second chamber, which contains a pyrolysis source situated perpendicular to the path of the droplet beam. Fulvenallene was chosen as a pyrolysis precursor for the production of fulvenallenyl. Gaseous fulvenallene was synthesized by flash vacuum pyrolysis of homophthalic anhydride vapor and purified by trap-to-trap distillation, according to previously reported methods.[16, 23, 27] Thermal decomposition and rearrangement products of fulvenallene were produced as the gas passed through the hot-zone of a continuous-wave SiC pyrolysis

source (10 mm length, 1 mm inner diameter) heated to ~1500 K (4.8 amps).[28] The fulvenallene density in the pyrolysis source (~10^{10} cm^{-3}) was optimized such that droplets captured either nothing or a single dopant as they passed by the outlet of the SiC furnace. Dopants captured by the droplets are rapidly cooled to 0.4 K via He atom evaporation.[29, 30]

After this process, the droplet beam travels downstream where it interacts with counterpropagating IR light from an optical parametric oscillator laser system.[31] Resonant vibrational excitation of helium-solvated molecules results in the evaporation of He atoms as the excess vibrational energy is quenched (1 atom for every ~5 cm^{-1} of energy).[30] Photo-induced He-atom loss leads to a reduction in the geometric and ionization cross sections of the droplets, the latter of which is detected by monitoring ion signal using a quadrupole mass spectrometer. A lock-in amplifier processes the ion current associated with a specified mass channel (*vide infra*) while the IR beam is chopped at 80 Hz and tuned from 2800 to 3400 cm^{-1}. The recorded spectrum corresponds to the ion signal difference with and without the laser present, which is then normalized to the laser power. When comparisons are available, it has been shown that the vibrational band origins of hydrocarbon molecules in helium droplets are usually within 1 cm^{-1} of the gas-phase values; this allows for the direct comparison of band origins measured in helium droplets to those predicted *ab initio*.

4.3 Computational Details

4.3.1 VPT2+K

All electronic structure computations were performed using the CFOUR package.[32] The CCSD(T)[33-35] method, combined with the atomic natural orbital basis sets[36]ANO0 and ANO1, was used for all species considered: fulvenallene, fulvenallenyl, and the three isomers of ethynylcyclopentadiene, all of which are shown in Figure 4.1. Optimized geometries and harmonic frequencies were computed with both basis sets; semi-diagonal quartic force fields were computed only with the ANO0 basis set. Infrared spectra were simulated with the VPT2+K (Second-Order Vibrational Perturbation Theory with Resonances) method,[37-39] implemented with in-house Mathematica scripts.[40] This method has been reviewed,[37] and details of its application to the CH stretching spectra of hydrocarbons can be found elsewhere.[41-43] Most interactions were treated with perturbation theory, but couplings between CH stretch fundamentals and overtones/combinations of high frequency bending modes were treated explicitly, in addition to couplings with select 3 and 4-quanta states.[39, 44] The electrical harmonicity approximation was made. For each molecule studied, the ANO1 harmonic frequencies were substituted for their ANO0 counterparts in the quartic force fields.[44]

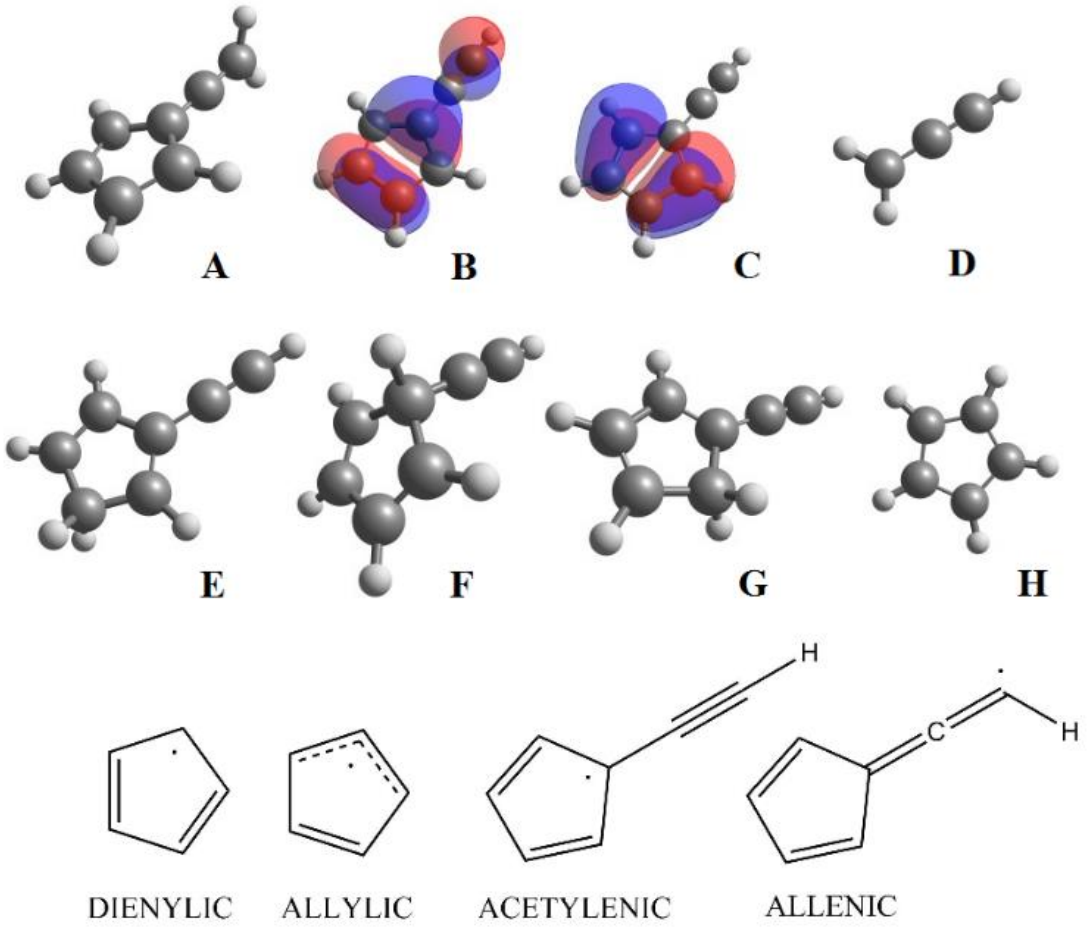

Figure 4.1: Structures and orbitals of theoretically investigated molecules and bonding nomenclature. (A) fulvenallene (B) B_1 fulvenallenyl SOMO (C) A_2 fulvenallenyl SOMO (D) propargyl (E) 2-ethynylcyclopentadiene (F) 5-ethynylcyclopentadiene (G) 1-ethynylcyclopentadiene (H) cyclopentadienyl. The four bonding patterns discussed in the text are shown schematically: dienylic, allylic, acetylenic, and allenic. The fulvenallenyl radical can be viewed as a *resonantly stabilized free radical* (RSFR), for which the electron density is delocalized and characterized as a superposition between acetylenic and allenic resonance structures.

4.3.2 Fulvenallenyl Electronic Structure

For fulvenallenyl, both UHF and ROHF reference wavefunctions were tested. Because of the significant amount of spin contamination found with UHF ($\langle S^2 \rangle > 1.1$), an ROHF reference was the preferred choice. It has been shown that near-instabilities in the reference wavefunction can degrade the accuracy of computed force constants for open-shell systems, especially those containing double and triple bonds.[45] We checked for this in one dimension: the CC "triple" bond stretching normal coordinate, as the harmonic frequencies associated with this coordinate displayed a significant reference wavefunction dependence. The CCSD(T)/ANO1 harmonic frequencies were 2108 cm^{-1} and 2069 cm^{-1} with UHF and ROHF references, respectively. A plot of both potential functions and their second derivatives is shown in Figure 4.2. Energy points were calculated with both UHF- and ROHF-CCSD(T)/ANO1, along the HF-CCSD(T)/ANO0 CC triple bond stretching normal coordinate. The quadratic force constants are found to be 2122 (UHF) and 2044 (ROHF) cm^{-1} when evaluated in the UHF-CCSD(T)/ANO0 normal coordinate, similar to the exact CCSD(T)/ANO1 harmonic frequencies. The potential energy surfaces are continuous in this energy regime, and they have second derivatives that are nearly linear. This is normal behavior, and it leads us to trust that wavefunction instabilities are not a concern for the computation of fulvenallenyl harmonic frequencies (at least not for this coordinate). Because of the spin contamination in the UHF reference and because neither CC stretching force constant displayed unphysical behavior in the region around the equilibrium geometry, an ROHF-based force field was used in anharmonic simulations.

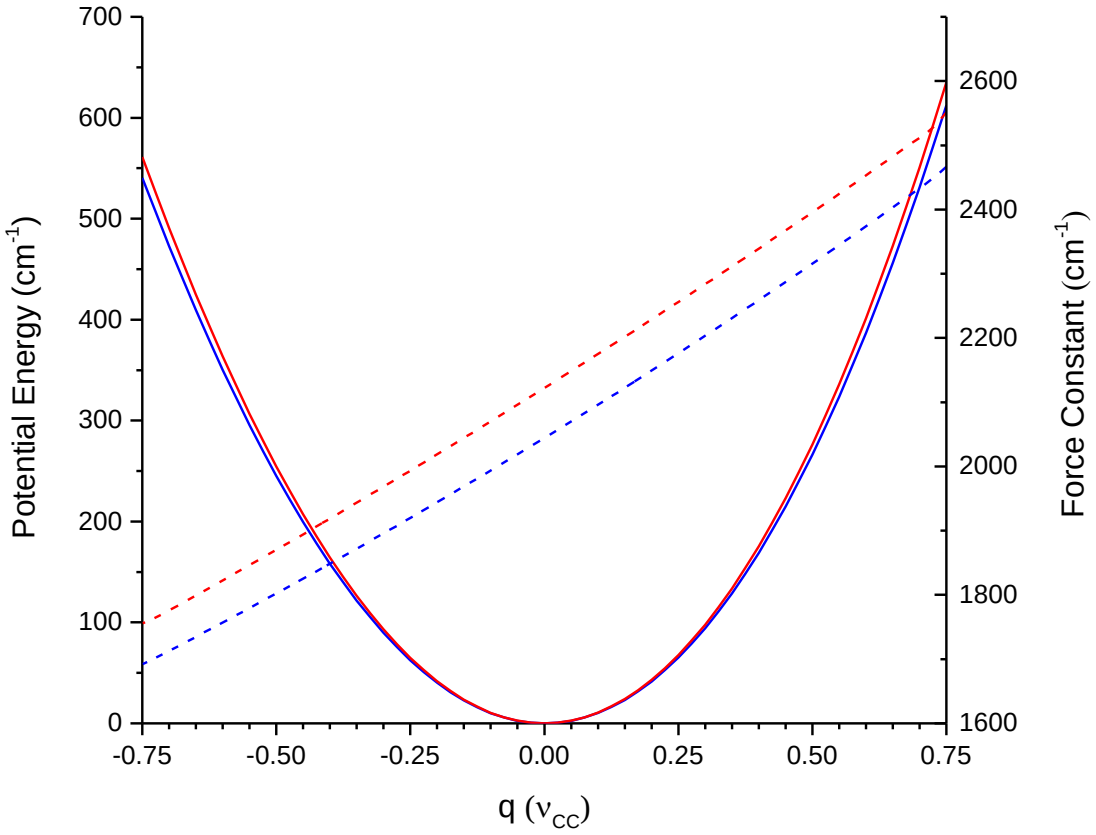

Figure 4.2: Plot of the CCSD(T)/ANO1 potential energy (primary Y-axis) using UHF (red) and ROHF (blue) reference wavefunctions. Displacements are made, from the corresponding equilibrium structures, in the UHF-CCSD(T)/ANO0 dimensionless normal coordinate associated with acetylenic CC bond stretching. The second derivatives of the potentials are plotted on the secondary Y-axis; these correspond roughly with the CCSD(T)/ANO1 harmonic frequencies when q = 0.

The electronic symmetry of ground state fulvenallenyl radical was not assumed to be known. Various orbital occupations were considered, spanning all four irreducible representations of the C_{2v} point group. No stable structures of A_1 electronic symmetry were identified, and B_2 electronic states were quite high in energy. The ground state was identified as having B_1 symmetry, in agreement with previous theoretical work.[24] However, a low-lying A_2 symmetry electronic state was also found. It was less than 8,000 cm^{-1} higher in energy than the B_1 state, at the B_1 optimized geometry. Upon optimizing the geometry and comparing adiabatic energy differences, the A_2 state was found to lie only 1471 cm^{-1} above the ground electronic state (ROHF-CCSD(T)/ANO0).

CCSD(T) computations predicted the A_2 structure to be a minimum, having one unusually large B_1 symmetry ring-stretching harmonic frequency. In order to investigate this further, we used EOMIP-CCSD,[46] with the closed shell anion as the reference. With this method, the A_2 structure is now a transition state, with a B_1 symmetry imaginary mode similar to the ring-stretch found by CCSD(T) to have a very large frequency. Accordingly, we relaxed symmetry constraints and attempted to reoptimize the A_2 structure to a C_s minimum, but all attempts to do so resulted in optimization to the B_1 ground state structure, which has the same symmetry (A'') in C_s space.

We decided that the A_2 stationary point does not actually represent a unique conformer of fulvenallenyl; rather, we view it as a vestige of the Jahn-Teller cyclopentadienyl radical potential surface. On the cyclopentadienyl potential, 5 equivalent allylic transition states connect 5 equivalent dienylic wells in the brim of a Mexican hat (see Figure 4.1 for structures associated with this nomenclature).[47, 48] The allylic stationary points are so named because they have a resonantly-stabilized allyl

moiety. The dienylic bonding pattern instead resembles cyclopentadiene, having a pair of conjugated C=C bonds and a more localized radical site. Ethynyl substitution, yielding fulvenallenyl, reshapes the potential surface, breaking the fivefold symmetry and washing out much of this structure. In fulvenallenyl, a single A_2 allylic saddle point serves to carry the dienylic B_1 equilibrium structure back into itself, during a planar pseudorotational process. The A_2 saddle point represents the barrier to this process (1893 cm^{-1} at EOMIP-CCSD/ANO1). Further exploratory computations were performed for the allylic and dienylic cyclopentadienyl stationary points to test the behavior of the applied levels of theory. For cyclopentadienyl, similar to fulvenallenyl, CCSD(T) predicts that both the allylic and dienylic structures are minima; whereas, the EOMIP-CCSD potential surface shows dienylic minima connected by allylic saddle points (located 0.3 cm^{-1} above the minima), each one possessing a ring stretching frequency of about 40 cm^{-1} (40*i* for the allylic points).

Attempts to locate other C_s stationary points were also made. These were envisioned to be similar to the other 8 (equivalent by symmetry) stationary points of cyclopentadienyl. Guess structures were generated, adjusting the CC bond lengths in the ring such that they exhibited either allylic or dienylic bonding patterns. Then they were optimized, constrained to at least C_s symmetry. All optimizations to a minimum returned to the B_1 equilibrium structure. Optimizations targeting allylic transition states either failed to converge or found the A_2 transition state. We conclude that C_s symmetry minima either do not exist or are exceedingly shallow.

Because of its prediction of an A_2 electronic "allylic" minimum, one may be skeptical of the ability of CCSD(T) to describe fulvenallenyl. Comparisons between the

harmonic frequencies of the B_1 equilibrium structure, obtained with EOMIP-CCSD and ROHF-CC methods reveal far more commonalities than differences (Table S1). The similarity of the harmonic frequencies between EOMIP-CCSD and ROHF-CCSD suggests to us that the EOM family of methods (and their capacity to correctly describe strong electronic couplings) are not essential for predictions of the fulvenallenyl vibrational spectrum. In addition to this, CASSCF computations were performed in the full π space (9 electrons in 9 orbitals), with ORCA.[49-52] Using the cc-pVTZ basis[53] set, we found that the leading configuration comprises 84% of the total wavefunction, and the next most significant configuration, a double-excitation, accounts for only 1.5%. On the basis of these calculations, we feel that a highly-correlated single reference method is appropriate for predicting fulvenallenyl's CH stretch fundamentals.

4.4 Results and Discussion

4.4.1 C_7H_6 Potential Energy Surface

Figure 4.3 shows a simplified zero-Kelvin enthalpic potential energy surface adapted from Cavallotti and co-workers.[2, 3] In addition to fulvenallene, the C_7H_6 global minimum (C_{2v} symmetry), three C_s symmetry ethynylcyclopentadiene isomers are present. Computations by Polino *et al.* confirm that fulvenallenyl (+H) formation represents the lowest energy fulvenallene dissociation pathway. The thermodynamic barrier for fulvenallenyl formation *via* H-atom loss is 82.5 kcal/mol. This energy is also sufficient to overcome the H-atom transfer barrier leading directly to 1-ECPD. The

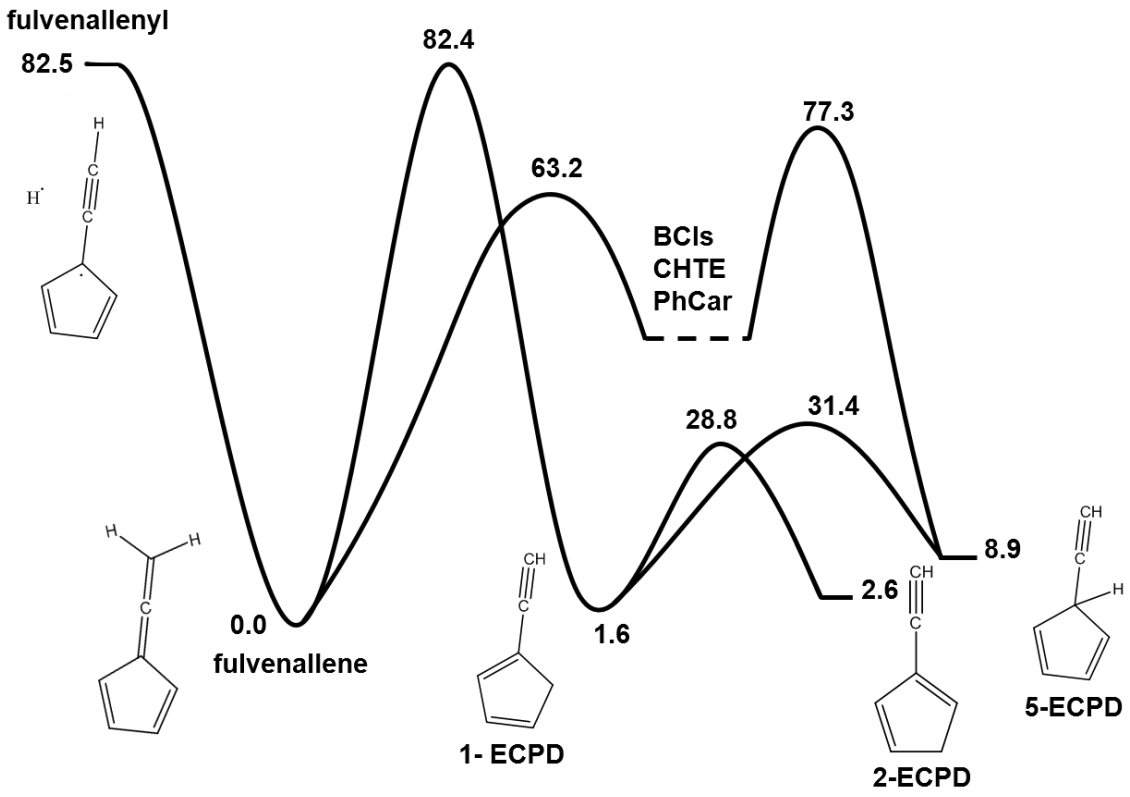

Figure 4.3: Schematic C_7H_6 potential energy surface (kcal/mol). The surface is adapted from previous works by Polino, Famulari, and Cavallotti.[2, 3] BCIs, CHTE, PhCar, and ECPD are acronyms for bicyclic intermediates, cycloheptatetraene, phenylcarbene, and ethynylcyclopentadiene respectively. The transition state at 77.3 kcal/mol separates PhCar and 5-ECPD.

1-ECPD species can rearrange to form 2- and 5-ECPD *via* barriers lying lower in energy (28.8 and 31.4 kcal/mol, respectively). A lower energy interconversion pathway (77.3 kcal/mol barrier) leading to 5-ECPD has been discussed in detail by Polino *et al*. This pathway involves a rather complicated rearrangement of fulvenallene to a series of bicyclic species, cycloheptatetraene, and singlet phenylcarbene, which ring-opens to form 5-ECPD. It has been shown definitively in previous mass-selected photoelectron spectroscopy studies that pyrolysis of fulvenallene in a 1500 K SiC furnace leads to the production of fulvenallenyl.[19, 22] Therefore, we fully expect that our source, being similar in design, will also produce fulvenallenyl; nevertheless, given the computed barrier heights, our analysis of IR spectra also considers the possibility that other species, such as ECPD, are produced *via* the rearrangement of fulvenallene.

4.4.2 Mass Spectrometry

The ionization of doped helium droplets by electron bombardment has been described previously.[30, 54] In short, He cluster ions are formed from electron impact ionization of pure droplets *via* the mechanism given in equation 4.1.

$$(He)_n + e^- \rightarrow He^+(He)_{n-1} + 2e^- \rightarrow He_2^+(He)_{n-2} + 2e^- \rightarrow He_m^+ + (n-m)(He) + 2e^- \quad \textbf{(Eq. 4.1)}$$

For doped He droplets, charge transfer ionization (equation 4.2) may also occur in competition with the production of He cluster ions.

$$(M)(He)_m + e^- \rightarrow (M)(He)^+(He)_{m-1} + 2e^- \rightarrow (M)^{+*} + m(He) + 2e^- \quad \textbf{(Eq. 4.2)}$$

The large energetic mismatch between the He and dopant ionization potentials typically leads to the complete desolvation and fragmentation of the molecular ion.

Figure 4.4 shows the mass spectra associated with the neat He droplet beam (trace A) and the precursor doped droplet beam under cold pyrolysis conditions (trace B). In the neat droplet spectrum, only He_n^+ ions are observed above 59 u. Upon doping fulvenallene into the droplets (under conditions that render fulvenallene dimer formation negligible), clusters of peaks are observed in the vicinity of 63 u ($C_5H_3^+$) and 89 u ($C_7H_5^+$). Most of these peaks arise from the charge transfer ionization and fragmentation of fulvenallene, evidence of which is shown in Figure 4.5. Fulvenallene is synthesized directly from the pyrolysis of homophthalic anhydride, but the sample is not completely free from contaminants. For example, water can be co-trapped with fulvenallene during the final stages of synthesis, which explains the increase in mass 18 u in going from trace A to B. Furthermore, over the course of a few days, the peaks at 90, 91 and 92 u increase relative to 89 u, presumably due to the low stability of the room temperature fulvenallene sample.[23] We note that peaks at 90, 91, and 92 u were previously observed in the electron ionization mass spectrum of a molecular beam produced *via* a similarly synthesized fulvenallene sample.[16]

4.4.3. Infrared Spectroscopy (2800 – 3140 cm^{-1})

Because 89 u appears as the most intense signature of He-solvated fulvenallene, an IR spectrum from 2800 − 3140 cm^{-1} was first recorded by monitoring ion depletion in this channel. We note, however, that the same spectrum was subsequently reproduced on

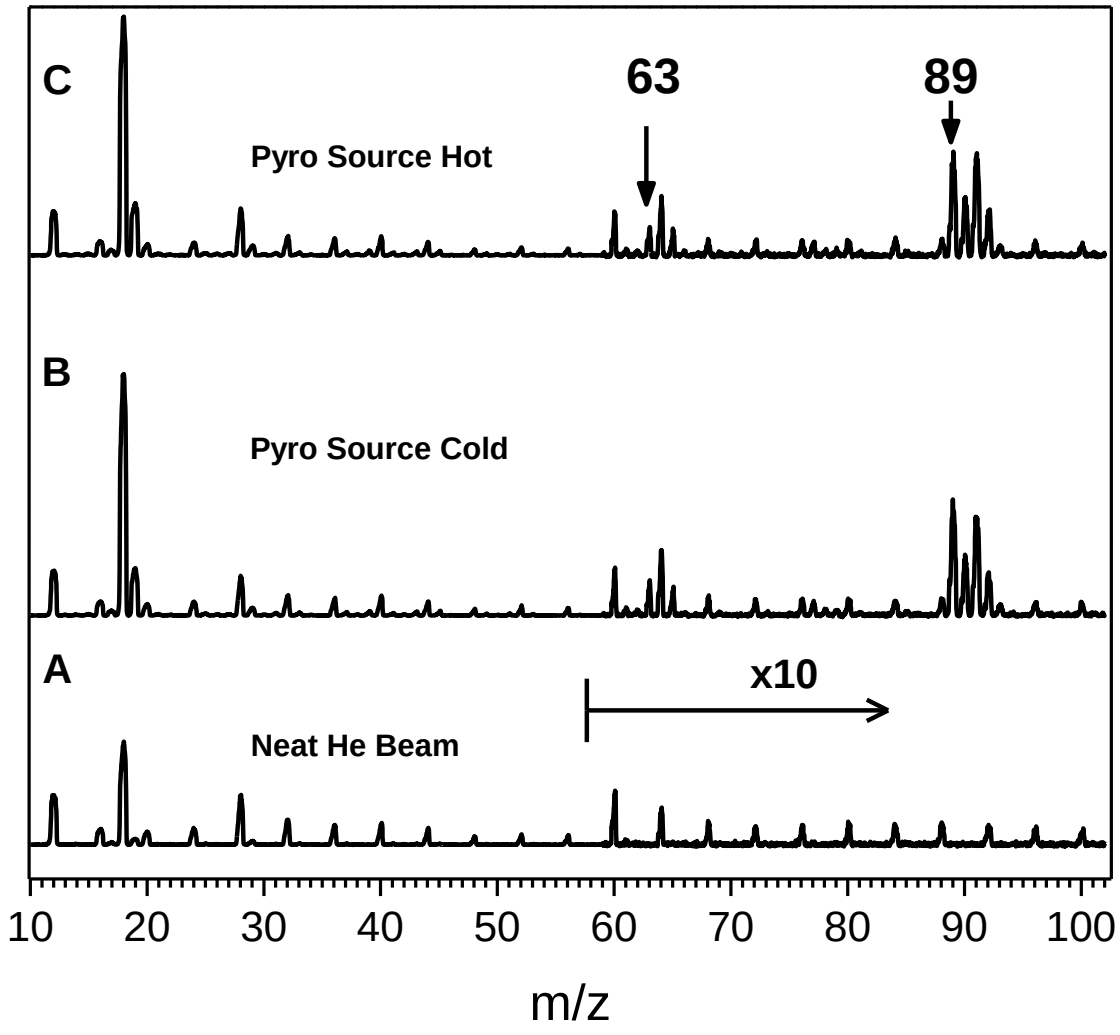

Figure 4.4: (A) Electron ionization mass spectrum of the neat droplet beam, showing peaks every 4 u (He_n^+ ions) and residual water at 18 u. (B) Mass spectrum of droplets doped with fulvenallene, which was metered into the apparatus through the cold pyrolysis tube. (C) Mass spectrum of droplets doped with pyrolysis products resulting from the thermal decomposition of fulvenallene; the only significant change in going from cold to hot source conditions is a slight reduction in 89 u. The IR spectrum of fulvenallene was recorded by monitoring depletion of either 63 or 89 u, whereas the acetylenic CH stretch band observed for the fulvenallenyl radical could only be observed as a depletion in channel 63 u (see text).

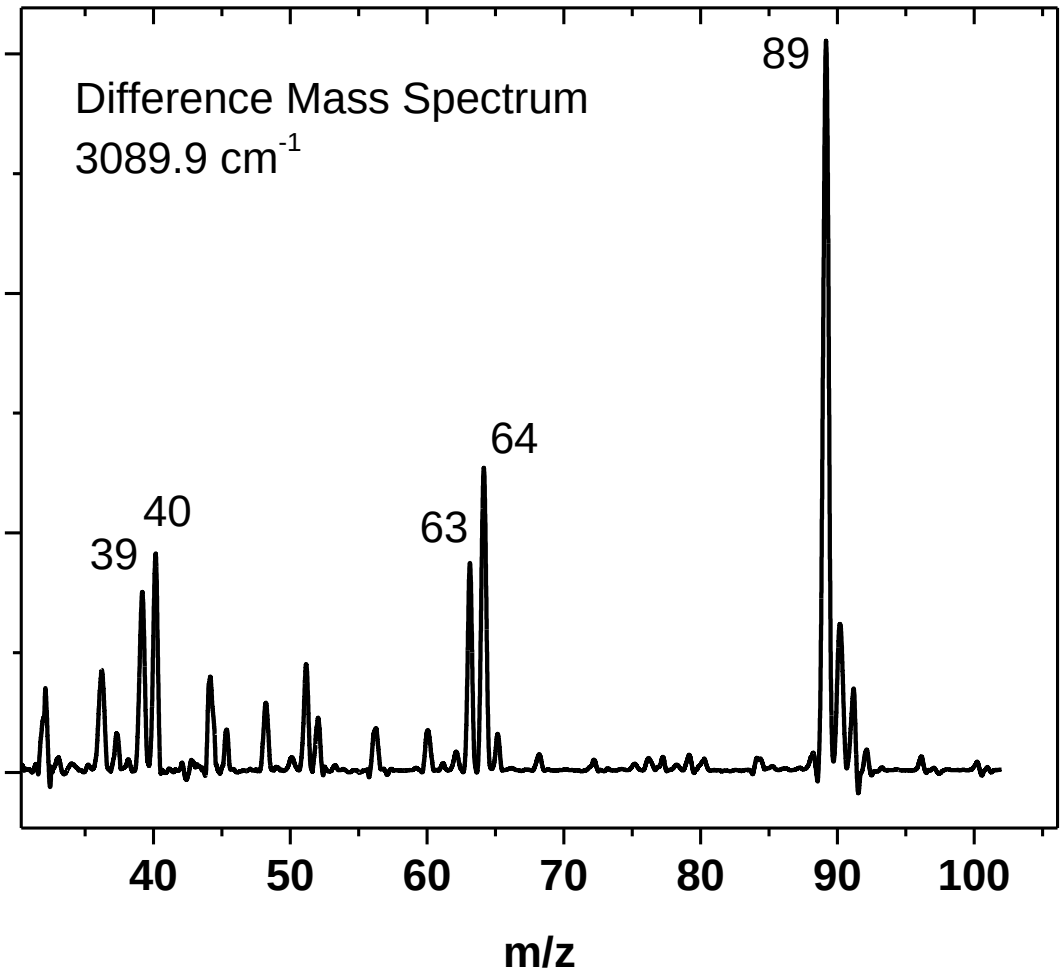

Figure 4.5: Difference depletion mass spectra measured with the laser frequency fixed to 3089.9 cm^{-1}. With the pyrolysis source at room temperature, the IR laser is tuned to 3089.9 cm^{-1}, *i.e.* the most intense resonant frequency for fulvenallene. The laser frequency is fixed and amplitude modulated at 80 Hz while the quadrupole mass spectrometer is slowly scanned across all mass channels. When processed with a lock-in amplifier, the resulting *difference* mass spectrum corresponds to the electron-impact ionization mass spectrum of *only* the subset of droplets that contain resonantly excited molecules. In this figure, mass channel 89 is by far the most intense, indicating that this channel carries the largest laser-induced ion depletion signal at 3089.9 cm^{-1} when the pyrolysis source is kept at room temperature, *i.e.* indicating that this is the largest mass channel associated with fulvenallene doped helium droplets.

63 u, albeit with a poorer signal to noise ratio (Figure 4.6). The 89 u depletion spectrum is shown in Figure 4.7, along with an inset showing intense features centered near 3090 cm^{-1} and a diagram of fulvenallene having labels relevant to the vibrational band assignments summarized in Table 4.1. In addition to the more intense features above 3089 cm^{-1}, there are many weak, reproducible features observed at lower energy. The assignments suggested in Table 4.1 are based on comparisons to our VPT2+K computations. Many of the more intense bands observed in the helium droplet spectrum were previously observed in a lower resolution gas-phase spectrum,[18] and where available, gas-phase band origins are compared to the droplet spectra in Table 4.1. A comprehensive list of fulvenallene harmonic frequencies and mode descriptions is given in Table 4.2.

Figure 4.4 C shows that there is very little change in the mass spectrum in going from cold to hot pyrolysis source conditions, despite the source being turned up towards its highest operating temperature. The most obvious change is a small reduction in the intensity of mass 89 u. Because nothing in the mass spectrum appeared to be "growing in" as the SiC temperature was raised, we initially chose to measure the hot pyrolysis IR spectrum as depletion in channel 89 u. Figure 4.8 shows the comparison between the cold and hot pyrolysis 89 u depletion spectra between 3000 and 3140 cm^{-1}. As shown clearly in the inset, in addition to all of the bands observed in the cold pyrolysis spectrum, two additional features appear at 3058 and 3074 cm^{-1} in the hot pyrolysis spectrum. A spectrum was also measured as depletion in channel 63 u for both cold and hot pyrolysis conditions (Figure 4.6). There are no discernible differences between the two spectra on channel 63 u.

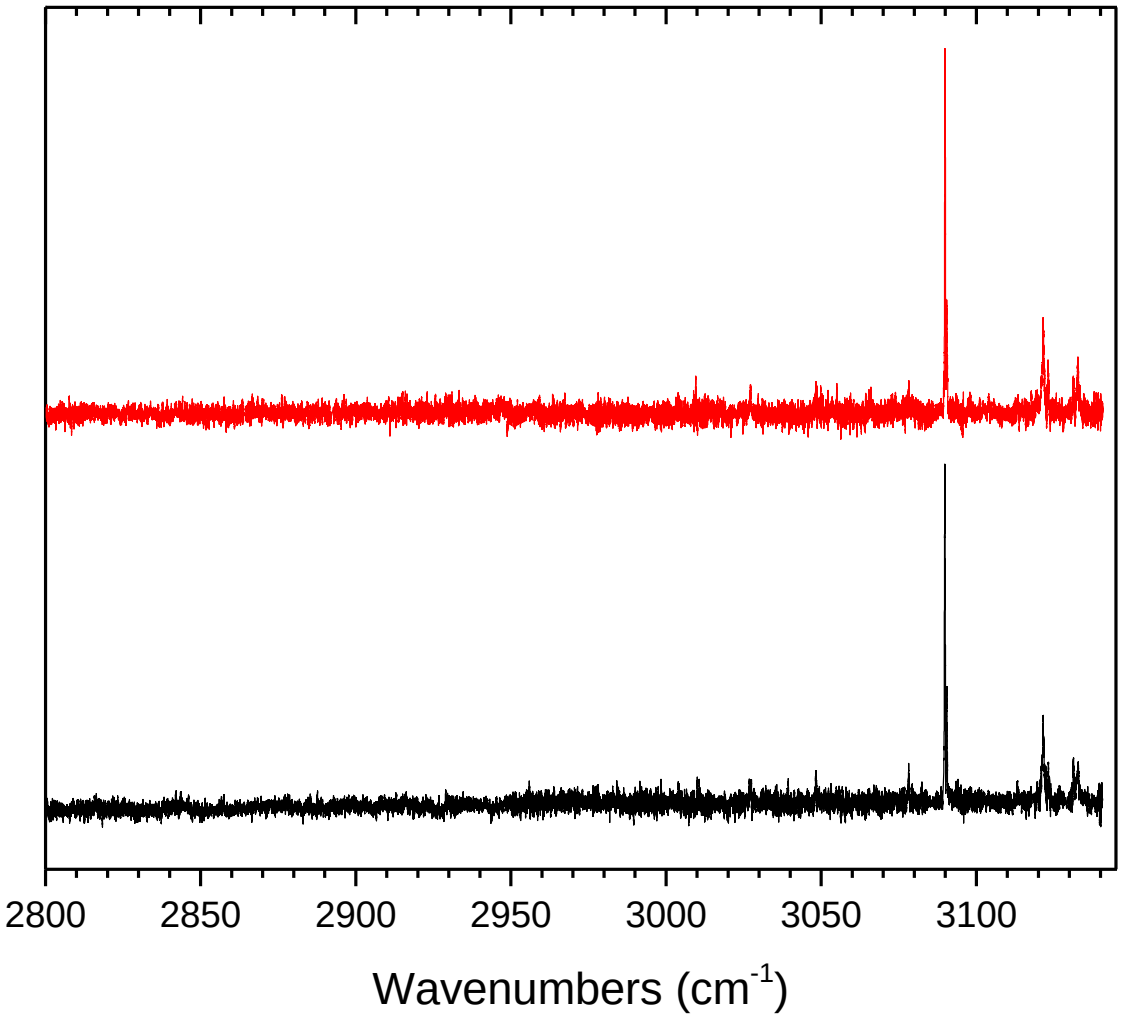

Figure 4.6: Mass channel 63 u comparison for cold pyro (black) and hot pyro (red). No obvious difference is observed between the two spectra aside from very weak features near the signal to noise limit.

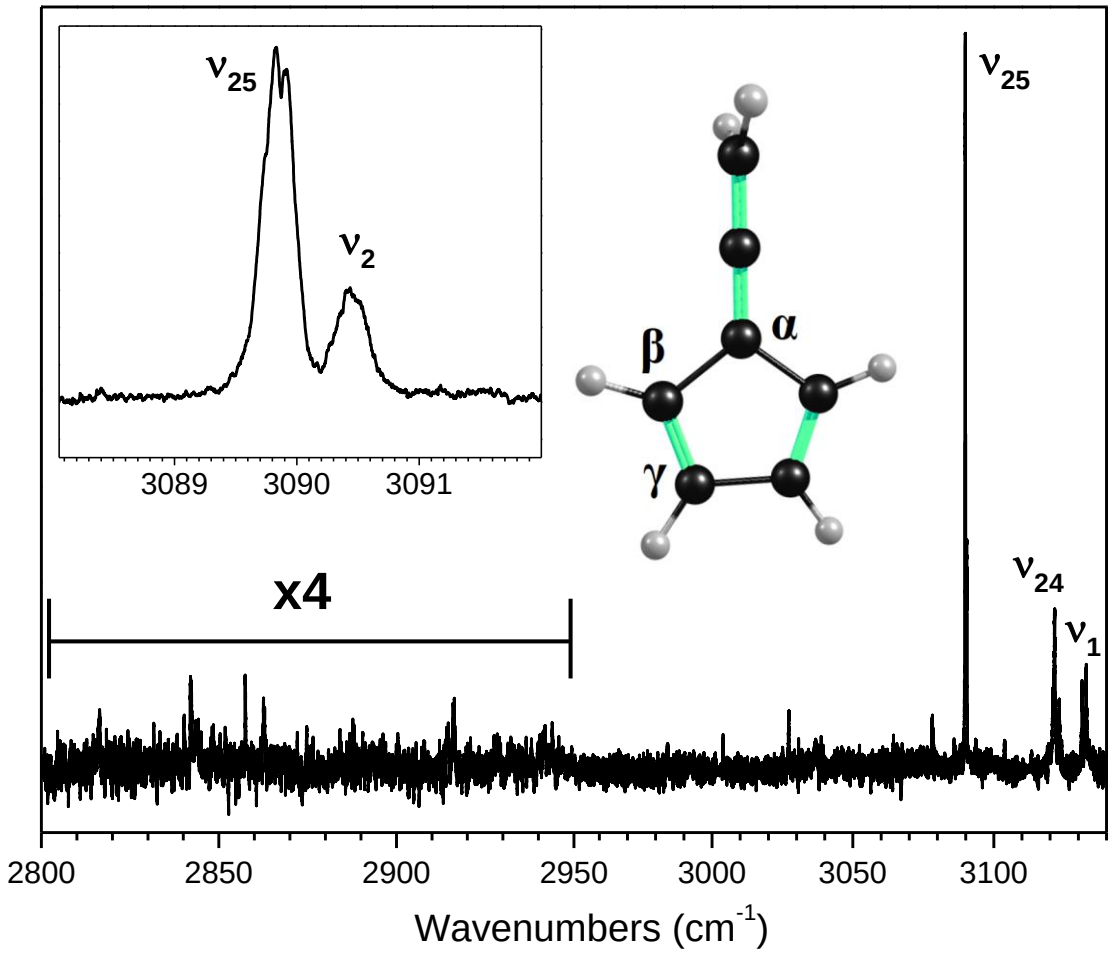

Figure 4.7: Infrared spectrum of fulvenallene in the CH stretching region, measured on mass channel 89 u. The inset is a higher resolution scan of the bands near 3090 cm^{-1}.

Table 4.1: Fulvenallene: comparison of experimental bands to VPT2+K predictions (cm^{-1}).

Gas Phase[a] (cm^{-1})	HENDI (cm^{-1})	VPT2+K (Intensity, km/mol)	Description	Assignment (Symmetry)
	2816.3	2826.4 (0.1)	CH bend combination with out-of-phase C=C stretch (ring)	$\nu_{27} + \nu_{26}$ (b_2)
	2841.9	2836.3 (0.002)	in-phase C=C stretch (ring) combination with CH bend	$\nu_5 + \nu_7$ (a_1)
	2857.3	2854.5 (0.01)	CH_2 scissor overtone	$2\nu_6$ (a_1)
	2862.5	2898.5 (0.1)	CH bend combination with out-of-phase C=C stretch (ring)	$\nu_7 + \nu_{26}$ (b_2)
	2915.9, 2916.3	2916.5 (0.01)	in-phase C=C stretch (ring) combination with CH_2 scissor	$\nu_5 + \nu_6$ (a_1)
2966		2957.0 (0.1)	in-phase C=C stretch (ring)	$2\nu_5$ (a_1)
	2984.2	2984.2 (0.1)	antisymmetric C=C ring stretch combination with CH_2 scissor	$\nu_6 + \nu_{26}$ (b_2)
3010	3003.9	3008.0 (0.1)	CH_2 symmetric stretch	ν_3 (a_1)
	3027.2	3015.9 (0.4)	in-phase C=C ring stretch in combination with out-of-phase C=C stretch (ring)	$\nu_5 + \nu_{26}$ (b_2)
3071	3078.2	3070.6 (0.01)	CH_2 antisymmetric stretch	ν_{17} (b_1)
3092	3089.9	3089.1 (3.4)	antisymmetric ring γ-CH stretch	ν_{25} (b_2)
	3090.4	3087.9 (1.7)	antisymmetric C=C ring stretch (2 quanta), out-of-phase CH stretch	$2\nu_{26}$ (a_1)
		3099.0 (3.5)	out-of-phase ring CH stretch	ν_2 (a_1)
3122	3121.6, 3123.2	3122.7 (4.7)	antisymmetric ring β-CH stretch	ν_{24} (b_2)
3134	3131.3, 3132.7	3132.5 (4.4)	symmetric in-phase CH stretch, antisymmetric C=C ring stretch (2 quanta)	ν_1 (a_1)

[a] Reference[18]

Table 4.2: Qualitative descriptions, symmetries, and CCSD(T)/ANO1 harmonic frequencies and intensities of the normal modes of vibration of fulvenallene.

Mode	Γ	ω (cm^{-1})	I (km/mol)	Shorthand	Description
1	a_1	3255.00	6.36	ν_s^{in}(CH)	symmetric in-phase CH stretch (ring)
2	a_1	3228.98	3.69	ν_s^{out}(CH)	symmetric out-of-phase CH stretch (ring)
3	a_1	3137.58	0.09	$\nu_s(CH_2)$	symmetric CH_2 stretch
4	a_1	2006.11	124.98	ν_{as}(C=C=C)	antisymmetric C=C stretch (allene)
5	a_1	1526.38	29.90	ν^{in}(C=C)	in-phase C=C stretch (ring)
6	a_1	1467.40	3.23	$\delta(CH_2)$	CH_2 scissor
7	a_1	1393.58	8.17	δ(CH)	CH bend
8	a_1	1270.40	1.06	ν_s(C=C=C)	symmetric C=C stretch (allene)
9	a_1	1085.61	5.06	δ(CH)	CH bend
10	a_1	996.56	1.60	ν(C-C)	C-C stretch (ring)
11	a_1	893.00	19.34	δ(ring)	ring deform (horizontal)
12	a_1	556.32	0.00	δ(ring)	ring deform (vertical)
13	a_2	922.81	0.00	ρ_w(CH)	CH wag
14	a_2	730.63	0.00	ρ_t(CH)	CH twisting
15	a_2	638.64	0.00	$\rho_t(CH_2$+ring)	out-of-phase ring twisting + CH_2 twisting
16	a_2	479.42	0.00	$\rho_t(CH_2$+ring)	in-phase ring twisting + CH_2 twisting
17	b_1	3221.19	0.01	$\nu_{as}(CH_2)$	antisymmetric CH_2 stretch
18	b_1	998.25	0.09	$\rho_r(CH_2)$	CH_2 rock
19	b_1	919.51	0.01	ρ_w(CH)	CH wag
20	b_1	768.27	75.56	ρ_t(CH)	CH twisting
21	b_1	613.38	21.70	ρ_w(ring)	ring puckering
22	b_1	350.32	0.74	δ(C=C=C)	C=C=C bend
23	b_1	131.48	2.83	δ(skeletal)	skeletal bend
24	b_2	3250.18	5.33	β-ν_{as}(CH)	β-CH antisymmetric stretch
25	b_2	3218.08	3.62	γ-ν_{as}(CH)	γ-CH antisymmetric stretch
26	b_2	1590.60	0.04	ν^{out}(C=C)	out-of-phase C=C stretch (ring)
27	b_2	1314.61	0.00	δ(skeletal)	α-skeletal bend
28	b_2	1187.24	2.13	ν_{as}(C-C)	antisymmetric C-C stretch (ring)
29	b_2	1095.77	7.84	δ(CH)	CH bend
30	b_2	863.49	44.97	$\rho_w(CH_2)$	CH_2 wag
31	b_2	814.80	2.24	δ(ring)	antisymmetric ring deform
32	b_2	538.26	2.95	δ(C=C=C)	C=C=C bend
33	b_2	150.65	1.16	δ(skeletal)	skeletal bend

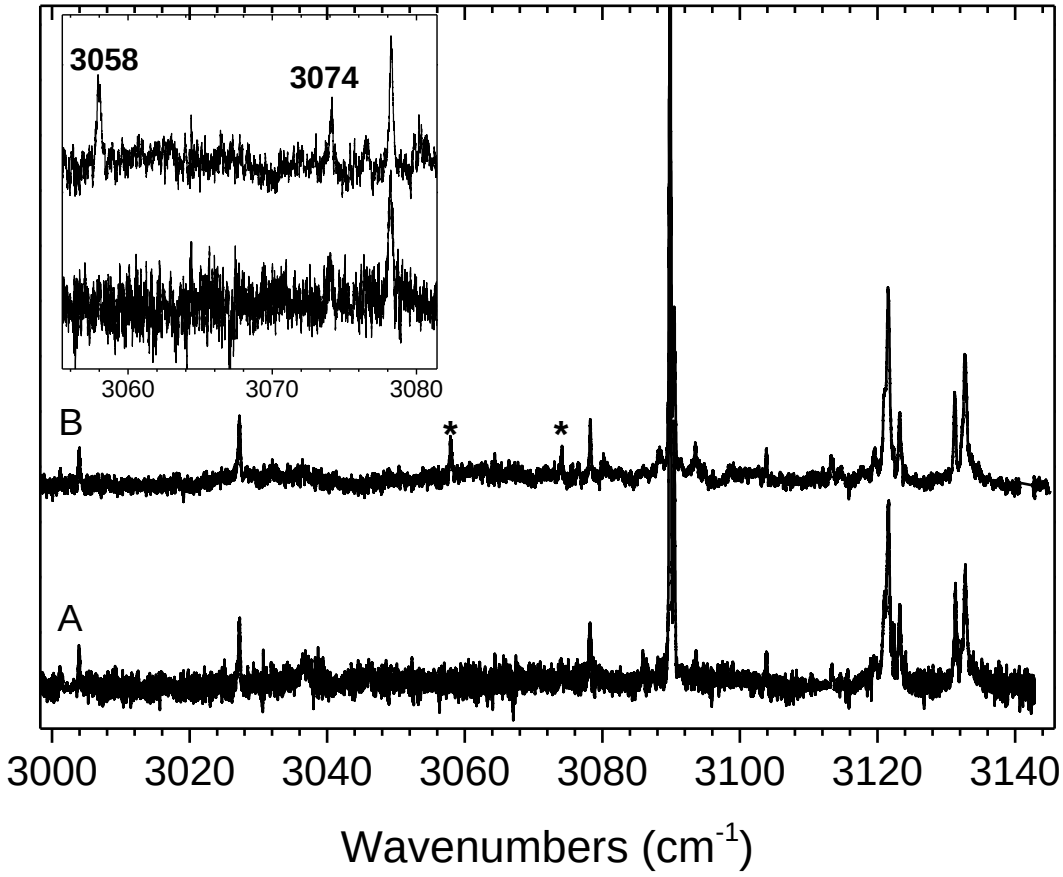

Figure 4.8: Comparison of 89 u depletion spectra between 3000 and 3140 cm^{-1} with cold (A) and hot (B) pyrolysis source conditions. The hot pyrolysis spectrum shows two additional features at 3058 and 3074 cm^{-1} (see inset), marked by *.

Because one anticipates the production of fulvenallenyl from the thermal decomposition of fulvenallene under hot pyrolysis source conditions, VPT2+K computed spectra of fulvenallene and fulvenallenyl are compared in Figure 4.9. The fulvenallene CH stretch vibrations localized on the ring are computed to fall between 3089 and 3133 cm^{-1}, in agreement with experiment (Table 4.1). Analogous computations for fulvenallenyl are summarized in Tables 4.3 and 4.4. Similar to fulvenallene, fulvenallenyl ring CH stretch vibrations are predicted with similar intensity in the same spectral region (3093 to 3126 cm^{-1}); despite this, nothing new is observed in this region upon heating the SiC furnace (see Figure 4.8). Apparently, fulvenallene pyrolysis under our experimental conditions does not produce fulvenallenyl in sufficient abundance to observe the ring CH stretch vibrations.

Figure 4.9 also shows predicted spectra for the ECPD isomers which also contain ring CH stretch vibrations above 3080 cm^{-1} (see Tables 4.5-4.7). The dashed lines in Figure 4.9 mark the locations of the two features that appear in the hot pyrolysis scan (3058 and 3074 cm^{-1}). Neither of these two bands can be assigned to fulvenallenyl nor ECPD via comparison to the predicted spectra shown in Figure 4.9, especially considering that no new features appear between 3080 and 3140 cm^{-1} where the more intense ring CH stretches are predicted. An intriguing possible assignment involves the species cycloheptatetraene and phenylcarbene, both of which can be accessed via fulvenallene rearrangement over the 63.2 kcal/mol barrier shown in Figure 4.3. Indeed, both of these species have strong vibrational bands in the same spectral region as those observed to grow in under hot pyrolysis conditions. Bally and co-workers measured IR

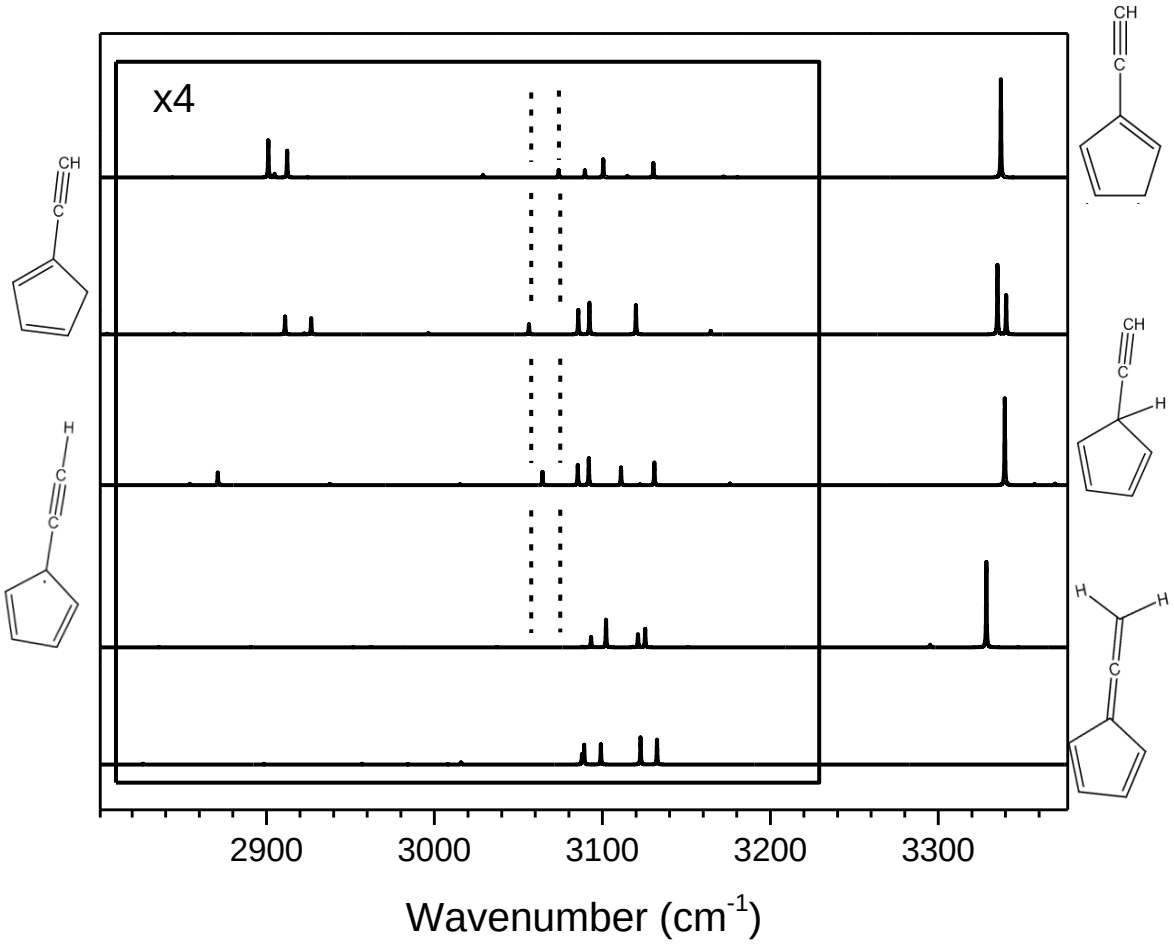

Figure 4.9: VPT2+K spectra of (bottom to top) fulvenallene, fulvenallenyl, 5-ethynylcyclopentadiene, 1-ethynylcyclopentadiene, and 2-ethynylcyclopentadiene. The acetylenic CH stretches are predicted to be 10 to 20 times more intense than the lower energy CH stretch transitions. The vertical dashed lines mark the locations of the only experimentally observed bands to appear in the CH stretch region following the pyrolysis of fulvenallene (3058 and 3074 cm^{-1}).

Table 4.3: Experimental frequencies (cm^{-1}), intensities and assignments of the acetylenic CH stretch region measured with hot pyrolysis conditions.

Experimental (Normalized Intensity)[a]			**VPT2+K (Intensity, km/mol)**	**Description**	**Symmetry**
---			3093.4 (1.9); ν_{22}	Fulvenallenyl: antisymmetric γ-CH ring stretch	b_2
---			3102.6 (4.8); ν_3	Fulvenallenyl: out-of-phase ring CH stretch	a_1
---			3121.1 (2.3); ν_{21}	Fulvenallenyl: antisymmetric ring β-CH stretch	b_2
---			3125.7 (3.3); ν_2	Fulvenallenyl: symmetric in-phase ring CH stretch	a_1
	63 u	**89 u**			
3327.1	(77.2)	(0)	3331.1 (59.1); ν_1	Fulvenallenyl: acetylenic CH stretch	a_1
3331.8	(100)	(100)	3335.3 (48.4); ν_1 3337.2 (68.6); ν_1 3339.6 (60.5); ν_1 3340.42 (27.3); $\nu_{6+}\nu_{12}$	1-ethynylcyclopentadiene: C≡C stretch in combination with CH ring bend, acetylenic CH stretch (more acetylenic stretch character)	a'
3333.1	(24.8)	(15.4)		2-ethynylcyclopentadiene: acetylenic CH stretch	a'
3333.7	(40.1)	(29.7)		5-ethynylcyclopentadiene: acetylenic CH stretch	a'
3340.6 or 3342.6	(0.8) (6.4)	(3.7) (6.0)		1-ethynylcyclopentadiene: C≡C stretch in combination with CH ring bend, acetylenic CH stretch (less acetylenic stretch character)	a'

[a] Integrated intensities are based on a least squares fit of acetylenic CH stretch region to six (m/z=63) or five (m/z=89) Lorentzians.

Table 4.4: Qualitative descriptions, symmetries, and ROHF-CCSD(T)/ANO1 harmonic frequencies and intensities of the normal modes of vibration of fulvenallenyl.

Mode	Γ	ω (cm^{-1})	I (km/mol)	Shorthand	Description
1	a_1	3459.47	61.52	ν(CH)	acetylenic CH stretch
2	a_1	3260.67	3.38	ν_s^{in}(CH)	symmetric in-phase CH stretch (ring)
3	a_1	3235.51	5.05	ν_s^{out}(CH)	symmetric out-of-phase CH stretch (ring)
4	a_1	2068.94	28.36	ν(C≡C)	C≡C stretch
5	a_1	1505.06	3.87	ν^{in}(C=C)	in-phase C=C stretch (ring)
6	a_1	1403.93	53.21	δ(CH)	CH bend
7	a_1	1287.23	2.53	ν(C-C)	C-C stretch (ethynyl)
8	a_1	1082.76	0.02	δ(CH)	CH bend
9	a_1	987.55	5.01	ν_{ring}(C-C)	C-C stretch (ring)
10	a_1	906.03	5.05	δ(ring)	ring deform (horizontal)
11	a_1	553.94	0.03	δ(ring)	ring deform (vertical)
12	a_2	899.44	0.00	ρ_w(CH)	CH wag
13	a_2	719.42	0.00	ρ_t(CH)	CH twisting
14	a_2	514.07	0.00	ρ_t(ring)	ring twisting
15	b_1	891.64	3.21	ρ_w(CH)	CH wag
16	b_1	745.71	89.83	ρ_t(CH)	CH twisting
17	b_1	629.97	6.03	ρ_w(ring)	ring puckering
18	b_1	587.04	41.27	δ(CH)	CH bend
19	b_1	388.92	0.89	δ(C≡C-C)	ethynyl bend
20	b_1	141.63	3.35	δ(skeletal)	skeletal bend
21	b_2	3255.90	2.40	β-ν_{as}(CH)	β-CH antisymmetric stretch
22	b_2	3225.24	1.98	γ-ν_{as}(CH)	γ-CH antisymmetric stretch
23	b_2	1519.39	0.17	ν^{out}(C=C)	out-of-phase C=C stretch (ring)
24	b_2	1279.95	0.08	δ(CH)	CH bend
25	b_2	1115.38	18.67	δ(skeletal)	α-skeletal bend
26	b_2	1036.84	0.66	ν_{as}(C-C)	“dienylic” C-C stretch (ring)
27	b_2	646.13	28.27	ν_{as}(C-C)	“allylic” C-C stretch (ring)
28	b_2	624.50	16.99	δ(ring)	CH bend
29	b_2	500.84	0.46	δ(C≡C-C)	ethynyl bend
30	b_2	154.37	1.41	δ(skeletal)	skeletal bend

Table 4.5: Symmetries, identities, and VPT2+K frequencies and intensities of vibrational transitions of 5-ethynylcyclopentadiene between 2800 and 3400 cm^{-1}.

Γ	**ν (cm^{-1})**	**I (km/mol)**	**Character**
a′	3369.54	1.17	$\nu_5+\nu_8$
a′	3357.40	0.87	$\nu_8+\nu_9+\nu_{10}$
a′	3339.60	60.49	ν_1
a′	3175.97	0.34	$2\nu_{22}$
a′	3111.09	3.10	ν_2
a′	3091.89	4.70	ν_3
a′	3015.20	0.20	$2\nu_6$
a′	2872.41	0.14	$\nu_6+\nu_7$
a′	2871.00	2.22	ν_4
a′	2854.30	0.26	$\nu_{22}+\nu_{23}$
a″	3130.96	4.00	ν_{20}
a″	3122.36	0.18	$\nu_{22}+\nu_{10}+\nu_{17}$
a″	3085.34	3.53	ν_{21}
a″	3064.32	2.33	$\nu_6+\nu_{22}$
a″	2937.71	0.26	$\nu_7+\nu_{22}$

Table 4.6: Symmetries, identities, and VPT2+K frequencies and intensities of vibrational transitions of 1-ethynylcyclopentadiene between 2800 and 3400 cm^{-1}.

Γ	ν (cm^{-1})	I (km/mol)	Character
a'	3379.96	0.42	$\nu_6+\nu_{11}$
a'	3340.42	27.29	$\nu_6+\nu_{12}$
a'	3335.26	48.41	ν_1
a'	3164.56	0.62	$2\nu_7$
a'	3119.96	5.09	ν_2
a'	3092.28	5.53	ν_3
a'	3085.64	4.27	ν_4
a'	3056.27	1.77	$\nu_7+\nu_8$
a'	2996.38	0.23	$2\nu_8$
a'	2922.38	0.19	$\nu_7+\nu_{10}$
a'	2911.07	3.10	ν_5
a'	2844.86	0.15	$\nu_8+\nu_{10}$
a'	2805.10	0.12	$\nu_7+\nu_{12}$
a''	2926.60	2.85	ν_{23}

Table 4.7: Symmetries, identities, and VPT2+K frequencies and intensities of vibrational transitions of 2-ethynylcyclopentadiene between 2800 and 3400 cm^{-1}.

Γ	**ν (cm^{-1})**	**I (km/mol)**	**Character**
a′	3377.49	0.32	$\nu_6+\nu_{11}$
a′	3337.28	68.60	ν_1
a′	3172.07	0.21	$2\nu_7$
a′	3130.37	2.53	ν_2
a′	3114.84	0.27	$\nu_8+\nu_{26}+\nu_{28}$
a′	3100.55	3.16	ν_3
a′	3089.59	1.25	ν_4
a′	3073.97	1.28	$\nu_7+\nu_8$
a′	3028.89	0.47	$2\nu_8$
a′	2904.84	0.65	$\nu_8+\nu_9$
a′	2901.10	6.48	ν_5
a″	2912.30	4.67	ν_{23}

spectra of these species in an Ar matrix,[55] observing three CH stretch bands for each species, the strongest of which were at 3048 cm^{-1} for cycloheptatetraene and 3073 cm^{-1} for phenylcarbene. Despite this suggestion, we hesitate to definitively assign the 3058 and 3074 cm^{-1} bands observed in the present study.

4.4.4 Infrared Spectroscopy (3270 – 3350 cm^{-1})

Returning to the VPT2+K computed spectra in Figure 4.9, it is clear that the strongest spectral signatures in the CH stretch region are the acetylenic CH stretch bands predicted at 3331 cm^{-1} for fulvenallenyl and 3335 − 3339 cm^{-1} for the ECPD isomers (see Table 3). Indeed, for these species, the acetylenic CH stretch intensities are predicted to be 10 to 20 times larger than the ring CH stretch bands. Moreover, fulvenallene does not possess an acetylenic CH bond, so the spectra in this region will be free from fulvenallene contamination. Therefore, spectra were measured in this region under hot pyrolysis conditions on channels 63 and 89 u, as shown in Figure 4.10. Depletion in channel 89 u is observed at 3331.8, 3333.1, 3333.7, 3340.6 and 3342.6 cm^{-1}, along with a small feature at 3280 cm^{-1}. Depletion in channel 63 u is observed at all of these frequencies; additionally, a relatively intense band is observed at 3327.1 cm^{-1}. These features are completely absent under cold pyrolysis source conditions; therefore, fulvenallene is clearly being converted in the SiC source to species that contain acetylenic CH bonds.

A possible assignment of these features is suggested in Figure 4.11, which shows a close up view of the 69 u experimental depletion spectrum between 3323 and

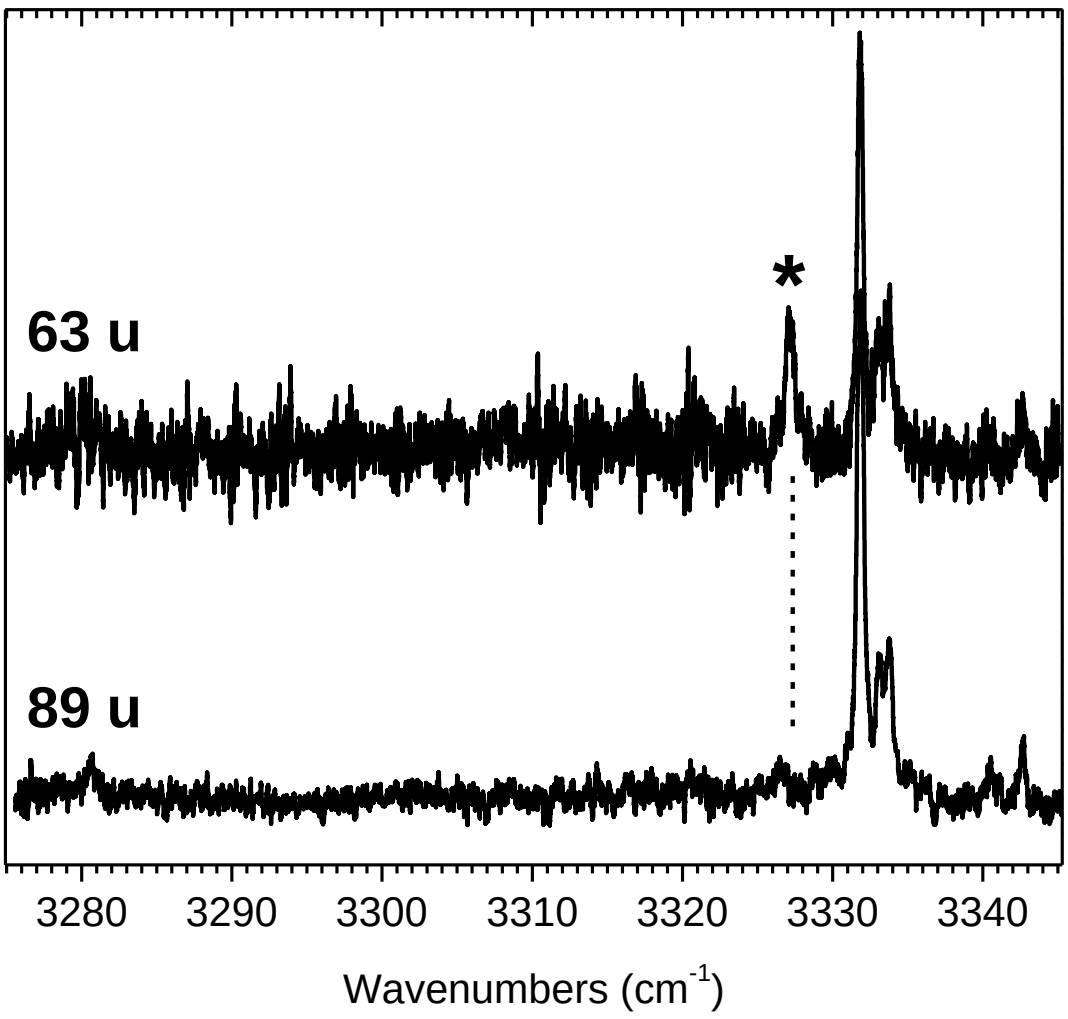

Figure 4.10: Acetylenic CH stretching region measured on mass channels 89 and 63 u. Both spectra are measured under hot pyrolysis source conditions. The band at 3327.1 cm^{-1} (marked by an asterisk) only appears on channel 63 u. As this is the most red-shifted band (*i.e.* most "allenic"), we assign it to the fulvenallenyl radical. The other bands at 3331.8, 3333.1, 3333.7, 3340.6 and 3342.6 cm^{-1} are attributed to C_7H_6 ethynylcyclopentadiene species (see Figures 4.3 and 4.11). All features are absent under cold pyrolysis conditions.

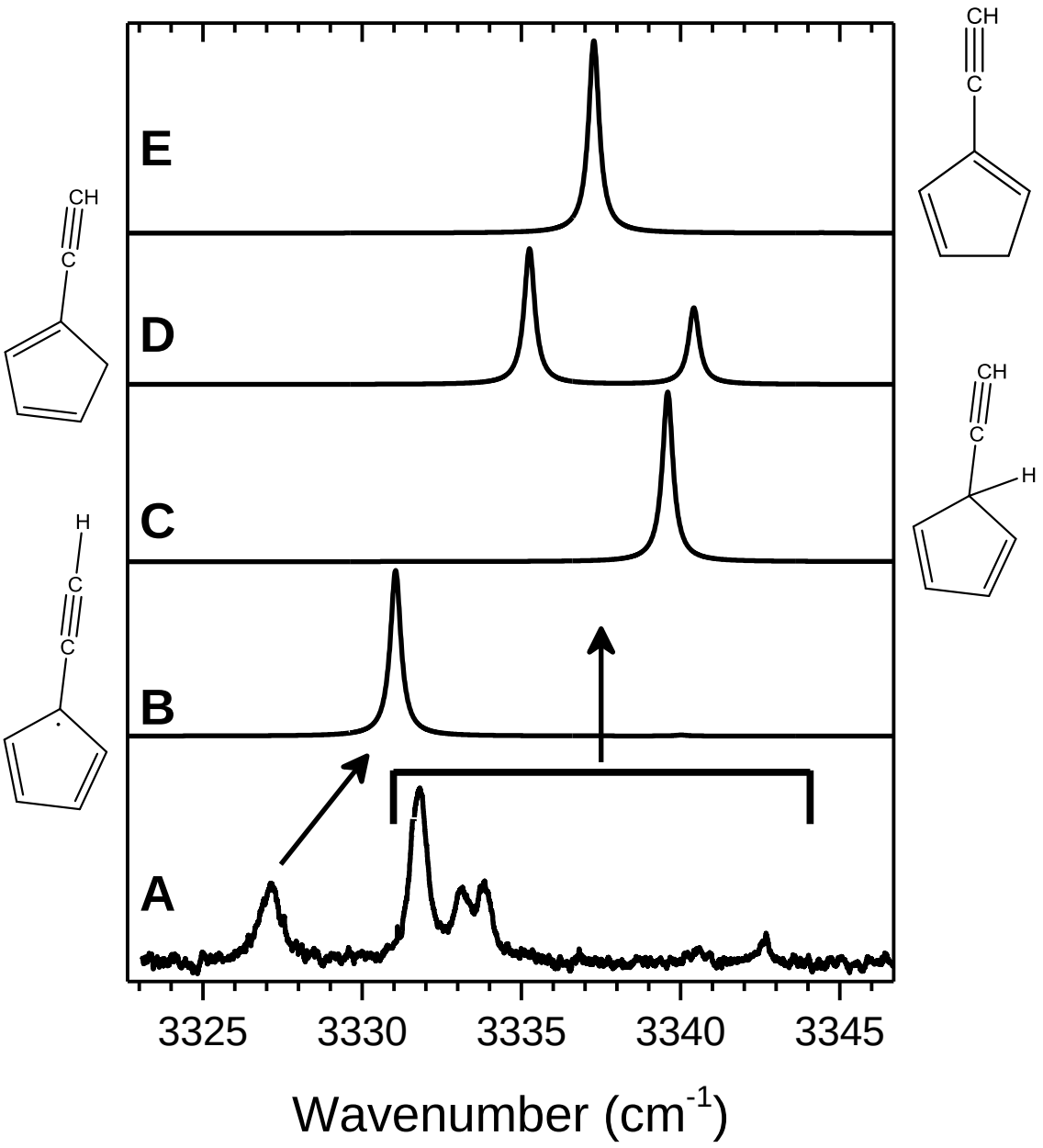

Figure 4.11: (A) Experimental acetylenic CH stretch spectral region (channel 63 u) compared to VPT2+K simulations for fulvenallenyl radical (B), and three C_7H_6 isomers: (C) 5-ethynylcyclopentadiene, (D) 1-ethynylcyclopentadiene, and (E) 2-ethynylcyclopentadiene.

3347 cm^{-1}, along with the VPT2+K predictions for fulvenallenyl and 1-, 2-, and 5- ECPD. The predicted fulvenallenyl band is the most red shifted, suggesting that the 3327.1 cm^{-1} band, appearing only as depletion in channel 63 u, should be assigned to the acetylenic CH stretch vibration of the radical. The red shift of the fulvenallenyl acetylenic CH stretch, in comparison to those associated with the closed shell species, originates from the delocalization of the unpaired electron, as discussed in more detail below. It is interesting that the band at 3327.1 cm^{-1} is the only one not to appear on channel 89 u (*i.e.* the mass of fulvenallenyl). Perhaps this may be viewed as further support for the assignment, as charge transfer ionization of fulvenallenyl will leave it with approximately 16 eV of internal energy (the difference between the He and fulvenallenyl ionization potentials), and this may lead to its prompt fragmentation *via* loss of C_2H_2 to produce signal at 63 u. On the other hand, the fragmentation of an ionized ECPD isomer *via* H atom loss could produce signal at 89 u.

Given the comparison of VPT2+K predictions to experiment (and the computed barriers on the potential energy surface), it is at least plausible that all three ethynylcyclopentadiene isomers are formed *via* rearrangement of fulvenallene, and it is then *these* species that contribute to the spectrum above 3330 cm^{-1}. An alternative explanation must be ruled out, *i.e.* self-reaction of fulvenallenyl within the SiC source and subsequent capture of the reaction products by helium droplets. Indeed, fulvenallenyl self-reaction would lead to C-C bond formation at the radical centers, which would quench the resonance delocalization and shift the acetylenic CH stretch vibrations to the blue of monomeric fulvenallenyl. For fulvenallenyl self-reaction to be the explanation, the bands to the blue of 3330 cm^{-1} should grow at the expense of the 3327 cm^{-1} band as

the density of fulvenallenyl increases in the SiC furnace. However, experimentally, we observe all features in the 63 u depletion spectrum to go up and down together as the fulvenallene density is slowly adjusted with a very-fine metering valve attached to the inlet of the pyrolysis source. Moreover, the density at which all bands optimize is similar to several previous measurements of *monomeric* hydrocarbon radicals, carried out with the same experimental setup.[41, 42, 56-59] We take this as evidence that the acetylenic CH stretch bands observed here are due to products resulting from the dissociation (fulvenallenyl) and rearrangement (ethynylcyclopentadiene) of monomeric fulvenallene.

It is interesting to compare the spectra in Figures 4.10 and 4.11 to previous work by Ellison and co-workers, who studied benzyl pyrolysis by passing ethyl benzene through a 1800 K SiC furnace and trapping the products in a neon matrix.[10] IR spectra in the acetylenic CH stretch region revealed acetylene, the propargyl radical (C_3H_3), and three or four unassigned bands between 3330 and 3340 cm^{-1}. In other regions, they observed strong spectral evidence for the production of fulvenallene, and they speculated that the unassigned peaks in the acetylenic CH stretch region could be due to fulvenallenyl or other fulvenallene decomposition products. It is typical for vibrational bands observed in neon matrix isolation spectra to be slightly red shifted in comparison to the band origins observed using helium nanodroplet isolation. Therefore, assuming our 3327 cm^{-1} assignment is correct, the bands observed by Ellison and co-workers are too high in energy to be assigned to fulvenallenyl, although it is possible that they arise from the ethynylcyclopentadiene species.

4.4.5 On the Nature of Fulvenallenyl Electron Delocalization

Fulvenallenyl can be viewed as a *resonantly stabilized free radical* (RSFR), for which the electron density is delocalized and characterized as a superposition between *acetylenic* and *allenic* resonance structures. These limiting resonance structures are shown schematically in Figure 4.1. The allenic unpaired electron resides on the terminal carbon atom, whereas the acetylenic unpaired electron is delocalized in the ring. A closely related RSFR is propargyl (C_3H_3), which can similarly be viewed as a superposition of acetylenic and allenic resonance structures. Ellison and co-workers performed spin density calculations for the propargyl radical, and using Mulliken population analysis, they determined (*via* atomic partitioning of the CCSD(T)/ANO1 spin density) that propargyl is 35% allenic and 65% acetylenic.[60] Spin density calculations at the ROHF-CCSD(T)/ANO1 level of theory were carried out for fulvenallenyl, and an isosurface at ρ=0.01 e a^{-3} is shown in Figure 4.12. From this, it is evident that the alpha spin density (blue shading in Figure 4.12) is delocalized over *both* the terminal acetylenic carbon *and* the α/γ-ring carbon atoms. With the same atomic partitioning scheme used for propargyl,[60] we find that fulvenallenyl is approximately 24% allenic and 76% acetylenic. In comparison to propargyl, fulvenallenyl is more acetylenic, because for this resonance structure, the radical center can be delocalized within the cyclopentadienyl-like moiety.

Among other properties of the system, the frequency of the acetylenic CH stretch is a rather sensitive marker of the extent of this electron delocalization. The acetylenic CH stretch for propargyl (35% allenic) is 3322.3 cm^{-1},[61] which can be compared to the CH stretch of HCCD at 3337.2 cm^{-1}.[62] Another useful comparison is to a closely related,

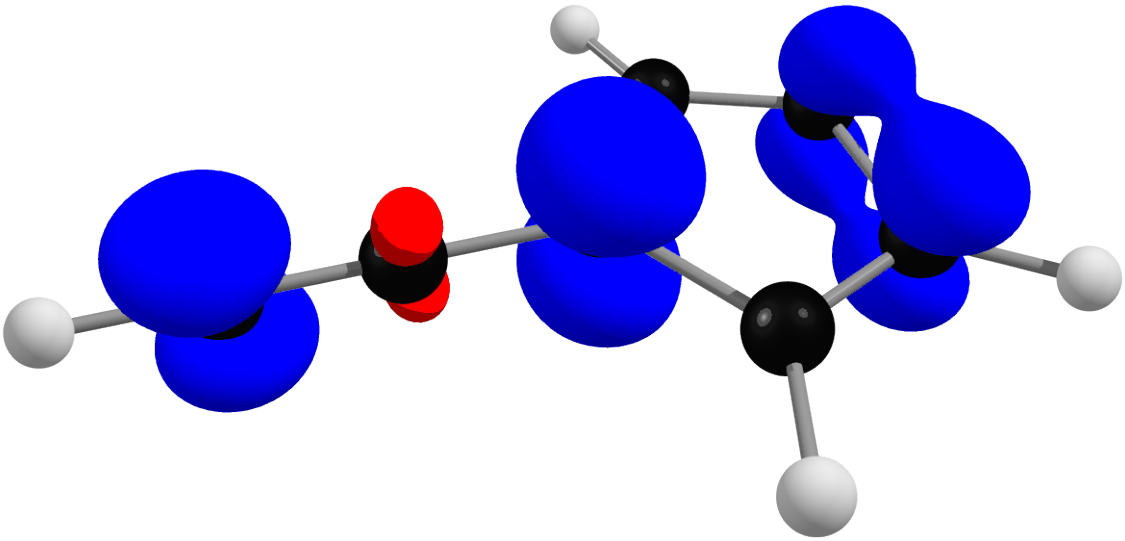

Figure 4.12: ROHF-CCSD(T)/ANO1 spin density plot for fulvenallenyl radical (ρ=0.01 e a_0^{-3}). Blue regions represent excess alpha spin while red represents excess beta spin. An atomic partitioning of the spin density based on Mulliken populations reveals that fulvenallenyl radical possesses 24% allenic character and 76% acetylenic bonding character.

closed shell system containing an acetylenic moiety, such as propargyl bromide (3332.56 cm^{-1}).[63] Clearly, propargyl experiences a substantial red shift of its acetylenic CH stretch due to its partial allenic character (*i.e.* the slight rehybridization of the terminal carbon atom to have more *p* character than is typical for an *sp* hybridized ethynyl moiety). Again, our computations predict fulvenallenyl to have somewhat less allenic character (24%), in comparison to propargyl (35%). Consistent with this, the fulvenallenyl acetylenic CH stretch at 3327.1 cm^{-1} is to the red of the closed shell acetylenic systems, but to the blue of propargyl.

4.5 Conclusions

Fulvenallene was doped into helium nanodroplets, and the IR spectrum between 2800 and 3140 cm^{-1} is in good agreement with previous lower resolution gas-phase spectra.[18] Several new vibrational bands are assigned in this region *via* comparison of experimental spectra to VPT2+K anharmonic frequency computations. Pyrolysis of fulvenallene in a 1500 K SiC furnace results in the appearance of new vibrational bands at 3058 and 3074 cm^{-1} along with several features in the acetylenic CH stretch region near 3330 cm^{-1}. The 3058 and 3074 cm^{-1} bands are not definitively assigned here; we note, however, that they are centered close to the most intense CH stretch bands observed in Ar matrix-isolation spectra of cycloheptatetraene and phenylcarbene.[54] On the basis of VPT2+K computations and their dependence on experimental conditions, the bands observed in the acetylenic CH stretch region are assigned to the fulvenallenyl radical and multiple ethynylcyclopentadiene isomers. The 3327.1 cm^{-1} assignment to fulvenallenyl is

most convincing, as this resonantly stabilized free radical is predicted to have 24% allenic and 76% acetylenic character, the signature of which is a red shift of the acetylenic CH stretch. In comparison, the bands assigned to the closed shell ethynylcyclopentadiene species are all observed at 3331.8 cm^{-1} and above.

The potential energy surface from Cavallotti and co-workers[2] is used to motivate all assignments put forth in this work. Interconversion of fulvenallene to other C_7H_6 isomers, such as cycloheptatetraene and phenylcarbene is predicted to occur *via* a pathway having an initial barrier equal to 63.2 kcal/mol (relative to fulvenallene); ring-opening of phenylcarbene to produce 5-ethynylcyclopentadiene is predicted to occur *via* a barrier at 77.3 kcal/mol. Both of these barriers are lower than the predicted barrier for the homolytic barrierless dissociation of fulvenallene to produce fulvenallenyl (82.5 kcal/mol). Although the dissociation pathway is favored entropically, the lower barriers associated with rearrangement seem to allow these pathways to be competitive at 1500 K; indeed, there is perhaps evidence for this here, assuming the assignments we have put forth for the acetylenic CH stretch region. Unfortunately, given the "action spectroscopy" scheme and mass channel bias inherent in the detection scheme, it is not possible for us to confidently report dissociation:rearrangement branching ratios. Furthermore, the sensitivity of the experiment is insufficient in the ring-CH stretch region to definitively confirm the assignment of the higher frequency bands to ethynylcyclopentadiene, and these assignments must necessarily be viewed as tentative.

References

(1) Wong, M. W.; Wentrup, C. Interconversions of Phenylcarbene, Cycloheptatetraene, Fulvenallene, and Benzocyclopropene. A Theoretical Study of the C_7H_6 Energy Surface. *J. Org. Chem.* **1996**, *61*, 7022-7029.

(2) Polino, D.; Famulari, A.; Cavallotti, C. Analysis of the Reactivity on the C_7H_6 Potential Energy Surface. *J. Phys. Chem. A.* **2011**, *115*, 7928-7936.

(3) Polino, D.; Cavallotti, C. Fulvenallene Decomposition Kinetics. *J. Phys. Chem. A.* **2011**, *115*, 10281-10289.

(4) Hansen, N.; Kasper, T.; Klippenstein, S. J.; Westmoreland, P. R.; Law, M. E.; Taatjes, C. A.; Kohse-Höinghaus, K.; Wang, J.; Cool, T. A. Initial Steps of Aromatic Ring Formation in a Laminar Premixed Fuel-Rich Cyclopentene Flame. *J. Phys. Chem. A.* **2007**, *111*, 4081-4092.

(5) Zhang, T. C.; Zhang, L. D.; Hong, X.; Zhang, K. W.; Qi, F.; Law, C. K.; Ye, T. H.; Zhao, P. H.; Chen, Y. L. An Experimental and Theoretical Study of Toluene Pyrolysis with Tunable Synchrotron VUV Photoionization and Molecular-Beam Mass Spectrometry. *Combust. Flame.* **2009**, *156*, 2071-2083.

(6) Li, Y.; Zhang, L.; Tian, Z.; Yuan, T.; Wang, J.; Yang, B.; Qi, F. Experimental Study of a Fuel-Rich Premixed Toluene Flame at Low Pressure. *Energy Fuels.* **2009**, *23*, 1473-1485.

(7) Cavallotti, C.; Derudi, M.; Rota, R. On the Mechanism of Decomposition of the Benzyl Radical. *Proc. Combust. Inst.* **2009**, *32*, 115-121.

(8) da Silva, G.; Cole, J. A.; Bozzelli, J. W. Thermal Decomposition of the Benzyl Radical to Fulvenallene (C_7H_6) + H. *J. Phys. Chem. A.* **2009**, *113*, 6111-6120.

(9) Derudi, M.; Polino, D.; Cavallotti, C. Toluene and Benzyl Decomposition Mechanisms: Elementary Reactions and Kinetic Simulations. *Phys. Chem. Chem. Phys.* **2011**, *13*, 21308-21318.

(10) Buckingham, G. T.; Ormond, T. K.; Porterfield, J. P.; Hemberger, P.; Kostko, O.; Ahmed, M.; Robichaud, D. J.; Nimlos, M. R.; Daily, J. W.; Ellison, G. B. The Thermal Decomposition of the Benzyl Radical in a Heated Micro-Reactor. I. Experimental Findings. *J. Chem. Phys.* **2015**, *142*, 044307.

(11) Shapero, M.; Cole-Filipiak, N. C.; Haibach-Morris, C.; Neumark, D. M. Benzyl Radical Photodissociation Dynamics at 248 nm. *J. Phys. Chem. A.* **2015**, *119*, 12349-12356.

(12) da Silva, G.; Trevitt, A. J. Chemically Activated Reactions on the C_7H_5 Energy Surface: Propargyl Plus Diacetylene, i-C_5H_3+Acetylene, and n-C_5H_3+Acetylene. *Phys. Chem. Chem. Phys.* **2011**, *13*, 8940-8952.

(13) da Silva, G.; Bozzelli, J. W. The C_7H_5 Fulvenallenyl Radical as a Combustion Intermediate: Potential New Pathways to Two- and Three-Ring PAHS. *J. Phys. Chem. A.* **2009**, *113*, 12045-12048.

(14) da Silva, G. Reaction of Benzene with Atomic Carbon: Pathways to Fulvenallene and the Fulvenallenyl Radical in Extraterrestrial Atmospheres and the Interstellar Medium. *J. Phys. Chem. A.* **2014**, *118*, 3967-3972.

(15) Giegerich, J.; Fischer, I. Photodissociation Dynamics of Fulvenallene, C_7H_6. *Phys. Chem. Chem. Phys.* **2013**, *15*, 13162-13168.

(16) Ramphal, I. A.; Shapero, M.; Haibach-Morris, C.; Neumark, D. M. Photodissociation Dynamics of Fulvenallene and the Fulvenallenyl Radical at 248 and 193 nm. *Phys. Chem. Chem. Phys.* **2017**, *19*, 29305-29314.

(17) Sakaizumi, T.; Katoh, F.; Ohashi, O.; Yamaguchi, I. The Microwave Spectra of Fulvenallene and Its Deuterated Species. *J. Mol. Spectrosc.* **1993**, *159*, 112-121.

(18) Angell, C. L. The Vapor-Phase Infrared Spectrum and Structure of Fulvenallene. *J. Mol. Struct.* **1971**, *10*, 265-273.

(19) Steinbauer, M.; Hemberger, P.; Fischer, I.; Bodi, A. Photoionization of C_7H_6 and C_7H_5: Observation of the Fulvenallenyl Radical. *ChemPhysChem.* **2011**, *12*, 1795-1797.

(20) Botter, R.; Jullien, J.; Pechine, J. M.; Piade, J. J.; Solgadi, D. Ionization Potentials of Unstable Species: Photoelectron Spectrum of Fulvenallene. *J. Electron Spectrosc. Relat. Phenom.* **1978**, *13*, 141-143.

(21) Mueller, C.; Schweig, A.; Thiel, W.; Grahn, W.; Bergman, R. G.; Vollhardt, K. P. C. Theory and Application of Photoelectron Spectroscopy. 80. Photoelectron Spectra of 2,5-Dehydrotropylidene, 3,6-Dehydrooxepin, and Fulvenallene. *J. Am. Chem. Soc.* **1979**, *101*, 5579-5581.

(22) da Silva, G.; Trevitt, A. J.; Steinbauer, M.; Hemberger, P. Pyrolysis of Fulvenallene (C_7H_6) and Fulvenallenyl (C_7H_5): Theoretical Kinetics and Experimental Product Detection. *Chem. Phys. Lett.* **2011**, *517*, 144-148.

(23) Thapa, J.; Spencer, M.; Akhmedov, N. G.; Goulay, F. Kinetics of the OH Radical Reaction with Fulvenallene from 298 to 450K. *J. Phys. Chem. Lett.* **2015**, *6*, 4997-5001.

(24) Chakraborty, A.; Fulara, J.; Maier, J. P. The Electronic Spectrum of the Fulvenallenyl Radical. *Angew. Chem.-Int. Edit.* **2016**, *55*, 228-231.

(25) Liang, T.; Flynn, S. D.; Morrison, A. M.; Douberly, G. E. Quantum Cascade Laser Spectroscopy and Photoinduced Chemistry of Al–(CO)n Clusters in Helium Nanodroplets. *J. Phys. Chem. A.* **2011**, *115*, 7437-7447.

(26) Knuth, E.; Schilling, B.; Toennies, J. P. Proceedings of the 19th International Symposium on Rarefield Gas Dynamics, 1995.

(27) Spangler, R. J.; Ho Kim, J. The Pyrolysis of Homophthalic Anhydride. Simple Synthesis of Benzocyclobutenone and Fulveneallene. *Tetrahedron Lett.* **1972**, *13*, 1249-1251.

(28) Kohn, D. W.; Clauberg, H.; Chen, P. Flash Pyrolysis Nozzle for Generation of Radicals in a Supersonic Jet Expansion. *Rev. Sci. Instrum.* **1992**, *63*, 4003-4005.

(29) Toennies, J. P.; Vilesov, A. F. Superfluid Helium Droplets: A Uniquely Cold Nanomatrix for Molecules and Molecular Complexes. *Angew. Chem.-Int. Edit.* **2004**, *43*, 2622-2648.

(30) Choi, M. Y.; Douberly, G. E.; Falconer, T. M.; Lewis, W. K.; Lindsay, C. M.; Merritt, J. M.; Stiles, P. L.; Miller, R. E. Infrared Spectroscopy of Helium Nanodroplets: Novel Methods for Physics and Chemistry. *Int. Rev. Phys. Chem.* **2006**, *25*, 15-75.

(31) Morrison, A. M.; Liang, T.; Douberly, G. E. Automation of an "Aculight" Continuous-Wave Optical Parametric Oscillator. *Rev. Sci. Instrum.* **2013**, *84*, 013102.

(32) CFOUR, A Quantum Chemical Program Package Written by, J. F. Stanton, J. Gauss, M. E. Harding, P. G. Szalay with Contributions from A. A. Auer, R. J. Bartlett, U. Benedikt, C. Berger, D. E. Bernholdt, Y. J. Bomble, et. al., and the Integral Packages Molecule (J. Almlöf and P. R. Taylor), Props (P. R. Taylor), Abacus (T. Helgaker, H. J. Aa. Jensen, P. Jørgensen, and J. Olsen), and ECP Routines by A. V. Mitin and C. Van Wüllen.

(33) Raghavachari, K.; Trucks, G. W.; Pople, J. A.; Head-Gordon, M. A Fifth-Order Perturbation Comparison of Electron Correlation Theories. *Chem. Phys. Lett.* **1989**, *157*, 479-483.

(34) Hampel, C.; Peterson, K. A.; Werner, H.-J. A Comparison of the Efficiency and Accuracy of the Quadratic Configuration Interaction (QCISD), Coupled Cluster (CCSD), and Brueckner Coupled Cluster (BCCD) Methods. *Chem. Phys. Lett.* **1992**, *190*, 1-12.

(35) Deegan, M. J. O.; Knowles, P. J. Perturbative Corrections to Account for Triple Excitations in Closed and Open Shell Coupled Cluster Theories. *Chem. Phys. Lett.* **1994**, *227*, 321-326.

(36) Almlöf, J.; Taylor, P. R. General Contraction of Gaussian Basis Sets. I. Atomic Natural Orbitals for First- and Second-Row Atoms. *J. Chem. Phys.* **1987**, *86*, 4070-4077.

(37) Rosnik, A. M.; Polik, W. F. VPT2+K Spectroscopic Constants and Matrix Elements of the Transformed Vibrational Hamiltonian of a Polyatomic Molecule with Resonances Using Van Vleck Perturbation Theory. *Mol. Phys.* **2014**, *112*, 261-300.

(38) Matthews, D. A.; Vázquez, J.; Stanton, J. F. Calculated Stretching Overtone Levels and Darling–Dennison Resonances in Water: A Triumph of Simple Theoretical Approaches. *Mol. Phys.* **2007**, *105*, 2659-2666.

(39) Martin, J. M. L.; Lee, T. J.; Taylor, P. R.; François, J. P. The Anharmonic Force Field of Ethylene, C_2H_4, by Means of Accurate Ab Initio Calculations. *J. Chem. Phys.* **1995**, *103*, 2589-2602.

(40) Wolfram Research Inc., Mathematica, Version 10.0, Champaign, IL (2014).

(41) Franke, P. R.; Tabor, D. P.; Moradi, C. P.; Douberly, G. E.; Agarwal, J.; Schaefer, H. F.; Sibert, E. L. Infrared Laser Spectroscopy of the n-Propyl and i-Propyl Radicals: Stretch-Bend Fermi Coupling in the Alkyl CH Stretch Region. *J. Chem. Phys.* **2016**, *145*, 224304.

(42) Brown, A. R.; Franke, P. R.; Douberly, G. E. Helium Nanodroplet Isolation of the Cyclobutyl, 1-Methylallyl, and Allylcarbinyl Radicals: Infrared Spectroscopy and Ab Initio Computations. *J. Phys. Chem. A.* **2017**, *40*, 7576-7587.

(43) Franke, P. R.; Douberly, G. E. Rotamers of Isoprene: Infrared Spectroscopy in Helium Droplets and Ab Initio Thermochemistry. *J. Phys. Chem. A.* **2018**, *122*, 148-158.

(44) Schneider, H.; Vogelhuber, K. M.; Schinle, F.; Stanton, J. F.; Weber, J. M. Vibrational Spectroscopy of Nitroalkane Chains Using Electron Autodetachment and Ar Predissociation. *J. Phys. Chem. A.* **2008**, *112*, 7498-7506.

(45) Crawford, T. D.; Stanton, J. F.; Allen, W. D.; Henry F. Schaefer, I. Hartree–Fock Orbital Instability Envelopes in Highly Correlated Single-Reference Wave Functions. *J. Chem. Phys.* **1997**, *107*, 10626-10632.

(46) Stanton, J. F.; Gauss, J. Analytic Energy Derivatives for Ionized States Described by the Equation-of-Motion Coupled Cluster Method. *J. Chem. Phys.* **1994**, *101*, 8938-8944.

(47) Applegate, B. E.; Miller, T. A.; Barckholtz, T. A. The Jahn–Teller and Related Effects in the Cyclopentadienyl Radical. I. The Ab Initio Calculation of Spectroscopically Observable Parameters. *J. Chem. Phys.* **2001**, *114*, 4855-4868.

(48) Leicht, D.; Kaufmann, M.; Schwaab, G.; Havenith, M. Infrared Spectroscopy of the Helium Solvated Cyclopentadienyl Radical in the CH Stretch Region. *J. Chem. Phys.* **2016**, *145*, 074304.

(49) Neese, F. The ORCA Program System. *Wiley Interdiscip. Rev.: Comput. Mol. Sci.* **2012**, *2*, 73-78.

(50) Roos, B. O.; Taylor, P. R.; Siegbahn, P. E. M. A Complete Active Space SCF Method (CASSCF) using a Density Matrix Formulated Super-CI Approach. *J. Chem. Phys.* **1980**, *48*, 157-173.

(51) Siegbahn, P. E. M.; Almlöf, J.; Heiberg, A.; Roos, B. O. The Complete Active Space SCF (CASSCF) Method in a Newton–Raphson Formulation with Application to the HNO Molecule. *J. Chem. Phys.* **1981**, *74*, 2384-2396.

(52) Malmqvist, P.-Å.; Roos, B. O. The CASSCF State Interaction Method. *Chem. Phys. Lett.* **1989**, *155*, 189-194.

(53) Kendall, R. A.; Jr., T. H. D.; Harrison, R. J. Electron Affinities of the First-Row Atoms Revisited. Systematic Basis Sets and Wave Functions. *J. Chem. Phys.* **1992**, *96*, 6796-6806.

(54) Hernandez, F. J.; Brice, J. T.; Leavitt, C. M.; Liang, T.; Raston, P. L.; Pino, G. A.; Douberly, G. E. Mid-Infrared Signatures of Hydroxyl Containing Water Clusters: Infrared Laser Stark Spectroscopy of OH–H_2O and OH(D_2O)n (n = 1-3). *J. Chem. Phys.* **2015**, *143*, 164304.

(55) Matzinger, S.; Bally, T. Spectroscopic Characterization of Matrix-Isolated Phenylcarbene and Cycloheptatetraene. *J. Phys. Chem. A.* **2000**, *104*, 3544-3552.

(56) Morrison, A. M.; Raston, P. L.; Douberly, G. E. Rotational Dynamics of the Methyl Radical in Superfluid ^{4}He Nanodroplets. *J. Phys. Chem. A.* **2013**, *117*, 11640-11647.

(57) Morrison, A. M.; Agarwal, J.; Schaefer, H. F.; Douberly, G. E. Infrared Laser Spectroscopy of the CH_3OO Radical Formed from the Reaction of CH_3 and O_2 within a Helium Nanodroplet. *J. Phys. Chem. A.* **2012**, *116*, 5299-5304.

(58) Leavitt, C. M.; Moradi, C. P.; Acrey, B. W.; Douberly, G. E. Infrared Laser Spectroscopy of the Helium-Solvated Allyl and Allyl Peroxy Radicals. *J. Chem. Phys.* **2013**, *139*, 234301.

(59) Moradi, C. P.; Morrison, A. M.; Klippenstein, S. J.; Goldsmith, C. F.; Douberly, G. E. Propargyl + O_2 Reaction in Helium Droplets: Entrance Channel Barrier or Not? *J. Phys. Chem. A.* **2013**, *117*, 13626-13635.

(60) Jochnowitz, E. B.; Zhang, X.; Nimlos, M. R.; Varner, M. E.; Stanton, J. F.; Ellison, G. B. Propargyl Radical: Ab Initio Anharmonic Modes and the Polarized Infrared Absorption Spectra of Matrix-Isolated $HCCCH_2$. *J. Phys. Chem. A.* **2005**, *109*, 3812-3821.

(61) Yuan, L.; DeSain, J.; Curl, R. F. Analysis of the K-Subband Structure of the ν_1 Fundamental of Propargyl Radical $H_2CC{\equiv}CH$. *J. Mol. Spectrosc.* **1998**, *187*, 102-108.

(62) Nauta, K.; Miller, R. E. The Vibrational and Rotational Dynamics of Acetylene Solvated in Superfluid Helium Nanodroplets. *J. Chem. Phys.* **2001**, *115*, 8384-8392.

(63) Küpper, J.; Merritt, J. M.; Miller, R. E. Free Radicals in Superfluid Liquid Helium Nanodroplets: A Pyrolysis Source for the Production of Propargyl Radical. *J. Chem. Phys.* **2002**, *117*, 647-652.

CHAPTER 5

A RESEARCH-BASED ACTIVITY FOR USE IN A SCALE-UP CLASSROOM ON STUDENTS' DEFINITIONS OF ENTROPY: CREATION, IMPLEMENTATION AND RESULTS

5.1 Introduction

According to the 2012 President's Council of Advisors on Science and Technology (PCAST) Undergraduate STEM Education Report, the United States must produce at least 1 million more science, technology, engineering, and math (STEM) major graduates by 2022 in order to meet the demands of society and to continue the country's tradition of innovation in these fields.[1] From 2012 data, this equated to a necessity for a 34% increase in the number of college graduates with a STEM degree. One suggestion for a simple way to begin to accomplish this feat is to increase retention of STEM major students within their first two years of college. This strategy alone would produce approximately 750,000 new graduates over the 10-year span. Another recommendation for increasing the STEM graduation rate is for higher education institutions to adopt evidence-based teaching practices that actively engage students; these have been shown to improve student learning and critical thinking skills at the university level.[2, 3] Interest in STEM fields can become stagnant or decline when traditional lecture is the sole teaching method. [4, 5] However, when students are actively

involved in learning, such as in a chemistry laboratory course, they are more likely to develop a positive attitude towards the material and enjoy it more than the lecture component.[6-8]

Active learning environments, such as Student-Centered Active Learning Environments for Upside-down Pedagogies (SCALE-UP), have been shown to increase overall performance and lower drop/fail/withdrawal (DFW) rates in STEM courses.[3] In their meta-analysis of 225 previously published and unpublished studies, Freeman et al. concluded that active learning improved exam scores by 6% when compared to traditional lecture sections; students in traditional classrooms were 1.5 times more likely to fail the course than those in an active learning course. These results were found to hold true across all STEM disciplines as well as a variety of class sizes, and examination types.

The SCALE-UP pedagogical model was developed by Robert Beichner at North Carolina State University for introductory, large-enrollment physics courses. This method focuses on student collaborative groups to solve problems and work through activities that reinforce topics covered in the course.[9, 10] Rather than listening to a lecture for an entire class period, students work together with their group members and neighboring groups to complete these activities. During this time the instructor facilitates class wide discussions, asks questions to guide the students/groups in a semi-Socratic type fashion, and provide a "big picture" view of the topic for the session.[11, 12] Preliminary research from courses at NC State agree with the Freeman study in that active learning environments (specifically the SCALE-UP method) help students perform better on exams than traditional settings and promotes a more positive attitude toward learning.[13, 14]

Since its inception, this approach has been modified for use in a variety of STEM and non-STEM courses at over 500 institutions worldwide.[15]

In 2016, the University of Georgia began an active learning initiative, which prompted the building of a new Science Learning Center (SLC) that houses two of these SCALE-UP classrooms. See Figure 5.1 for a simplified schematic of the room design in the SLC. These rooms were modeled after those at NC State University which were designed carefully to promote an engaging classroom environment.[10] This included performing research on the shape, orientation, and number of tables to be used as well as the use of technology within the classroom and the number of students per group.[9, 10] Tables in the SLC are equipped with desktop computers, and within the room itself, there are multiple projectors and monitors that both the students and instructor can use to display information. White boards line the classroom walls and are used by instructors and by students as they are working in groups.

Physical chemistry is, in general, a difficult course for undergraduate students because of the abstract concepts presented. It can become more difficult when students lack motivation and when teacher-centered pedagogies are used.[16] Students also enter the class with preconceived notions about the difficulty of the course and their personal abilities, making it difficult to foster success.[17, 18] Specifically, thermodynamics is a challenging section of the course for many reasons including the novelty of concepts as well as the lack of required math skills; although, it is thought that this latter difficulty stems from students not being able to transfer previously learned math skills or to make connections between mathematical formulas and their physical meanings.[17, 19-22] In thermodynamics, entropy is often viewed as a difficult topic, and students will often use

analogies to make the connection to their previous knowledge.[23] A prevalent definition involves disorder, but this definition does not hold for all situations and can often lead to future misconceptions and confusion.[24-28] For example, entropy is often equated to the disorder that occurs in a college dorm room over time. During move-in, every object has its place, and the room is orderly. After a few weeks' time has passed, the room becomes untidy and disorganized, which is attributed to the increase in entropy that occurs over time. Another description of entropy involves a microscopic interpretation, in which it is viewed as the spread of energy within molecular states; this is a much more specific definition, in which misunderstanding can be limited.[29] Disorder should not be regarded as a "bad" definition, but without proper context, students often transfer this explanation to other situations and can compromise their intuition.[25]

Although active learning in chemistry has become prevalent, only a handful of activities are geared towards upper level courses such as physical chemistry; few are designed solely for use in a SCALE-UP classroom.[15, 30-42] As a way to combat this issue at the University of Georiga and help provide students with alternative definitions of entropy, the activity described herein was created for use in the one-semester physical chemistry course (CHEM 3110). Students work through the meaning of entropy and enthalpy and how they relate to molecules such as the model dipeptide N-acetylglycine methylamide (NAGMA) while gaining experience reading a current research article and learning about research techniques in physical chemistry.[43] We believe that this activity is the first of its kind in that it relates current physical chemistry research to physical chemistry SCALE-UP curriculum at the University of Georgia.

5.2 Project Methods

5.2.1 Creation and Implementation of Activity

From the fall semester of 2015 through spring 2016, a preliminary version of the activity was created to be used in the CHEM 3110: Fundamentals of Physical Chemistry course at the University of Georgia. During the fall 2016 semester, students in the course were asked to participate in an education project. Their consent was documented on the form shown in Figure 5.2. They were made aware that the activity was newly created and that their answers and opinions about the activity would be used in two ways: as data to fulfill the education project requirements of the graduate school's Interdisciplinary Certificate in University Teaching and to improve the activity for use in subsequent years. All students opted to participate in the process. Students self-selected into groups of 3-4 students and, over the course of two 50 minute class periods, worked together to read the article[43] and complete the corresponding questions. The activity used in the initial project is shown in Figure 5.3. Results of this initial phase of the project (i.e. students' answers from the activity) were analyzed to find trends in wording and phrases as they answered the questions from the activity. This is a similar procedure to what Luft and coworkers used in their latest article.[44] A more thorough explanation of this analysis process is described below in the following section. From the analysis of questions 1 and 2 from this initial activity, it was concluded that students had a variety of different definitions of entropy and that this topic should be explored further. Student opinions of the process and activity were elicited and recorded with an online survey. Pertinent

results from this survey are shown in Figure 5.4. Feedback from this survey was used to revise the activity for use the following year.

Results from the 2016 analysis were used to structure the final project, which was performed during the fall semester of 2017 and used to fulfill the requirements of the certificate program. The revised NAGMA activity, shown in Figure 5.5, was implemented for the CHEM 3110 course in one of the SLC's new SCALE-UP rooms to facilitate group collaboration. The initial project, however, was housed in a traditional classroom with individual desks that students moved when forming their groups. A pre-test and post-test were created to serve as reference points for student knowledge before and after completing the activity. This methodology is common practice and was also used by Bennett and Sözbilir to study students' understanding of entropy in a physical chemistry course.[28]

Before beginning the activity, students were given the details of the project and asked to sign a consent form (Figure 5.6) if they agreed to have their work used as data. All students agreed to participate. During one 50 minute class session, students discussed the research article, which they were asked to read before the class session, and asked questions about the experiment or the data before they started the activity. Students were also asked to complete the pre-test questionnaire during this class period (Figure 5.7).

The following class period, students met in one of the SLC SCALE-UP rooms and self-selected into sub-groups of 2-3, which were seated with 2 additional groups to form a table of 8-9 students. For the period, students were told to complete the questions associated with the article (Figure 5.5) and that they were allowed to use the article, their notes, their books, and the internet to find answers. Students were also encouraged to

work together with the peers in their sub-group as well as students in their larger group to come up with and discuss their answers. They were also allowed to ask the instructor for help during the activity since this would be a normal occurrence during any other class session. Throughout the period, the instructor of record (IOR) for the course walked around the room to aid students with the activity and to prompt and answer questions that arose during discussions. To limit bias, only the IOR was allowed to interact with students and was told the same information about this project that the students were told. Although some students were able to finish the assignment within the 50 minute class period, instructions were given that the activity could be finished outside of class and turned in during the following class session. Since students were able to use a variety of resources within the classroom, there was no worry
about letting students finish the assignment outside of class.

During a third class session, students turned in the activity and were asked to take the post-test questionnaire and a survey about the activity, the TA, and their overall experience (Figure 5.8). The activity and typical answers were also discussed with the class so that students had correct answers to look back on when reviewing the concepts covered in the activity. Once all materials were collected, the answers to the pre- and post-tests as well as the activity questions were analyzed to look for trends in students' answers.

5.2.2 Methods for Analysis of Student Work

Following the initial project in 2016, answers to each of the activity's questions were analyzed. Different types of questions were analyzed with different methods; for example, free-response questions were analyzed based on trends in the language used by students,[44] whereas questions that asked students to rank a series of objects were analyzed based on correct vs. incorrect responses. Questions 1 and 2 from the original activity had the most potential for gathering meaningful data for a follow-up project (see Figure 5.3). Because question 1 was a simplified matching question, most of the information came from the second question which asked students to explain their answer. These responses indicated that these particular students hold many different views about entropy and enthalpy and a few common words and phrases began to appear. From these responses, a list of structural codes was generated to indicate answers with similar language.[45] If a student used the word "disorder" in their answer or mentioned phrases that are consistent with a macromolecular viewpoint (i.e. chaos, or another "real-world" analogy), these answers were grouped together. Other groupings included answers with a molecular viewpoint (i.e. degrees of freedom, spread of energy) or answers with viewpoints different from these two. Coded responses were formed into a table for ease of analysis.[46] The information gathered from these responses led to the question: How do CHEM 3110 students' definitions of entropy change as a function of completing this activity?

Responses from the final project were analyzed in a similar fashion. Pre-test question 1 was coded by the same method as the initial project's open-ended question. Questions 2 and 3 were scored based on correct vs. incorrect responses and any

additional explanations provided by the students were coded like other open-ended questions. Since the purpose of the project was to track student definitions of entropy before and after completing the activity, the activity itself was not analyzed. The post-test questions were analyzed the same way as the pre-test.

5.3 Results and Discussion

Because this project was created specifically for CHEM 3110 students at the University of Georgia, the following results should not be used to generalize physical chemistry students' learning in other types of courses or at other universities. After analyzing student responses, a few trends in the data appeared. First, 91.17% of students mentioned "chaos" or disorder" in their definitions of entropy in the pre-test and only 76.47% in the post-test. Although not a dramatic change, this still shows us that students are starting to think of entropy in a way other than disorder. Another definition of entropy involves the distribution of energy among states of the molecule; this definition (or similar) was used 14.70% in the post-test as opposed to 11.76% in the pre-test. For question one, students' answers also became more clear and concise from 20.58% having an incorrect or unclear definition for the pre-test and only 5.88% for the post-test. We believe that these results indicate that students are learning more about the concept of entropy and feel more comfortable discussing it after completion of the activity.

Question two showed a macroscopic view of entropy, and not surprisingly, students mentioned "chaos" and "order" or "disorder" 76.47% in the pre-test and 79.41% in the post-test. Whether or not students realized that this definition fits with a

macroscopic point of view is not definitive, but it is promising to know that more students possibly recognized this when answering this question for the post-test. Another interesting result came about from this question; 5.88% mentioned "organization" or "arrangement" in the pre-test while 17.64% mentioned similar phrases in the post-test. In this macroscopic example, it is appropriate to mention these phrases, but it's important to note that these phrases do not always carry over to a microscopic view. Care should be taken to dispel any of these misconceptions before moving to a molecular view. Students were able to rank these pictures from least to greatest entropy fairly easily. Only 5.88% answered incorrectly in the pre-test and 2.94% in the post-test, so it seems that students have a good grasp of this macroscopic view of entropy. This should not be surprising because students learn this definition of entropy as early as general chemistry and often make up analogies to make it easier to understand.

When asked to rank the given molecules from least to greatest entropy in question 3, 47.06% were able to in the pre-test as opposed to 50% in the post-test. There were multiple correct answers based on the information given to the students, so this value includes all possible correct answers. Based on DFT calculations performed at the B3LYP/6-311++G(3d,3p) level of theory, the molecules rank from least to greatest entropy as formaldehyde, acetic acid, and benzonitrile having entropy values of 218.631, 287.707, and 323.242 J/mol K, respectively. This would correspond to an answer of 2, 1, 3 on the pre- and post-test questions. Another acceptable answer would be to switch the ordering of benzonitrile and acetic acid due to the torsional motion of the OH group of acetic acid; this could be conceived to have a greater effect on the molecule's entropy than the greater number of atoms for benzonitrile. Using this logic would give an

ordering of 3, 1, 2 for the pre- and post-test questions. These values are for molecules at room temperature (298 K). A bar graph of the responses from the pre- and post-tests is shown in Figure 5.9. For reference, the correct answers are shown as green bars with the legend labels 213 and 312. The increase in the percentage of correct answers from pre- to post-test could be because students are becoming more comfortable with their new definitions of entropy and are able to apply their new knowledge, but there is no definitive way to conclude this given the current data. However, results show that students talked about the structure of the molecule 67.64% in the pre-test and 82.35% in the post-test, which is another promising result. Students did not mention anything about the structure of a molecule in their definitions from the pre-test question 1, so it seems that this activity has forced them to think about entropy in this new light as well.

5.4 Conclusions

An activity for use in an undergraduate SCALE-UP classroom has been created for a physical chemistry course at the University of Georgia. Through several iterations, the original activity was improved upon and used during the fall 2017 semester as an intervention in an educational project. Students' definitions of entropy were recorded before and after the intervention by means of a pre- and post-test questionnaire. This was done to compare their answers and determine if the intervention had any effect on their definitions. Students rely heavily on an analogy of "disorder" when thinking about entropy. Promising results show that students used this definition 14.7% less in the post-test than in the pre-test discussion questions after completing the activity.

Although this was a small sample size (34 students) and was only studied in one course at one university, it seems that this activity was successful in giving students new ways to look at entropy. It also gave them an opportunity to differentiate between macroscopic and microscopic points of view. In general, the class' definitions of entropy changed from a macroscopic (chaos, disorder) point of view to a microscopic (energy distribution, states, molecular structure) point of view. For future reference, more class discussions should involve connecting the macroscopic and microscopic views more and make their relationship more explicit. This should help students separate these two views and pick which definition fits best with a given scenario. It would be interesting to see if students from other physical chemistry courses at UGA were impacted similarly to students in the CHEM 3110 class. Although outside the scope of this project, the effects that this activity have on students' definitions could be studied across multiple universities with varying class sizes in order to get a broad consensus of student learning.

Along with these results, students had an overall positive experience with the activity and liked that it connected their lessons with a real-world application. Other students disliked that it did not connect enough with class material and that they were not graded on learning the information from the activity. Aligning this activity to their assessments in future classes should help with this. Also having students read more examples of research papers prior to this activity should help with their confidence in understanding this paper. Despite having the dedicated class session to discussing the paper, some students still felt like the paper was too advanced and that they would like to have had a better understanding of it before beginning the activity. Overall, this activity seems to have been successful in that students enjoyed learning about this new side of

entropy and are more aware of their own previous definitions of this complicated concept.

References

(1) PCAST STEM Undergraduate Working Group *Engage to Excel: Producing One Million Additional College Graduates with Degrees in Science, Technology, Engineering, and Mathematics*; Office of the President: Washington, 2012.

(2) Prince, M. Does Active Learning Work? A Review of the Research. *J. Eng. Educ.* **2004**, *93*, 223-231.

(3) Freeman, S.; Eddy, S. L.; McDonough, M.; Smith, M. K.; Okoroafor, N.; Jordt, H.; Wenderoth, M. P. Active Learning Increases Student Performance in Science, Engineering, and Mathematics. *Proc. Natl. Acad. Sci. U. S. A.* **2014**, *111*, 8410-8415.

(4) Tobias, S. *Revitalizing Undergraduate Science: Why Some Things Work and Most Don't*; Research Corporation: Tucson, Arizona, 1992.

(5) MacGregor, J. C., James; Smith, Karl A.; Robinson, Pamela *Strategies for Energizing Large Classes: From Small Groups to Learning Communities*; Jossey-Bass Inc. Publishers: San Francisco, CA, 2000; Vol. 81.

(6) Freedman, M. P. Relationship Among Laboratory Instruction, Attitude Toward Science, and Achievement in Science Knowledge. *J. Res. Sci. Teach.* **1997**, *34*, 343-357.

(7) Pringle, D. L.; Henderleiter, J. Effects of Context-Based Laboratory Experiments on Attitudes of Analytical Chemistry Students. *J. Chem. Educ.* **1999**, *76*, 100.

(8) Okebukola, P. A. An Investigation of Some Factors Affecting Students, Attitudes Toward Laboratory Chemistry. *J. Chem. Educ.* **1986**, *63*, 531.

(9) Beichner, R. J. The SCALE-UP Project: A Student-Centered Acitve Learning Environment for Undergraduate Programs. North Carolina State University, Ed. 2004.

(10) Beichner, R. J. The Student Centered Activities for Large Enrollment Undergraduate Programs (SCALE-UP) Project. In *Research-Based Reforms in University Physics*, 2007; Vol. 1.

(11) Morse, R. A. The Classic Method of Mrs. Socrates. *Phys. Teach.* **1994**, *32*, 276-277.

(12) Hake, R. R. Socratic Pedagogy in the Introductory Physics Laboratory. *Phys. Teach.* **1992**, *30*, 546-552.

(13) Oliver-Hoyo, M. T.; Allen, D.; Hunt, W. F.; Hutson, J.; Pitts, A. Effects of an Active Learning Environment: Teaching Innovations at a Research I Institution. *J. Chem. Educ.* **2004**, *81*, 441.

(14) Oliver-Hoyo, M. T.; Allen, D. Attitudinal Effects of a Student-Centered Active Learning Environment. *J. Chem. Educ.* **2005**, *82*, 944.

(15) North Carolina State University Physics Education Research Group SCALE-UP: Student-Centered Active Learning Environment with Upside-Down Pedagogies, scaleup.ncsu.edu (accessed February 6).

(16) Sözbilir, M. What Makes Physical Chemistry Difficult? Perceptions of Turkish Chemistry Undergraduates and Lecturers. *J. Chem. Educ.* **2004**, *81*, 573.

(17) Nicoll, G.; Francisco, J. S. An Investigation of the Factors Influencing Student Performance in Physical Chemistry. *J. Chem. Educ.* **2001**, *78*, 99.

(18) Carter, C. S.; Brickhouse, N. W. What Makes Chemistry Difficult? Alternate Perceptions. *J. Chem. Educ.* **1989**, *66*, 223.

(19) Tsaparlis, G.; Finlayson, O. E. Physical Chemistry Education: Its Multiple Facets and Aspects. *Chem. Educ. Res. Pract.* **2014**, *15*, 257-265.

(20) Derrick, M. E.; Derrick, F. W. Predictors of Success in Physical Chemistry. *J. Chem. Educ.* **2002**, *79*, 1013.

(21) Hahn, K. E.; Polik, W. F. Factors Influencing Success in Physical Chemistry. *J. Chem. Educ.* **2004**, *81*, 567.

(22) Becker, N.; Towns, M. Students' Understanding of Mathematical Expressions in Physical Chemistry Contexts: An Analysis Using Sherin's Symbolic Forms. *Chem. Educ. Res. Pract.* **2012**, *13*, 209-220.

(23) Bain, K.; Moon, A.; Mack, M. R.; Towns, M. H. A Review of Research on the Teaching and Learning of Thermodynamics at the University Level. *Chem. Educ. Res. Pract.* **2014**, *15*, 320-335.

(24) Wright, P. G. Entropy and Disorder. *Contemp. Phys.* **1970**, *11*, 581-588.

(25) Haglund, J. Good Use of a 'Bad' Metaphor. *Sci. Educ.* **2017**, *26*, 205-214.

(26) Ben-Naim, A. Entropy: Order or Information. *J. Chem. Educ.* **2011**, *88*, 594-596.

(27) Bucy, B. Physics Education Research Conference, 2006.

(28) Bennett, J. M.; Sözbilir, M. A Study of Turkish Chemistry Undergraduates' Understanding of Entropy. *J. Chem. Educ.* **2007**, *84*, 1204-1208.

(29) Leff, H. S. Thermodynamic Entropy: The Spreading and Sharing of Energy. *Am. J. Phys.* **1996**, *64*, 1261-1271.

(30) Southam, D. C. L., Jennifer E. Supporting Alternative Strategies for Learning Chemical Applications of Group Theory. *J. Chem. Educ.* **2013**, *90*, 1425-1432.

(31) Tsaparlis, G. G., Marianna Addition of a Project-Based Component to a Conventional Expository Physical Chemistry Laboratory. *J. Chem. Educ.* **2007**, *84*, 668-670.

(32) Hinde, R. J. K., Jeffrey Student Active Learning Methods in Physical Chemistry. *J. Chem. Educ.* **2001**, *78*, 93-99.

(33) Vázquez, A. V.; McLoughlin, K.; Sabbagh, M.; Runkle, A. C.; Simon, J.; Coppola, B. P.; Pazicni, S. Writing-To-Teach: A New Pedagogical Approach To Elicit Explanative Writing from Undergraduate Chemistry Students. *J. Chem. Educ.* **2012**, *89*, 1025-1031.

(34) Martini, S. R.; Hartzell, C. J. Integrating Computational Chemistry into a Course in Classical Thermodynamics. *J. Chem. Educ.* **2015**, *92*, 1201-1203.

(35) Johnson, L. E.; Engel, T. Integrating Computational Chemistry into the Physical Chemistry Curriculum. *J. Chem. Educ.* **2011**, *88*, 569-573.

(36) Muniz, M. N.; Oliver-Hoyo, M. T. Investigating Quantum Mechanical Tunneling at the Nanoscale via Analogy: Development and Assessment of a Teaching Tool for Upper-Division Chemistry. *J. Chem. Educ.* **2014**, *91*, 1546-1556.

(37) Iyengar, S. S.; deSouza, R. T. Teaching Thermodynamics and Kinetics to Advanced General Chemistry Students and to Upper-Level Undergraduate Students Using PV Diagrams. *J. Chem. Educ.* **2014**, *91*, 74-83.

(38) Hunnicutt, S. S.; Grushow, A.; Whitnell, R. Guided-Inquiry Experiments for Physical Chemistry: The POGIL-PCL Model. *J. Chem. Educ.* **2015**, *92*, 262-268.

(39) Castle, K. J.; Rink, S. M. Customized Laboratory Experience in Physical Chemistry. *J. Chem. Educ.* **2010**, *87*, 1360-1363.

(40) Hoffman, G. G. Using an Advanced Computational Laboratory Experiment To Extend and Deepen Physical Chemistry Students' Understanding of Atomic Structure. *J. Chem. Educ.* **2015**, *92*, 1076-1080.

(41) Miller, C. S.; Ellison, M. Walsh Diagrams: Molecular Orbital and Structure Computational Chemistry Exercise for Physical Chemistry. *J. Chem. Educ.* **2015**, *92*, 1040-1043.

(42) Reilly, J. T.; Strickland, M. A Writing and Ethics Component for a Quantum Mechanics, Physical Chemistry Course. *J. Coll. Sci. Teach.* **2010**, *39*, 35-41.

(43) Leavitt, C. M.; Moore, K. B.; Raston, P. L.; Agarwal, J.; Moody, G. H.; Shirley, C. C.; Schaefer, H. F.; Douberly, G. E. Liquid Hot NAGMA Cooled to 0.4 K: Benchmark Thermochemistry of a Gas-Phase Peptide. *J. Phys. Chem. A.* **2014**, *118*, 9692-9700.

(44) Nixon, R.; Toerien, R.; Luft, J. Knowing More Than Their Students: Characterizing Secondary Science Teachers' Subject Matter Knowledge. ResearchGate, 2019.

(45) Saldaña, J. *The Coding Manual for Qualitative Researchers*, 2 ed.; SAGE: Thousand Oaks, California, 2013.

(46) Miles, M. B.; Huberman, A. M.; Saldaña, J. *Qualitative Data Analysis: A Methods Sourcebook*, 3 ed.; SAGE: Thousand Oaks, California, 2014.

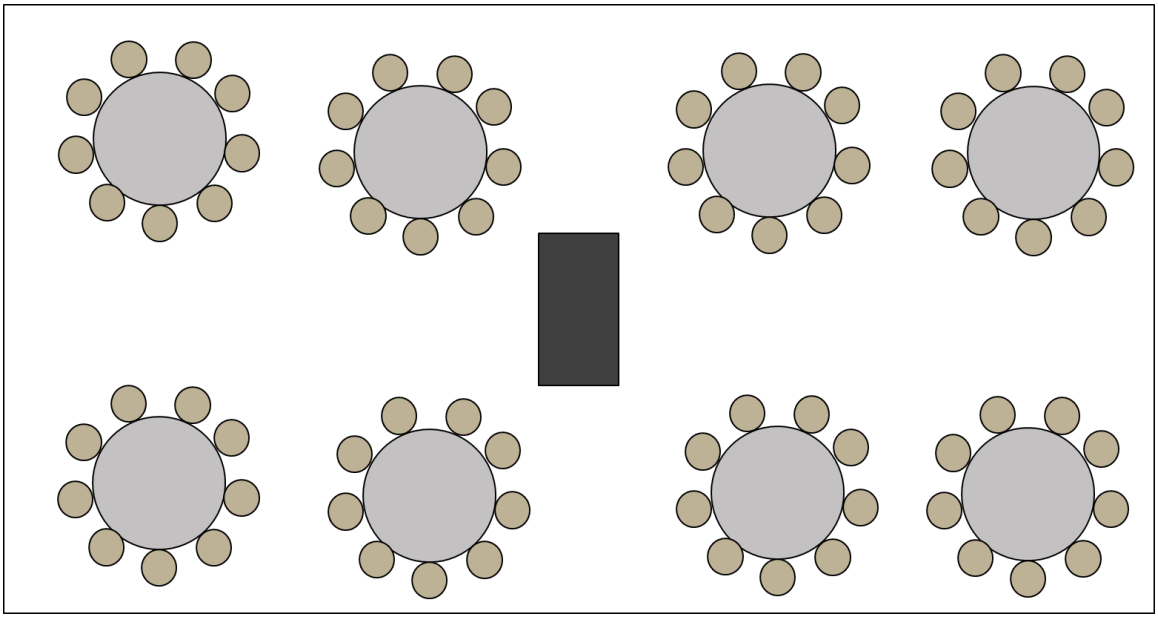

Figure 5.1: Simple schematic of a SCALE-UP classroom in the Science Learning Center at UGA. Each round table holds 9 students giving a total student count of 72 for this particular classroom. The tables are equipped with 3 desktop computers (1 for every group of 3) to be used during a class session. The dark rectangle at the center of the room represents the instructor podium which houses an additional desktop computer and controllers for the projectors and monitors. White boards line the walls of the room as well.

I, _____, give the instructor (Gary
(Please print name here)
Douberly) and TA (Alaina Brown) of CHEM 3110 permission to use my work from in-class activities and problems as part of an evaluation to improve the course and activities as a whole. In addition, I give permission for my work to be used in the TA's teaching portfolio as evidence of student work. (Note: your name will not be associated with your work in this portfolio.)

Signature:_____

Date: _____

Figure 5.2: Student consent form used in Fall 2016 CHEM 3110 course.

Figure 5.3: Preliminary activity used in fall 2016 class for CHEM 3110. In the text, this document is associated with the initial project.

THE JOURNAL OF PHYSICAL CHEMISTRY A

Article

pubs.acs.org/JPCA

Liquid Hot NAGMA Cooled to 0.4 K: Benchmark Thermochemistry of a Gas-Phase Peptide

Christopher M. Leavitt,[†] Kevin B. Moore III,[‡] Paul L. Raston,[†,§] Jay Agarwal,[‡] Grant H. Moody,[†] Caitlyne C. Shirley,[†] Henry F. Schaefer III,[‡] and Gary E. Douberly*[,†]

[†]Department of Chemistry and [‡]Center for Computational Quantum Chemistry, University of Georgia, Athens, Georgia 30602, United States

[§]Department of Chemistry, University of Adelaide, Adelaide, SA 5005, Australia

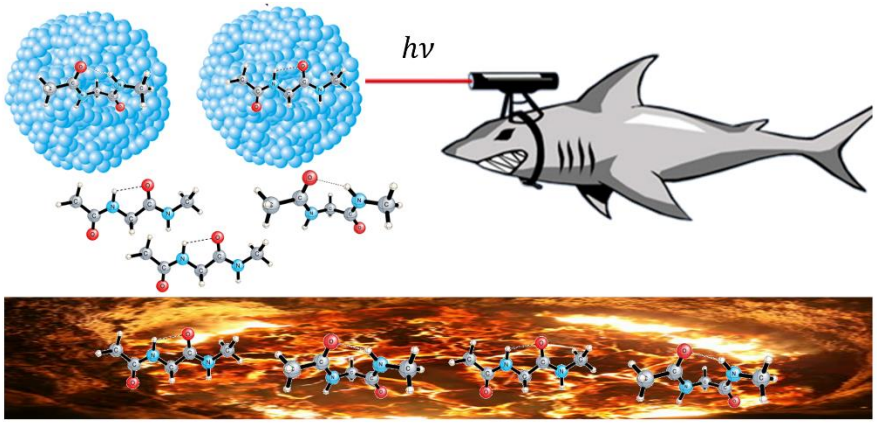

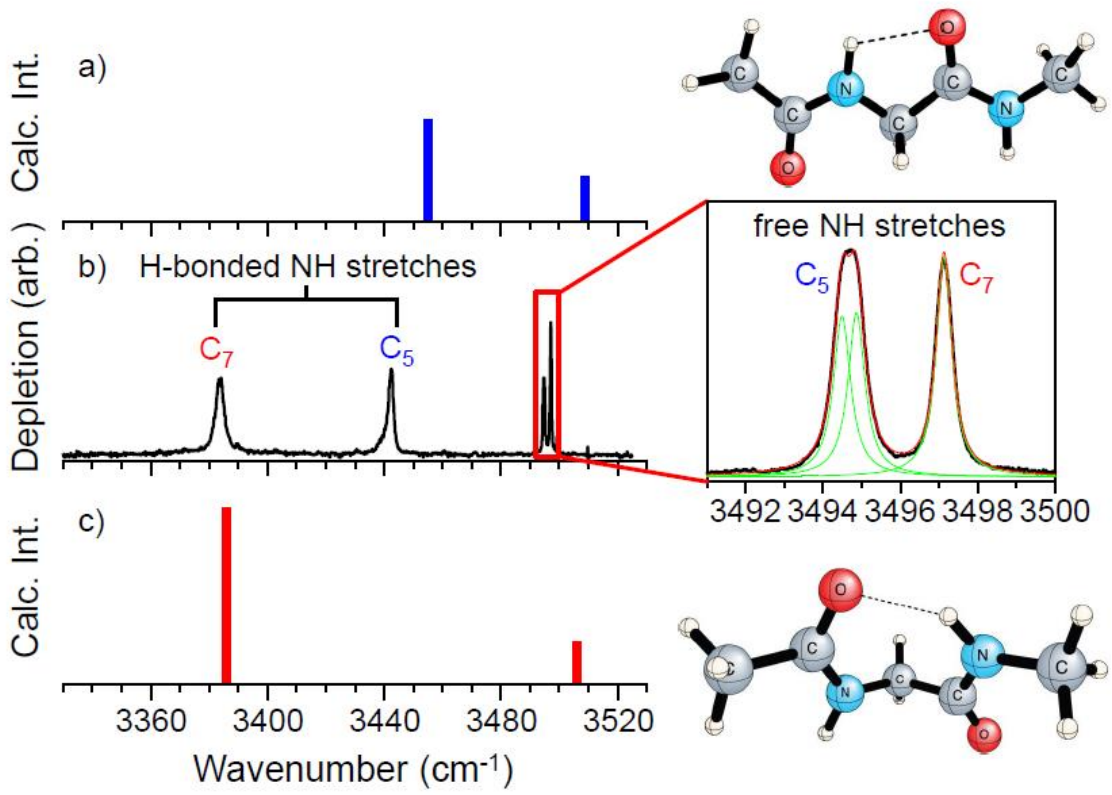

Experimental (frame b) and computed infrared spectra of the (a) C5 and (c) C7 isomers of N-acetylglycine methylamide (NAGMA).

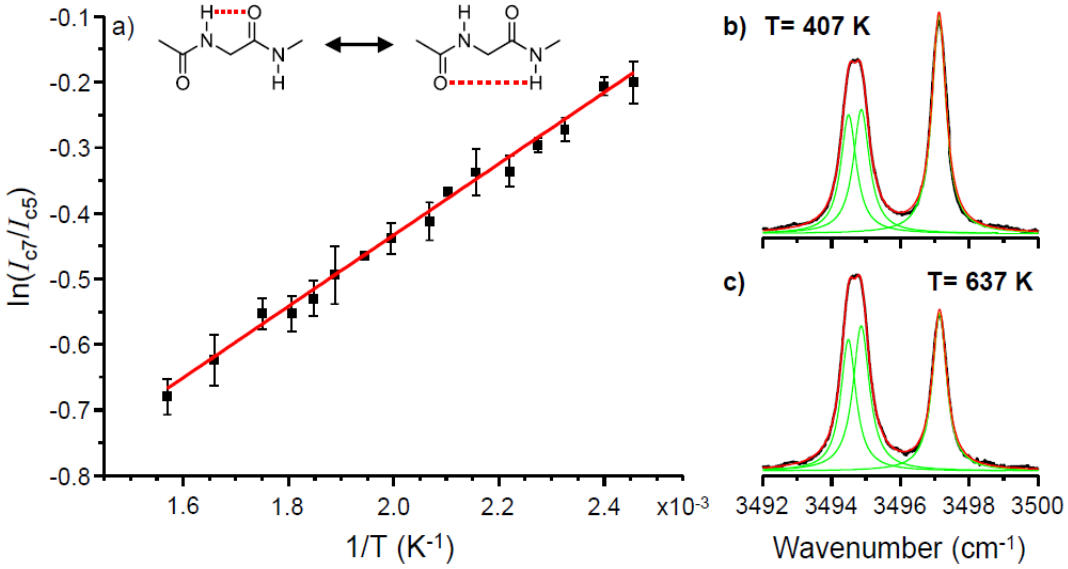

Van't Hoff Plot of NAGMA

1. Without doing any calculations, which isomer do you believe is enthalpically favored? Which one do you believe is entropically favored? (use your intuition!)

2. Describe the molecular level reasoning you used to answer question #1.

3. Re-derive the entire van't Hoff formula shown in equation 5, and list all assumptions. Start from the formula:

$$\Delta_r G = \Delta_r G^{\ominus} + RT \ln Q$$

4. How is ΔS and ΔH determined experimentally? Start by describing the spectroscopy technique used, and the critical assumptions that are made, which make this approach "valid".

5. Calculate ΔG for C5 to C7 isomerization at 400, 500, and 600 K. What does this tell us about the spontaneous direction of the reaction?

6. Calculate the temperature at which the spontaneous direction of the reaction changes, given the experimental thermodynamics. How does this differ from the temperature range explored experimentally?

7. What assumptions were made when computing the thermodynamics of this system using quantum mechanics? Is it reasonable to expect the quantum chemistry calculations to be capable of reproducing the experimental values at this level of approximation? What could be done better to improve the agreement between experiment and theory? Is it practical to do so?

8. Why not just do this experiment with a conventional FTIR spectrometer where the sample consists of NAGMA vapor isolated in a gas-cell? Why do we resort to such an expensive and “sophisticated” experimental technique to probe the gas-phase thermochemistry of dipeptide systems?

9. Who is the most famous author on the paper? Why?

Figure 5.4: Relevant survey questions and results from the 2016 survey given after the initial project.

To what extent do you agree with the following statements: Assignments for the problem solving sessions were useful for helping me learn the material.

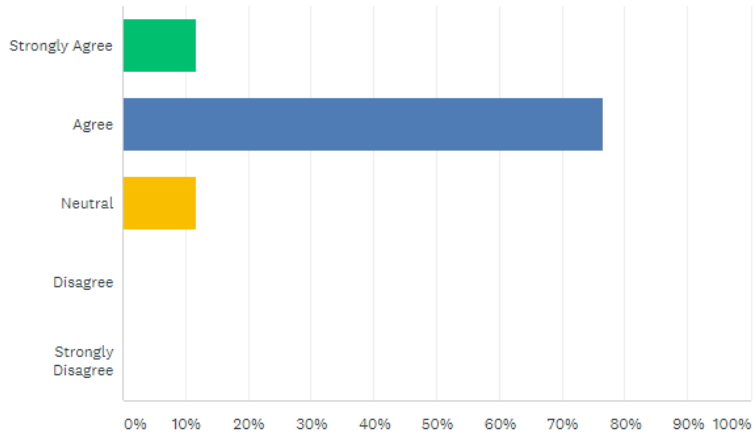

The activity and problem chosen for the problem solving sessions challenged me to think and learn.

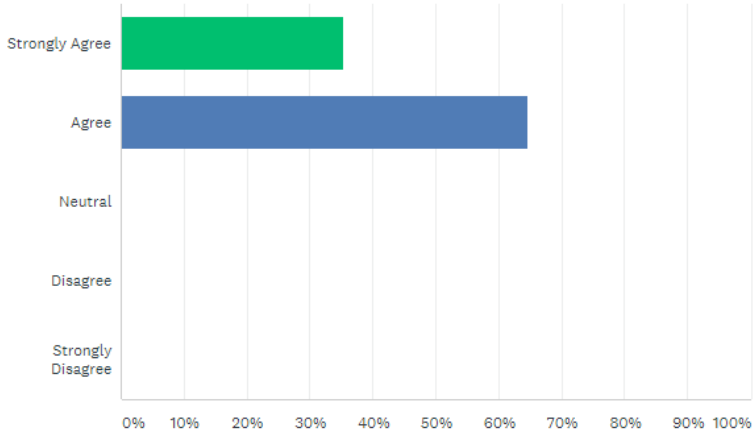

Please rate Activity 1 (NAGMA) based on a scale from 1-5; 1 being not helpful for learning class material and 5 being extremely helpful for learning class material.

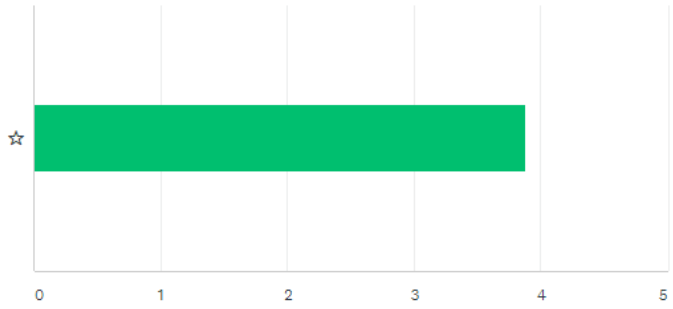

Figure 5.5: Modified activity used in CHEM 3110 fall 2017 semester. In the text, references to the final project utilized this activity.

Name_____

(Prior to completing these questions, please read Liquid Hot NAGMA Cooled to 0.4 K: Benchmark Thermochemistry of a Gas-Phase Peptide by Christopher M. Leavitt *et al*.)

1. What is the entropy (ΔS) for the isomerization from the C_5 conformer to the C_7 conformer?

2. What is the enthalpy (ΔH) for the isomerization from the C_5 conformer to the C_7 conformer?

3. How were both of these values determined experimentally? Start by describing the spectroscopy technique used, and the critical assumptions that are made, which make this approach "valid".

4. Calculate ΔG for C_5 to C_7 isomerization at 400, 500, and 600 K. What does this tell us about the spontaneous direction of the reaction?

5. Calculate the temperature at which the spontaneous direction of the reaction changes, given the experimental thermodynamics. How does this differ from the temperature range explored experimentally?

6. Which isomer is enthalpically favored? Which isomer is entropically favored? Describe your answer in terms of a molecular view of each isomer.

7. Re-derive the entire van't Hoff formula shown in equation 5, and list all assumptions. Start from the formula:

$$\Delta_r G = \Delta_r G^{\ominus} + RT \ln Q$$

8. What assumptions were made when computing the thermodynamics of this system using quantum mechanics? Is it reasonable to expect the quantum chemistry calculations to be capable of reproducing the experimental values at this level of approximation? What could be done better to improve the agreement between experiment and theory? Is it practical to do so?

9. Why not just do this experiment with a conventional FTIR spectrometer where the sample consists of NAGMA vapor isolated in a gas-cell? Why do we resort to such an expensive and "sophisticated" experimental technique to probe the gas-phase thermochemistry of dipeptide systems?

CHEM 3110 Fall 2017

You are being invited to participate in a project about student perceptions of entropy. This project is being conducted by Alaina Brown (Graduate Student) and is sponsored by Dr. Gary Douberly (Course Instructor), from the Department of Chemistry at the University of Georgia. This project is being performed to fulfill a requirement for the University of Georgia Graduate School Interdisciplinary Certificate in University Teaching.

There are no known risks if you decide to participate. There are no costs to you for participating in the project. The information you provide will allow us to improve the teaching of this subject area for future courses. To participate in the project, you will be responsible for filling out a pre-activity survey, as well as completing a post-activity survey. The pre- and post-surveys will take approximately 10 minutes total to complete. Additionally, there is an in-class activity that accompanies the pre- and post- surveys. Regardless of your participation in the project, everyone will complete the in-class activity.

The surveys as well as the activity will have your name associated with them, however, all answers collected will remain between you, the Graduate Student and the Course Instructor. There will be no grade associated with the surveys, but the activity will be graded at the discretion of the Course Instructor. Data collected from this project will be used for the purpose of fulfilling requirements for the University of Georgia Graduate School Interdisciplinary Certificate in University Teaching and will not affect your grade for the assignment or the course. Should the data be published (as in a dissertation), no individual information will be disclosed. Additionally, you are agreeing that any work you complete for the activity and surveys may be used as an example of student work in fulfilment of the University of Georgia Graduate School Interdisciplinary Certificate in University Teaching. No names will be associated with your work if it is used for this purpose.

Your participation in this project is voluntary. By signing this agreement, you are voluntarily agreeing to participate. You are free to decline to answer any particular question you do not wish to answer for any reason.

If you have any questions about the project, please contact Alaina Brown by email at alaina.brown@uga.edu.

_____

STUDENT NAME PRINTED

_____ _____

STUDENT SIGNATURE DATE

Figure 5.6: Student consent form used during the fall 2017 course.

Figure 5.7: Student pre-test questionnaire given to students in the fall 2017 course.

CHEM 3110 Fall 2017 Pre-Test Name _____
(Use additional paper if necessary.)

1. Define entropy. Use any examples necessary to explain your answer.

2. Which picture represents the system with higher entropy? Please explain your reasoning for choosing this picture.

A.

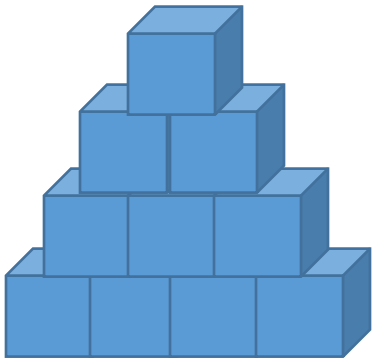

B.

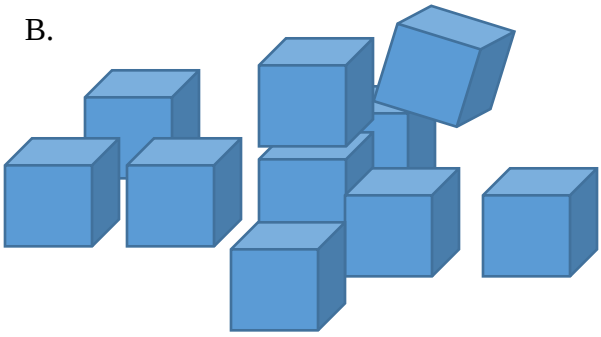

3. Rank the molecules from 1-3: 1 having the lowest entropy and 3 having the highest entropy. Please explain your reasoning for ranking these molecules as you have.

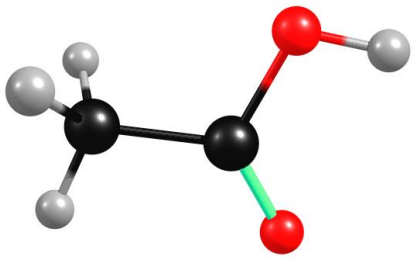

_____

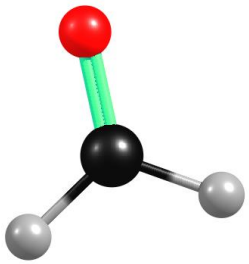

_____

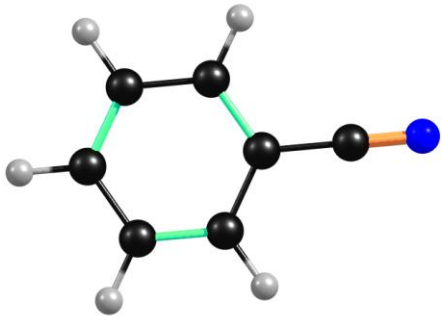

_____

Figure 5.8: Post-test questionnaire and accompanying survey questions given to students in the fall 2017 course.

CHEM 3110 Fall 2017 Post-Test Name _____
(Use additional paper if necessary.)

Answer the following questions after completing the "NAGMA" activity.

1. Define entropy. Use any examples necessary to explain your answer.

2. Which picture represents the system with higher entropy?

A.

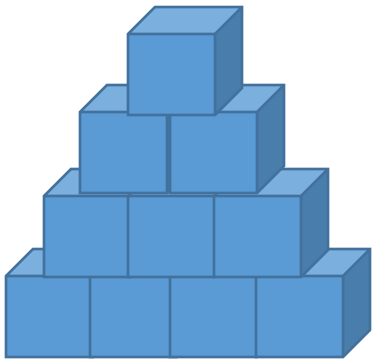

B.

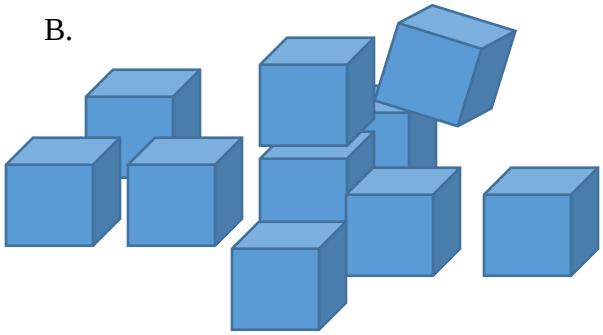

Please explain your reasoning for choosing this picture.

3. Rank the molecules from 1-3: 1 having the lowest entropy and 3 having the highest entropy.

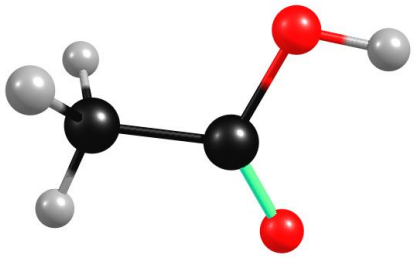

acetic acid _____

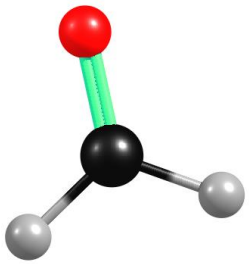

formaldehyde _____

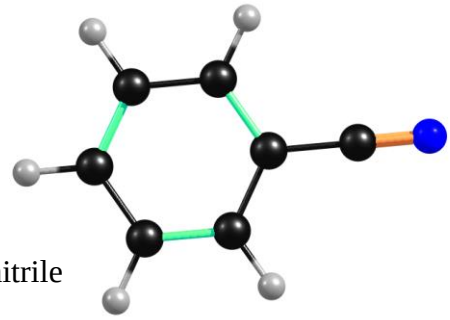

benzonitrile _____

Please explain your reasoning for ranking these molecules as you have.

Additional Survey Questions

1. The activity used during the problem solving session was useful for helping me learn the material.
   - Strongly Agree
   - Agree
   - Neutral
   - Disagree
   - Strongly Disagree

2. The activity used during the problem solving session challenged me to think and learn.
   - Strongly Agree
   - Agree
   - Neutral
   - Disagree
   - Strongly Disagree

3. Please rate the activity based on a scale from 1-5: 1 being not helpful for learning class material and 5 being extremely helpful for learning class material.

4. Please provide any additional feedback about this activity that would help us in the future.

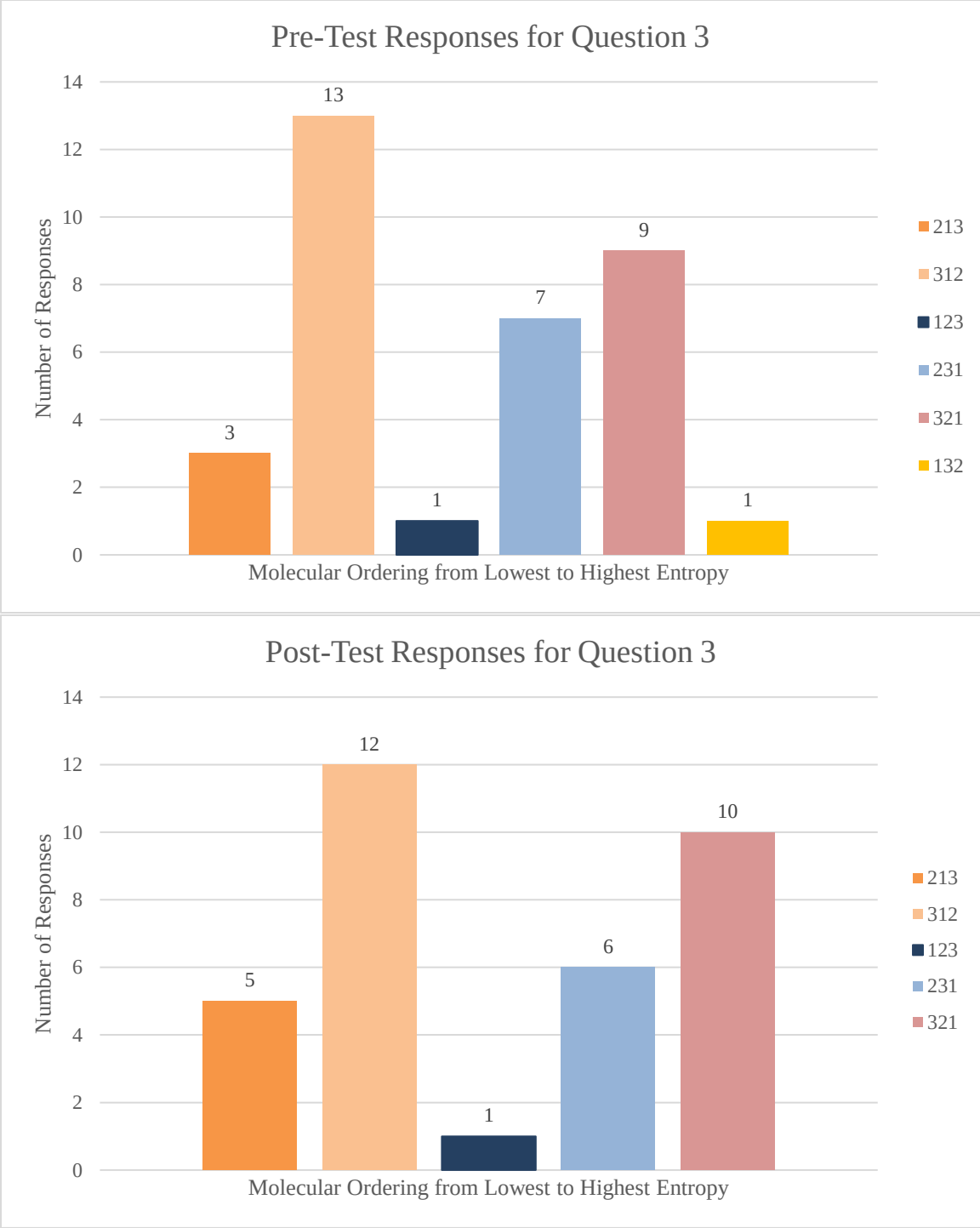

Figure 5.9: Bar graphs indicating student responses for question 3 of the pre-test (top) and post-test (bottom). The numberings found in the legends indicates the order in which students ranked the 3 molecules (acetic acid, formaldehyde and benzonitrile) from lowest to highest entropy.

CHAPTER 6

CONCLUSIONS AND OUTLOOK

Helium nanodroplet isolation (HENDI) was used to trap and characterize a variety of hydrocarbon molecules and radicals by infrared spectroscopy in the CH stretching region. In Chapter 3, the infrared spectrum of the cyclobutyl radical, whose pyrolytic precursor was cyclobutylmethyl nitrite, was shown. The 2800-3000 cm^{-1} region is complicated by the presence of resonance polyads, which appear because of anharmonic coupling between CH stretch fundamentals, and CH_2 bending combinations and overtones. The spectra of 1-methylallyl, and allylcarbinyl were also obtained. These radicals were also formed by pyrolysis of appropriate nitrite precursors through a quartz/tantalum source. The spectrum of 1,3-butadiene in helium droplets was also presented. Evidence of this species and 1-methylallyl was also confirmed to be in the original cyclobutyl spectrum by means of a spectrum recorded at a higher pyrolysis temperature. The presence of signatures of allylcarbinyl in the high temperature spectrum could not be validated; this may indicate it undergoes interconversion on a much faster timescale than that of the doping process. These results, along with a previously calculated C_4H_7 potential energy surface (PES), suggest that the cyclobutyl radical undergoes unimolecular decomposition via ring opening before being picked up by helium droplets.

Anharmonic frequencies for the cyclobutyl and 1-methylallyl radicals were predicted by VPT2+K simulations based upon a hybrid CCSD(T) force field. The frequencies predicted for a C_{2v} structure of the cyclobutyl radical match best with experimental values. Although not entirely conclusive, the experimental spectrum agrees with theoretical predictions for a combined contribution of both 1-methylallyl conformers. Multiple experimental values presented herein also agree well with the p-H_2 matrix work performed by Bahou et al.[1] Allylcarbinyl frequencies were predicted using a force field calculated with a DFT functional method, but agreements with experiment are overall poor. Future work should include a dedicated computational analysis of this particular radical possibly utilizing an orbital-optimized electronic structure method to alleviate any near-instabilities that may be occurring in this system.[2] Experimental future work of the C_4H_7 isomers should include exploring the spectra of cyclopropylmethylcarbinyl and 1-buten-1-yl radicals. These species have not been previously examined and could be the origin of the unassigned 3018 cm^{-1} band found in the high pyrolysis cyclobutyl spectrum.

The infrared spectrum of fulvenallene captured by helium droplets was displayed in Chapter 4. Although this molecule has been previously studied in the gas-phase, the work presented herein not only provides a higher resolution spectrum but also agrees with the previous results.[3] Anharmonic frequency calculations for this molecule were also presented and led to the assignment of several bands in the 2800-3140 cm^{-1} region. Fulvenallene was synthesized by flash vacuum pyrolysis of homophthalic anhydride as demonstrated previously in the literature.[4-6]

Fulvenallenyl was formed by the pyrolysis of fulvenallene through a SiC source and promptly solvated by the helium droplets.[7] The corresponding infrared spectrum of this species in the CH stretching region was also shown. Upon pyrolysis of fulvenallene, no evidence of pyrolytic decomposition was observed in the 2800-3140 cm^{-1} region of the spectrum when measured on mass channel 63 u. However, when the same frequency region was scanned on mass channel 89 u, two new vibrational bands appeared at 3058 and 3074 cm^{-1}. No formal assignments for these new bands were made. These bands are, however, centered close to the most intense bands of cycloheptatetraene and phenylcarbene measured in an Ar matrix.[8] Future work should explore this interesting possibility by assigning these bands and validating theoretical results on this interconversion process along the PES.[9, 10]

In the acetylentic CH stretching region, new bands appear between 3325 and 3345 cm^{-1} under pyrolysis conditions. This region of the spectrum has a high mass channel dependence. The band at 3327.1 cm^{-1} only appears on mass channel 63 u, while the bands at 3331.8, 3333.1, 3333.7, 3340.6, and 3342.6 cm^{-1} appear on mass channels 63 and 89 u. The experimental band for fulvenallenyl within this region of the spectrum is a sensitive marker for the extent of electron delocalization across the conjugated cyclopentadienyl and propargyl subunits. Spin density calculations were performed and aided in the assignment of the bands in this higher frequency region. Based on atomic partitioning of Mulliken populations, fulvenallenyl was shown to have 24% allenic and 76% acetylenic character. In comparison, the propargyl radical has values of 35% and 65%, respectively.[11] Looking at a closed shell system with an acetylenic unit, such as propargyl bromide (3332.56 cm^{-1}), we see that a substantial red shift of the acetylenic CH stretch

occurs for propargyl (3322.3 cm^{-1}) due to its partial allenic character.[12, 13] This can also be compared to the acetylenic CH stretch of HCCD which occurs at 3337.2 cm^{-1}.[14] Therefore, the fulvenallenyl acetylenic CH stretch was assigned to the band occuring at 3327.1 cm^{-1}. Based on the spin density analysis, which shows that fulvenallenyl has more acetylenic character than propargyl, and the corresponding spectral red shift, this conclusion is the most convincing argument. The other bands in this region of the spectrum were tentatively assigned to various isomers of ethynylcyclopentadiene based on the PES shown herein.[10, 15] Future work should explore these C_7H_6 isomers by recording their infrared spectra and comparing them to the spectra presented here.

Finally, an activity based on similar experimental physical chemistry research was created for use in an undergraduate course at the University of Georgia. As an application to current research, the activity shown provides a bridge for students as they begin to explore how concepts learned in the classroom are applicable to real-life situations and current research. The activity was based off an experiment that explores the thermodynamic characteristics of the model dipeptide N-acetylglycine methylamide (NAGMA) by recording its infrared spectrum in helium nanodroplets.[16] Through completion of pre- and post-test surveys, 34 students at UGA who opted to participate in the project explored their personal definitions of entropy before and after completing the activity, which consisted of reading the article and answering corresponding questions. For this particular set of students, their definitions of entropy shifted from a macroscopic point of view (i.e. “disorder”, “chaos”, etc.) to a microscopic point of view (i.e. “degrees of freedom”, “number of states”, etc.). As this project was not intended to give a generalized view of the results, future work should explore the activity’s effect on other

physical chemistry courses at UGA and other institutions. Creating other activities based on other physical chemistry research, such as what is presented in this dissertation, and gauging their effectiveness on instilling certain topics for chemistry undergraduates is another avenue of interest for further study.

References

(1) Bahou, M.; Wu, J. Y.; Tanaka, K.; Lee, Y. P. Infrared Absorption of Trans-1-Chloromethylallyl and Trans-1-Methylallyl Radicals Produced in Photochemical Reactions of Trans-1,3-Butadiene and Cl_2 in Solid Para-Hydrogen. *J. Chem. Phys.* **2012**, *137*, 084310.

(2) Szalay, P. G.; Vázquez, J.; Simmons, C.; Stanton, J. F. Triplet Instability in Doublet Systems. *J. Chem. Phys.* **2004**, *121*, 7624-7631.

(3) Angell, C. L. The Vapor-Phase Infrared Spectrum and Structure of Fulvenallene. *J. Mol. Struct.* **1971**, *10*, 265-273.

(4) Spangler, R. J.; Ho Kim, J. The Pyrolysis of Homophthalic Anhydride. Simple Synthesis of Benzocyclobutenone and Fulveneallene. *Tetrahedron Lett.* **1972**, *13*, 1249-1251.

(5) Thapa, J.; Spencer, M.; Akhmedov, N. G.; Goulay, F. Kinetics of the OH Radical Reaction with Fulvenallene from 298 to 450K. *J. Phys. Chem. Lett.* **2015**, *6*, 4997-5001.

(6) Ramphal, I. A.; Shapero, M.; Haibach-Morris, C.; Neumark, D. M. Photodissociation Dynamics of Fulvenallene and the Fulvenallenyl Radical at 248 and 193 nm. *Phys. Chem. Chem. Phys.* **2017**, *19*, 29305-29314.

(7) Kohn, D. W.; Clauberg, H.; Chen, P. Flash Pyrolysis Nozzle for Generation of Radicals in a Supersonic Jet Expansion. *Rev. Sci. Instrum.* **1992**, *63*, 4003-4005.

(8) Matzinger, S.; Bally, T. Spectroscopic Characterization of Matrix-Isolated Phenylcarbene and Cycloheptatetraene. *J. Phys. Chem. A.* **2000**, *104*, 3544-3552.

(9) Wong, M. W.; Wentrup, C. Interconversions of Phenylcarbene, Cycloheptatetraene, Fulvenallene, and Benzocyclopropene. A Theoretical Study of the C_7H_6 Energy Surface. *J. Org. Chem.* **1996**, *61*, 7022-7029.

(10) Polino, D.; Famulari, A.; Cavallotti, C. Analysis of the Reactivity on the C_7H_6 Potential Energy Surface. *J. Phys. Chem. A.* **2011**, *115*, 7928-7936.

(11) Jochnowitz, E. B.; Zhang, X.; Nimlos, M. R.; Varner, M. E.; Stanton, J. F.; Ellison, G. B. Propargyl Radical: Ab Initio Anharmonic Modes and the Polarized Infrared Absorption Spectra of Matrix-Isolated $HCCCH_2$. *J. Phys. Chem. A.* **2005**, *109*, 3812-3821.

(12) Küpper, J.; Merritt, J. M.; Miller, R. E. Free Radicals in Superfluid Liquid Helium Nanodroplets: A Pyrolysis Source for the Production of Propargyl Radical. *J. Chem. Phys.* **2002**, *117*, 647-652.

(13) Yuan, L.; DeSain, J.; Curl, R. F. Analysis of the K-Subband Structure of the ν_1 Fundamental of Propargyl Radical $H_2CC{\equiv}CH$. *J. Mol. Spectrosc.* **1998**, *187*, 102-108.

(14) Nauta, K.; Miller, R. E. The Vibrational and Rotational Dynamics of Acetylene Solvated in Superfluid Helium Nanodroplets. *J. Chem. Phys.* **2001**, *115*, 8384-8392.

(15) Polino, D.; Cavallotti, C. Fulvenallene Decomposition Kinetics. *J. Phys. Chem. A.* **2011**, *115*, 10281-10289.

(16) Leavitt, C. M.; Moore, K. B.; Raston, P. L.; Agarwal, J.; Moody, G. H.; Shirley, C. C.; Schaefer, H. F.; Douberly, G. E. Liquid Hot NAGMA Cooled to 0.4 K: Benchmark Thermochemistry of a Gas-Phase Peptide. *J. Phys. Chem. A.* **2014**, *118*, 9692-9700.